3-D Seismic processing in crystalline rocks using the Common Reflection Surface stack

Dissertation with the aim of achieving a doctoral degree
at the Faculty of Mathematics, Informatics and Natural Sciences
Department of Earth Sciences
University of Hamburg

submitted by
Khawar Ashfaq Ahmed

2015
Hamburg, Germany

Day of oral defense: 30.06.2015
The following evaluators recommended the admission of the dissertation:
Supervisor: Professor Dr. Dirk Gajewski
Co-supervisor: Dr. Claudia Vanelle

In the name of ALLAH, The Beneficent, The Merciful

Abstract

Seismic data from crystalline or hardrock environments usually exhibit a poor signal-to-noise (S/N) ratio due to low impedance contrasts in the subsurface. Moreover, instead of continuous reflections we observe a lot of steeply dipping events resembling parts of diffractions. The conventional seismic processing (CMP stack and DMO) is not ideally suited for imaging such type of data. Common-reflection-surface (CRS) processing considers more traces during the stack than CMP processing and the resulting image displays a better S/N ratio. In the last decade, the CRS method was established as a powerful tool to provide improved images, especially for low fold or noise contaminated data from sedimentary basins. The CRS stack and all attributes linked to it are obtained using a coherence-based automatic data-driven optimization procedure. In this research, the 3D CRS workflow was applying to 3D crystalline rock seismic data which were acquired near Schneeberg, Germany, for geothermal exploration. 3D seismic imaging is the challenge for data acquired in the hardrock environment. In 3D case, the data volume is big and it is not easy to process. For this purpose, before processing this big data, the 3D CRS code has been optimized with the hybrid approach (message passing interface MPI with OpenMP). This makes the program run in efficient fashion and can handle the big dataset up-to Tera-bytes with fast processing and also the output quality of the image is same as the original 3D CRS processed image.

The CRS stack itself provided an image of good S/N ratio. However, for data from environments with low acoustic impedance and poor velocity information, the coherence which is automatically obtained in the optimization procedure provides an alternative way to image the subsurface. Despite the reduced resolution, for this data the coherence image provided the best results for an initial analysis. Utilized as a weight, the coherence attribute can be used to further improve the quality of the stack. By combining the benefits of a decreased noise level with the high resolution and interference properties of waveforms, we argue that these results may provide the best images in an entirely data-driven processing workflow for the Schneeberg data. Because of the large number of diffractions in the data leading to numerous conflicting dips and crossing image patterns, stacks are difficult to interpret. Time-migrated data helped to identify several major fault structures, which coincide with geological features of the considered area.

Studies on these 3D crystalline rock data showed some interesting features which were not expected by the geologists. Schneeberg body was not expected before

survey. Conjugate faults cut through the Roter Kamm which is also a surprising fact. The behaviour of Roter Kamm is new for geologists. This include the faint seismic signature of the regional fault Roter Kamm. Before the 3D seismic survey, it was assumed to be the prominent feature. The distribution of diffraction apexes in the time-migrated section shows a distinct high where several fracture systems intersect. The fracture systems cross each other near the center of this block. If these diffractions are the response of open fractures the area could serve as a natural heat exchanger to generate geothermal energy. This is an ongoing discussion whether the cracks are open or mineralized.

Zusammenfassung

Seismische Daten aus dem Kristallinen oder Hardrock-Umgebungen weisen in der Regel aufgrund der niedrigen Impedanzkontraste im Untergrund ein schlechtes Signal-Rausch (S/N) Verhältnis auf. Außerdem beobachten wir anstelle von kontinuierlichen Reflexionen viele steil abfallende Ereignisse, die sich wie Diffraktionssegmente verhalten. Die konventionelle Bearbeitung seismischer Daten (CMP-Stapelung und DMO) ist nicht idealerweise zur Abbildung dieser Art von Daten geeignet ist. Die Bearbeitung mit dem Common-Reflection-Surface (CRS) Verfahren betrachtet mehr Spuren als das CMP-Verfahren und das resultierende Bild zeigt ein besseres S/N-Verhältnis. In den letzten zehn Jahren wurde die CRS-Methode als ein mächtiges Werkzeug eingeführt um verbesserte Bilder, vor allem für niedrig überdeckte oder verrauschte Daten aus Sedimentbecken zu erzeugen. Der CRS-Stack und alle mit ihm verbundenen Attribute werden unter Verwendung eines kohärenzbasierten, automatischen und datengesteuerten Optimierungsverfahren erhalten. In dieser Untersuchung wurde der 3D-CRS-Workflow auf 3D seismische Daten im kristallinen Gestein angewendet, die in der Nähe von Schneeberg, Deutschland für geothermische Exploration aufgezeichnet erworben wurden. Seismische 3D-Bildgebung ist eine Herausforderung für die in einer Hardrock-Umgebung erfassten Daten. Im 3D-Fall ist die Datenmenge groß und nicht einfach zu bearbeiten. Zu diesem Zweck wird vor der Bearbeitung dieser großen Daten der 3D-CRS-Code mit dem Hybrid-Ansatz (Message Passing Interface (MPI) mit OpenMP) optimiert. Das erlaubt, das Programm in effizienter Art und Weise auszuführen und die große Datenmenge, die Tera-Bytes betragen kann, schnell zu bearbeiten und auch die Qualität des Outputs ist die gleiche wie die des mit dem Original-3D-CRS bearbeiteten Bildes.

Der CRS-Stack selbst hat ein Bild mit gutem S/N-Verhältnis geliefert. Doch für Daten von Umgebungen mit niedriger akustischer Impedanz und schlechten Geschwindigkeitsinformationen, bietet die Kohärenz, die automatisch in der Optimierungsprozedur bestimmt wird, eine alternative Möglichkeit, den Untergrund abzubilden. Trotz der reduzierten Auflösung für diese Daten war das Kohärenzbild das beste Ergebnis für eine erste Analyse. Als Gewicht eingesetzt, kann das Kohärenzattribut verwendet werden, um die Qualität der Stapelung weiter zu verbessern. Durch die Kombination der Vorteile des verringerten Geräuschpegels mit der hohen Auflösung und den Interferenzeigenschaften von Wellenformen, argumentieren wir, dass diese Ergebnisse die besten Bilder in einem rein datengesteuerten Bearbeitungsworkflow für die Schneeberg-Daten liefert. Wegen

der großen Anzahl der Diffraktionen in den Daten, die zu zahlreichen 'conflicting dip' Situationen führen, sind die Stapelsektionen schwierig zu interpretieren. Zeitmigrierte Daten haben dazu beigetragen, mehrere große Verwerfungsstrukturen zu identifizieren, die mit geologischen Besonderheiten des betrachteten Bereich übereinstimmen.

Studien an diesen 3D Gesteinsdaten aus dem Kristallin zeigten einige interessante Features, die von den Geologen nicht erwartet wurden. Der Schneeberg-Körper wurde vor der Erhebung der Daten nicht erwartet. Konjugierte Störungen schneiden den Roten Kamm, was auch eine überraschende Tatsache ist. Das Verhalten des Roten Kamm ist neu für die Geologen. Dies beinhaltet die schwache seismische Signatur der regionalen Verwerfung Roter Kamm. Vor der Messung mit 3D-Seismik wurde davon ausgegangen, dass diese das hervorstechende Merkmal ist. Die Verteilung der Diffraktions-Apices in der zeitmigrierten Sektion zeigt ein deutliches Maximum dort wo sich mehrere Bruchsysteme schneiden. Die Bruchsysteme kreuzen einander nahe dem Zentrum dieses Blocks. Wenn diese Diffraktionen die Auswirkungen offener Risse sind, könnte der Bereich als natürlicher Wärmetauscher dienen, um geothermische Energie zu erzeugen. Es ist gegenstand anhaltender Diskussion ob die Risse offen oder mineralisiert sind.

Contents

List of Figures

List of Tables

1. Introduction

Crystalline or hardrock environments are present everywhere on earth depending upon the geological diversity and plate tectonics (Eaton et al., 2003). These areas act as the prospect zones for geothermal and mineral exploration. Some of the zones are metamorphosed, some are eroded and some are fractured due to the stress and tectonic forces. These fractures are mineralized sometimes due to the hydrothermal fluids and known to be the hydrothermal veins. Such environments are of great interests for geologists because of their mineralized zones. If the fractures are open, then they can act as the medium for the heat exchange by hot hydrothermal fluids. If the rock is dry, then they are the prospect zone for petrothermal energy exploration.

Heat collectors from petrothermal cracks are fractured zones of natural or artificially made cracks in the crystalline rocks of the basement. These rocks have high temperature and may serve as "heat exchanger". Detection of such "heat exchangers" are carried out by geophysical methods. When pumped out of wells and warmed to 100–300°C, waters function as a heat transfer for thermal energy supply and electric energy generation. If the technical problem of the rapid drilling of 6–10 km deep wells could be solved in an economic fashion, then petrothermal energy will become competitive to the traditional types of energy production and supply (Gnatus et al., 2011).

3D seismic imaging is a challenge for data from the subsurface comprising crystalline rocks. The reason for this is the small reflectivity/acoustic impedance and S/N ratio compared to data from sedimentary basins (see, e.g., Milkereit et al., 2000; Malehmir et al., 2012). Contrary to typical reflection data where we observe continuous events over large lateral distances hardrock data are usually dominated by diffractions or parts of diffraction events which leads to a criss-cross pattern and numerous conflicting dip features in the stacked sections. This challenges any kind of geological interpretation. Because of the small lateral extend of events in hardrock data, velocity determination is difficult, Moreover, the velocity in hardrock is usually high and the resulting moveouts are small which provides an additional challenge in the data processing. These problems in velocity analysis influence the quality of the stacked data and may lead to an unsatisfactory image

not very suitable for geological interpretation.

It was demonstrated previously that the common-reflection-surface (CRS) stacking method has advantages for low fold and/or low signal-to-noise (S/N) data when compared with CMP stacking (Mann et al., 1999; Jäger et al., 2001; Hertweck et al., 2007; Baykulov et al., 2011). This observation suggests to apply the CRS method to hardrock data. It is an important feature that the fold in CRS processing is considerably higher than the fold in CMP processing which helps to image weak events and to improve the S/N-ratio of the stacked section. The CRS method (Mann et al., 1999; Bergler et al., 2002) is an automatic entirely data driven approach. It provides next to the stack itself several kinematic wavefield attributes and the corresponding coherence for each sample in the stacked data volume. The wavefield attributes have many applications in CRS processing like multiple suppression (Dümmong and Gajewski, 2008), NIP-wave tomography (Duveneck, 2004), diffraction processing and imaging (Dell and Gajewski, 2011), pre-stack data enhancement, data interpolation and regularization (Baykulov and Gajewski, 2009) just to name a few.

In a joint project with the Leibniz Institute for Applied Geophysics (LIAG), Hannover, Germany and the TU Bergakademie Freiberg, Germany, a 3D reflection seismic experiment was conducted in the area of the city of Schneeberg, Saxony, Germany. The field work is part of a pre-site survey for a *petrothermal* exploration project. The subsurface in this area is complex and dominated by steep faulting in the crystalline rocks. The data show a lot of scattering due to the fractured zones and hydrothermal veins. The processing of this type of seismic data is a challenge because of the above mentioned reasons. Conventional CMP-DMO-based processing did not provide satisfactory results. Therefore, 3D CRS processing was applied here to achieve a better S/N ratio and to obtain an interpretable stacked volume.

Structure of the thesis

The thesis is structured as follows:

A short introduction to the 3-D reflection seismic imaging in hardrock environment is discussed with some overview of the petrothermal exploration.

In chapter **"Theoretical background"**, the seismic theory is explained with the

introduction of 3D seismic including the acquisition, preprocessing and 3D CRS processing. After processing, the stacked volume is also migrated.

New implementation for efficient performance of 3D CRS processing

In chapter **"Optimizing by Hybrid MPI and OpenMP"** optimization related work is discussed, as 3D CRS is costly because full attributes searches consume a lot of time compared to other processes. A hybrid parallelization approach has been implemented. As the code was already MPI based, OpenMP and concurrent programming is introduced at some tasks without changing the major routines of scientific calculation of CRS attributes. This gives a fast and robust approach to get the output of processed seismic 3D volume specially when the data is huge.

In chapter **"3D Seismic imaging in crystalline rock"**, 3D seismic imaging of the Schneeberg data is presented. 3D CRS itself improved the images, but the data volume was still not interpretable in detail. In this case, when the velocity information is not so good, coherence gave alternative and better interpretable images. Because of the criss-cross pattern, the time migration is also applied in the work flow which helped to improve the structural interpretation. It made the interpretation of faults and structures consistent and most features are according to the geological expectations.

In chapter **"Summary and outlook"**, the results are discussed with respect to the geophysical exploration in crystalline rock. The advantage of optimization is discussed and the results of studies on the optimized code is elaborated. The resultant achievement from this 3D hard rock seismic imaging via 3D CRS workflow is explained. This study show that the 3D CRS workflow can handle such type of data (low coherence and S/N ratio) better than the conventional CMP processing. Also, the coherence based seismic imaging gives more information about the sub-surface structure and tectonics.

Electronic material related to this application of 3D seismic study are given in appendix.

2. Theoretical background

2.1. 3D Seismics

Earth itself is a 3D structure and all geological features inside the earth are three dimensional (3D) which are of great interest for the exploration. The examples include duplex structures, hydrothermal veins, salt diapirs, faults and folds etc. A 2D seismic section is the response of the 3D reflection seismic along a profile. Although 2D sections contain the signal from all directions, including out of plane energy, 2D migration normally assumes that all signal originate from the plane in the profile. Only expert interpreter may recognize the response of signal which comes from out of the plane.

3D seismic surveys (data acquisition)

A typical 3D marine survey is carried out by shooting closely spaced parallel lines which are called shooting lines. The typical land seismic survey is carried out with the number of parallel receiver lines which are perpendicular to the direction of shooting lines. For land 3D seismic acquisition, the source and receiver lines may or may not be straight, depending upon the access and availability of the location. It also depends on the topography of the area. Also in 3D seismic acquisition, the receivers and sources can be in the form of groups designed in different configurations and shapes according to the demand and need of that acquisition. Different types of sources can be used in data acquisition such as vibroseis, dynamite, air gun, etc.

In seismic data acquisition, a typical $3D$ *seismic data* is a group of closely spaced seismic lines which are crossing each other and provide densely sampled measurements of the subsurface reflectivity. Typical receiver line spacing can range from 300 m to over 600 m, and typical distance between shot points and receiver groups is 25 m. It depends on the subsurface structure as well. If it is complex, line

spacing can be done more closely spaced e.g., 15 m (like in Schneeberg 3D seismic acquisition) and between 34 to 67 m (onshore). Bin sizes are commonly 25 m. The composite data set can be "cut" in any direction but still display is a well sampled seismic section. The original seismic lines are called in-lines. *In-line* is a seismic line within a 3D survey parallel to the direction in which the data were acquired as shown in Figure 2.1. In the figure, the dotted line shows the source lines, and the continuous line shows the receiver lines which coincide with the in-lines. The red stars show the sources. In marine seismic data, the in-line direction is that in which the vessel tows the streamers. Lines displayed perpendicular to in-lines are called $cross-lines$(x-line). *Azimuth* is the angle between the vertical projection of a line of interest into a horizontal surface and true north or magnetic north measured in a horizontal plane, typically measured clockwise from north as in Figure 2.2.

Acquisition geometry

In a typical 3D seismic land data acquisition, the source is usually vibroseis or dynamite, and the receiver cables are laid out in parallel lines (in-line direction) and the shots are located perpendicular to this direction. e.g., (cross-line direction).

Before designing the survey, the pre-site geophysical and geological surveys are performed, out of which gravity survey is important. Usually the survey is designed on the basis of gravity and a prior geological information.

2.2. Seismic data processing

Seismic data processing is a process in which the data is arranged and managed in an order to make it interpretable. It is a process in which the signal-to-noise ratio is enhanced, unnecessary frequencies are filtered out and seismic events are migrated and focused to their appropriate positions. It helps to improve the resolution of the seismic signal to make it easier for interpreters to understand the subsurface structures. There are two major types of processing the seismic data. One is called pre-processing, apart of which is done in the field during the acquisition of seismic data. The other is main processing, which is done in the labs.

3D seismic data pre-processing is almost similar to the 2D data pre-processing, and all the concepts applied during the processing are similar for 3D. The differences are the 3D geometry, statics, velocity analysis and 3D migration. Other steps such as trace editing, noise reduction, geometric spreading correction, deconvolution, trace

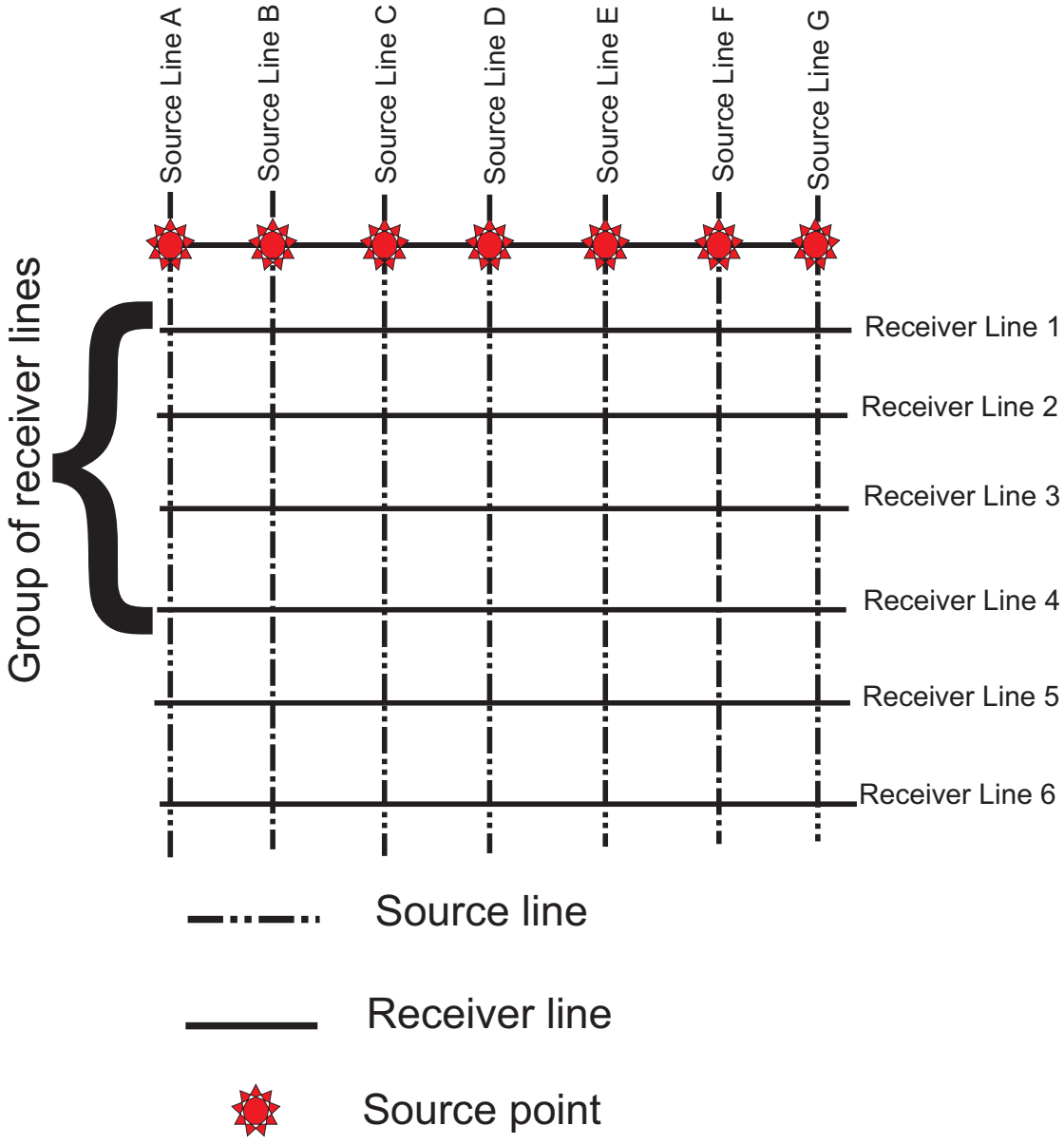

Figure 2.1.: 3D Seismic acquisition.

balancing, and statics are applied similar to the 2D surveys. One other difference is the binning. In 2D the traces are collected in common-midpoint (CMP) gathers, while in 3D, it is done in terms of cells known as CMP cell or bin.

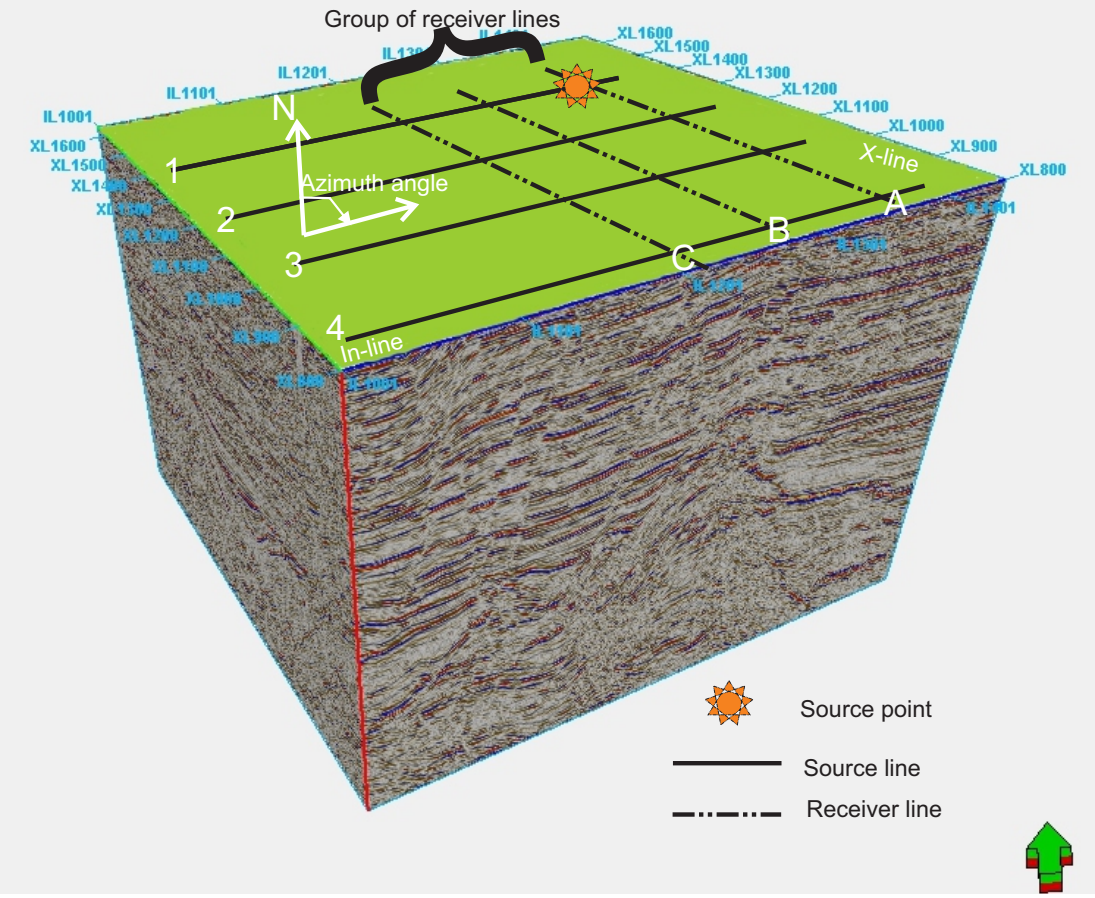

Figure 2.2.: 3D Seismic geometry.

3D data is often visualized in so called *time slices*. A *time slice* is a horizontal display or map view of 3D seismic data having a certain arrival time value, as opposed to a horizon slice that shows a particular reflection. A time slice is a quick, convenient way to evaluate changes in amplitude of seismic data (Schlumberger, 2015).

2.2.1. Pre-processing

Seismic pre-processing is a part of seismic data processing during which some steps are usually done immediately in the field during the seismic data acquisition. This is mandatory to assure the quality control of the seismic data acquisition and to evaluate the signal quality as well. Some pre-processing steps are listed here:

- *De-multiplex* : this is first step in which the traces of seismic data is converted

to (SEG-Y,D) from multiplexed format (SEG-A,B).

- *Re-sampling* : this is done in the field depending upon the signal quality. Normally the standard sampling interval is 2 ms.

- *Editing* : trace editing is done in-order to remove dead or bad traces.

- *Deconvolution* : it is inverse filtering in which the frequencies of a seismic signal is enhanced. It improves the resolution of seismic data which is badly affected by the convolution process when seismic energy is filtered by earth.

- *Noise attenuation* : different types of noise are present in the data when it is collected in the field during acquisition. This includes the ground rolls, noise produced by living beings, wind, electric poles etc. It is attenuated in the field by applying certain different types of filters.

- *Multiple attenuation* : Multiple is the multiply reflected seismic energy, or any event in seismic data that has incurred more than one reflection in its travel path. Multiples are the part of seismic data which are observed during seismic data acquisition. They have to be removed from the data to get a good approximation of the subsurface because most imaging methods assume primary only reflection data. Usually predictive deconvolution is used to remove the multiples. Water bottom multiples and sea surface interface are observed in common practice in marine seismic data which are suppressed by special seismic processing like, e.g., surface related multiples, removal (SRME), (see., Bruce et al. (2009)).

- *Static correction* : static corrections depend on the topography. If the area is flat, then static correction are not required. Also in marine acquisition, the static correction is not required if the tide are usually less then 6 m. If the topography is rough with landscapes, then it is crucial to apply it to bring the acquisition horizons to the datum. Static corrections compensate for differences in topography and differences in the elevations of sources and receivers. In land seismic, it is usually common practice to remove the effect of weathering layer near the surface where the velocity is very low. It is also known as weathering correction.

- *Quality Control (QC) of data* : it is done in the field to check the quality of the signal and to correct the geometry.

- *3D binning* : this is a process in which seismic data is divided into small parts according to the mid points between the sources and receivers. This is done before stacking data. In standard procedures, the binning space is 25 m by 25

m. But if its required, the binning can be done more closely spaced according to the demands.

Muting is a process, to remove the contribution of selected seismic events in a stack to minimize certain effects such as air waves, ground roll, near surface low frequency content or noise from first arrivals. The main targets of this process is the low frequency content specially present in the early parts of the dataset.

The change of amplitudes of oscillatory signal from original available input to the amplified output is known as *gain*. It is the time variant scaling function based on the desired criterion. For-example : *geometric spreading* correction is applied for the compensation of wavefront divergence. It should be applied with great care as its side effect can ruin the seismic signal. There are different types of gain. The most common practice used in seismic processing is automatic gain control (AGC). This is applied to improve the signal of the late arriving events in which the attenuation and wavefront divergence has caused the decay of the amplitude of the signal. AGC is a kind of trace equalizer as well. It balances out the amplitudes across the whole trace. Although the AGC is fast to apply, it has downsides as well. It uses the mean value on the basis of the average amplitude and no "true amplitudes" anymore.

Filtering is a procedure in which the undesired portion of the dataset is removed. This removal can be done in terms of frequency or amplitude or some other information from seismic dataset. This is done for increasing the signal-to-noise (S/N) ratio. Usually first of all, it is used to remove the coherent noise content from the data and to apply deconvolution. Sometimes, the unwanted frequency band is removed by band pass filtering. After pre-processing, certain filters such as low pass (high cut) or high pass (low cut) or band pass frequency filter is applied for certain band of frequencies which are unwanted in the signal processing. All of these filtering (other than deconvolution) almost follow the same principle to construct the zero phase wavelet with flat amplitude spectrum.

The mostly applied filter is known as a band pass filter because seismic data mostly contains low frequency content which acts as noise, such as ground roll, and some high frequency ambient noise. Band-pass filter is performed at various stages in seismic data processing. If necessary, it can also be applied before the deconvolution to suppress ground roll. Narrow band-pass filtering is applied before cross-correlation of traces in a CMP gather to estimate residual static shifts.

2.3. Conventional processing

After pre-processing of the seismic data, different steps are taken into account during the conventional seismic processing. These include velocity analysis, gain which could be AGC or clipping, filtering different undesired frequencies, and then stacking. The stacking may be of different kinds, like brute stack, common midpoint (CMP) stack, common reflection surface (CRS) stack, etc. After stacking, migration of the stacked data is performed to bring the reflection seismic events to their correct position. Two major types of migration are prestack and poststack migration. The sub-types include the time migration and depth migration.

The common-midpoint (CMP) stack

The common-midpoint (CMP) stacking was first time presented by (Mayne, 1962) under the assumption of a horizontally layered medium, in which the reflection events measured on different traces in a CMP gather stem from a common reflection point in the subsurface located directly beneath the CMP location.

$$t^2(h) = {t_0}^2 + \frac{4h^2}{\nu^2} \tag{2.1}$$

The CMP stack is a simulated zero-offset ssection which makes use of the redundancy in multicoverage seismic data by considering traces of a common midpoint but with varying offsets. Seismic signals are summed up in the form of stack based on the coherency of traces in the offset direction along the stacking curves. The resultant outcome has an improved signal-to-noise (S/N) ratio which are arranged with respect to the midpoint location. In Figure 2.3, h is the half offset distance. The reflection traveltimes $t(h)$ are measured in the CMP gather which is described in the equation 2.1 . ν is the stacking velocity which describes the least fitting moveout to the data.

Coherence is a measure of the similarity of two signals (here seismic events) in a dataset. The most commonly used coherence measure is *Semblance*. It is the statistic measure between the consistency of the two seismic events. It was first introduced by (Taner and Koehler, 1969). Semblance is the normalized coherency function (Luo and Hale, 2012). The semblance has been an indispensable tool for measure of velocity analysis in the seismic datasets (Fomel, 2009). Semblance based analysis is commonly performed in velocity analysis during the seismic data

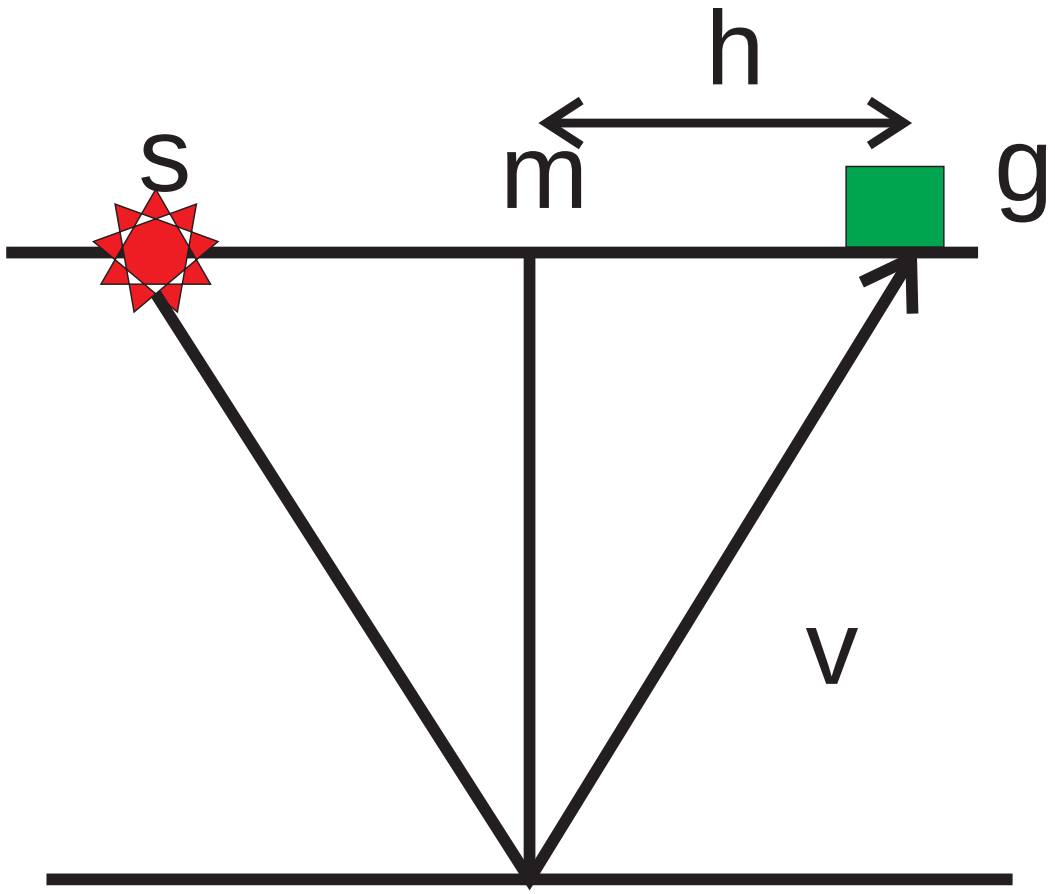

Figure 2.3.: Horizontal reflector in subsurface.

processing (Taner and Koehler, 1969; Neidell and Taner, 1971). In conventional velocity analysis of seismic data, seismic gathers are scanned for different values of stacking velocities, to obtain velocity spectra for picking of optimal stacking velocities (Yilmaz, 2001).

The coherence coefficient used in the current implementation of the common-reflection-surface stack (CRS) is given by (Neidell and Taner, 1971; Yilmaz, 2001) as:

$$S = \frac{1}{n} \frac{\sum_{t(0)-\frac{b}{2}}^{t(0)+\frac{b}{2}} \left(\sum_{i=1}^{n} f_{i,t(i)}\right)^2}{\sum_{t(0)-\frac{b}{2}}^{t(0)+\frac{b}{2}} \sum_{i=1}^{n} f_{i,t(i)}^2} \equiv \frac{\text{energy of stacked traces}}{\text{total energy}}, \tag{2.2}$$

where n denotes the number of traces in the gather. $t(0)$ is the ZO time, for which

Semblance S is evaluated and $t(i)$ is the operator traveltime for $(\Delta x_m, h)_i$. $f_{i,t(i)}$ denotes the amplitude on the i-th trace for $t = t(i)$. The stack is defined below:

$$\sum_{i=1}^{n} f_{i,t(i)} \tag{2.3}$$

Semblance is a normalized equality and its value ranges from 0 and 1. The drawback of the semblance criterion is that it assumes the amplitude and phase of the wavelet to be constant along the whole operator which unfortunately is not the case due to angle dependent reflection coefficient (Müller, 2007) and geometrical spreading. The coherence criteria which fulfills the definition of phase and amplitude incorporation is presented by (Gelchinsky et al., 1985) which ends up with high computational demands for the coherence estimation.

Seismic waves travel in the earth and give the indirect measurement of the velocity. The direct measure of velocity is only possible with the sonic logs. These information derive different types of velocities e.g., interval, root mean square (RMS), normal moveout (NMO), stacking, migration and average velocities. The stacking velocity is determined by the best fit of the operator.
The 'true' medium velocity is the interval velocity. There are many factors on which the velocity of the medium depends. Those include the type of lithology, pore shape, pore pressure, saturation content, temperature and overburden effects. The stacking velocity estimation requires the data recorded at non-zero offsets provided by common midpoint (CMP) recording (Yilmaz, 2001).

For a single layer horizontal layer, the reflection traveltime curve as function of offset is a hyperbola as given in equation above. The difference between the two way travel time at the given offset and the two way travel time at the zero offset is called normal moveout (NMO). The velocity required to correct the normal moveout is called normal moveout (NMO) velocity. In case of single horizontal reflector, the normal moveout velocity is the velocity above the reflector. In case of dipping reflector, the normal moveout velocity is velocity of medium divided by the cosine of the dip angle as given:

$$V_{NMO} = \frac{\nu_0}{\cos\phi} \tag{2.4}$$

If the reflector is observed in three dimensions, then there is additional a factor

involved which is known to be the azimuth. This azimuth is the angle between the dip direction and profile direction. For layered heterogeneous media, equation 1.1 is valid. This approximation is better for small offsets compared to the larger offsets. If offsets are small, the velocity of horizontal layered medium is equal to the root mean square (RMS) velocity. If there are dips in the reflecting medium or lateral velocity variations, the determination of medium velocities is complicated maximum and requires tomography. The formula shows here only for the 2D NMO velocity.

There is a difference between stacking and NMO velocities which is normally ignored in common practice. The NMO velocity is based on small spread hyperbolic traveltime (Taner and Koehler, 1969; Al-Chalabi, 1973), while stacking velocity is based on hyperbola which best fits the data over the entire spread length. In practice, generally both stacking velocity and NMO velocity are considered to be equal. The differences between stacking velocities and NMO velocities is known as *spread length bias* (Al-Chalabi, 1973; Hubral and Krey, 1980).

The most common way for velocity analysis is based on the hyperbolic assumption. There are different ways for the velocity analysis. One way of velocity analysis is to apply different NMO corrections to a CMP gather with the variety of range of velocities and to observe them. The velocity which flattens the reflectors (events) as a function of the offset is considered as the NMO velocity. In other way, small portion of the seismic line can be stacked with the constant velocity (with different constant values). These stacks are known to be the constant velocity stacks (CVS). The constant velocity that gives the best desired resultant stack is chosen as the final velocity for NMO correction.

Another approach of velocity analysis is based on the computation of velocity spectrum (Taner and Koehler, 1969). This is measure of coherency of velocity on a graph with two way zero offset traveltime. The velocity which gives higher coherency in the velocity spectra is chosen as the best fitted stacking velocity for the corresponding event.

A true reflection traveltime is not always hyperbolic even in the case of horizontal layered reflectors. One cause of the deviation from this hyperbolic fitting is the static time shifts which occurs because of the near surface velocity variations. Statics is a severe problem and distorts the fitting of hyperbola when there is rapid and large topographic elevation changes. Also if there is a big change in weathering layer, there is no perfect fitting. If the static corrections are not done well, then

the stacking velocity model for the near surface corresponding to those CMPs is unreliable.

Once the data is sorted into common cell gathers like CMPs or bins, velocity analysis is performed. In this whole procedure, there is no difference between the 3D velocity analysis compared to the 2D except one additional dimension for 3D case. The velocity analysis could be performed in certain intervals, e.g., every 500 m and also for every single CMP.

Once the normal moveout (NMO) velocity is estimated, the moveout is corrected. The NMO correction needs to be done prior to the trace summation of the CMP gathers. The normal moveout depends on many factors such as velocity above the reflector, offset, zero offset two way travel time, dip of the inclined/dipping reflector, azimuth of the acquisition geometry (azimuth of source, and receiver) with respect to the true dip of the reflector, and the degree of the complexity of the near surface and medium above the reflector.

If there is any frequency distortion in any event during NMO correction, its known to be the *NMO stretch*. It occurs during the NMO correction of shallow events or the events at large offsets. This can severely disturb the subsurface imaging in the large offsets or shallow events which are stretched. The only way to deal with it is to mute the stretched events to get rid of this problem. The threshold can be defined according to a certain percentage of signal stretch.

2.4. Basics of the 3D-CRS Workflow

The CRS stack (Mann et al., 1999; Jäger et al., 2001) was originally developed to obtain simulated zero-offset (ZO) sections or volumes from seismic multi-coverage data. The method is based on a stacking operator that is of second order in the midpoint and half-offset coordinates x_m and h, i.e., it is of hyperbolic shape. The CRS stacking operator at a given zero-offset location (x_0, t_0) is determined by a number of parameters related to the coefficients of the second order traveltime expansion. For each zero-offset sample to be simulated, the optimum stacking operator is found by varying these parameter values within predefined boundaries. The main attributes of this workflow are angle, normal incidence point curvature and normal wave curvature. These parameters or attributes define the shape of the operator. Stacking along this operator and performing a coherence analysis in

the pre-stack domain provides the attributes with the best fit to the data. The parameters which yield the highest coherence value describe the optimum stacking operator. The parameters are called kinematic wavefield attributes (Hubral, 1983). The travel time operator for the 3D-CRS is defined later on.

Automatic CMP stack

The first step in (non-conventional stacking procedure) 3D common-reflection-surface (CRS) stack is the generation of the automatic CMP stacked section. The procedure is similar to the conventional CMP stacking where the velocities are manually picked which is based on the highest achieved coherence values between the hyperbolas and recorded data. The CRS also follows the same criteria, but in automatic way of picking of highest coherence value. Here the stacking velocities are defined in terms of ν_0, α, M_{nip} and t_0.

The relationship for the stacking velocities in terms of ν_0, α and M_{nip} is given by equation.

$$V_{NMO} = \sqrt{\frac{2\nu_0 M_{nip}}{t_0 \cos^2 \alpha}} \tag{2.5}$$

Here in this case, the $m = 0$, so we can say that, the CMP is a special case of CRS in which the midpoint displacement is zero. We can say that the CRS is the extended version of CMP with one lateral extension in the midpoint (m) direction. In this search approach, a range of stacking velocity is delivered of which, a discrete number of stacking velocities are tested. Out of these, each defines the hyperbola in that CMP gather/bin, which is correlated with the prestack data. The velocity with the highest accuracy and coherency value is the value, which gives the best fit for hyperbola.

In conventional CMP search, the velocities of primaries are picked up manually. In automatic CMP stack, all coherent events are summed up which are described by the CRS parameters. Multiples are an issue for this automatic process, and in order to suppress multiples, the search procedure can be constrained. In-order to get rid of multiples, automatic CMP stack may be supplied with the reference velocity files/sections. This reference model can be build up by the conventional NMO analysis and can be used as the guided velocity function to compute the correct velocity for the events. This leads to the velocity analysis of the automatic

CMP stack which is constrained.

3D-Common-Reflection-Surface Stack

In the 3D case the 3D CRS operator (Bergler et al., 2002; Müller, 2003) reads:

$$t^2(\Delta\mathbf{x}_m, h) = (t_0 + \mathbf{p}\Delta\mathbf{x}_m)^2 + 2t_0\left(\Delta\mathbf{x}_m^T\mathbf{M}_n\Delta\mathbf{x}_m + \mathbf{h}^T\mathbf{M}_{nip}\mathbf{h}\right) \tag{2.6}$$

It depends on eight stacking parameters: a two component vector $\mathbf{p}$ and two symmetric 2×2 matrices $\mathbf{M}_{nip}$ and $\mathbf{M}_n$ (Figure 2.4). Because the CRS operator can be derived by a Taylor expansion in midpoint and half-offset coordinates these stacking parameters represent first and second order travel time derivatives with respect to mid-point and half-offset coordinates. As long as the processing stays in time, no physical interpretation of the parameter is required. The CRS method and the stacking parameter estimation is an entirely data driven fitting approach where the optimization of the operator is performed with the coherence as objective function. The coherence measure used is the semblance.

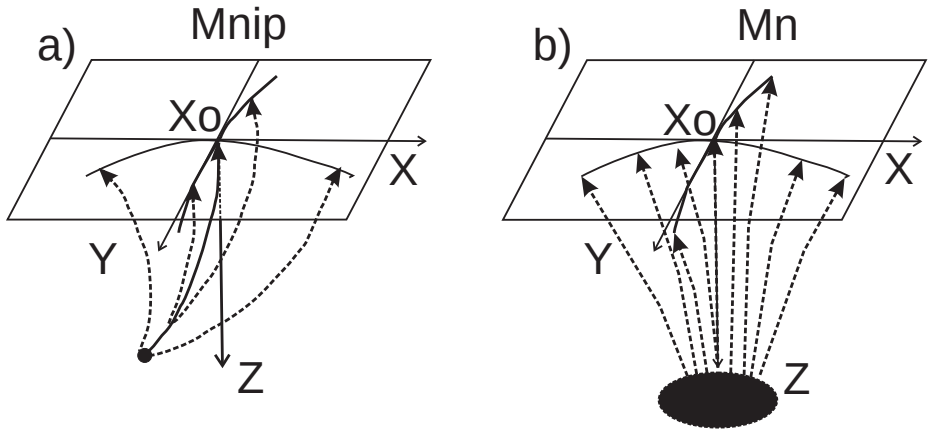

Figure 2.4.: (a) NIP wave and (b) N wave. The quantities $\mathbf{M}_{NIP}$ and $\mathbf{M}_N$ are related to wavefront curvatures associated with the hypothetical emerging NIP and normal waves at $\mathbf{X}_o$ on the measurement surface.

For the use of the attributes in processing and imaging a physical interpretation is available. If a locally constant near-surface velocity v_0 is known, the CRS operator can be written in a form which allows the interpretation of the stacking attributes as parameters describing two hypothetical emerging wave fronts at the considered surface location x_0. These are the so-called normal-incidence point (NIP) wave and the normal (N) wave (Hubral, 1983). The NIP wave would be observed at

x_0 if a point-source were placed at the NIP of the zero-offset ray on the reflector in the subsurface, while the N wave would be obtained if an exploding reflecting surface -the CRS- were placed around the NIP in the subsurface. Because of the link to wavefront curvatures the stacking parameters are also called kinematic wavefield attributes. I will use both terms synonymously. The relation of the stacking parameters to the kinematic wave-field attributes is given by the following relations:

$$\mathbf{p}_m = \frac{1}{v_0} \left(\cos\alpha \sin\beta, \sin\alpha \cos\beta\right)^T \tag{2.7}$$

$$\mathbf{M}_{nip} = \frac{1}{v_0} \mathbf{H}\mathbf{K}_{nip}\mathbf{H}^T \tag{2.8}$$

$$\mathbf{M}_n = \frac{1}{v_0} \mathbf{H}\mathbf{K}_n\mathbf{H}^T \tag{2.9}$$

where α is azimuth, β is dip angle and $\mathbf{H}$ is the 2×2 upper left sub matrix of the 3×3 transformation matrix from the wavefront coordinate system into the registration surface. p_m is the slowness vector. The 3D CRS stack is just one product of the method next to the simulated ZO section and a number of volumes containing the optimum kinematic wavefield attributes and coherence for each ZO sample.

Search strategy and aperture selection during 3D CRS processing

During the 3D CRS processing, the aperture selection is very important, as the proper aperture setting is very crucial to get the reliable image of the subsurface. It has been observed that the validity of the determination of the proper parameter search decreases with increasing the value of aperture distance in midpoint and offset directions. Appropriate choices of parameters (especially apertures) are necessary to estimate reliable attributes. If the apertures are too large the hyperbolic assumption is no longer valid. Small apertures lead to a declined quality of the CRS attributes because of decreased sensitivity. The apertures for the parameter searches can be chosen separately in individual steps. Depending upon the expected subsurface structure, larger apertures may improve the results of the CRS attributes, while smaller apertures can help to avoid smearing effects by stacking (Baykulov, 2009). The 3D CRS attributes can be updated by an optimization. Pragmatic approach is the option for optimizing the attributes. Simulated annealing is the best suitable technique used for solving the optimization problems where the desired goal is hidden among poor, local extrema (Müller, 2003). The implementation of the simulated annealing used in the 3D CRS optimization is the modification of downhill simplex or

amoeba method or Nelder–Mead method or flexible polyhedron search (Nelder and Mead, 1965) which is designed to find local minimum. The simplex is the polyhedron comprising N+1 vertices in the N-dimensional search space. In case of 2D, it is a triangle and in 3D it is tetrahedron. The search must start from N+1 points defining the simplex. At each vertex, the objective function (here coherence) is evaluated and depending on the value of this simplex, it takes the steps for alteration of shape, size and orientation of simplex, moving towards the local minimum in N-dimensional search space. The improved searched values are replaced by the old values updating with the highest objective function when the criteria is reached for optimal value of coherence. Usually this is an expensive computational process, therefore it was not used in the frame of this work. If the CRS parameters are chosen carefully and fit the curves best, then the optimized results are similar to the non-optimized CRS parameters.
Since the stack provides an image of the subsurface which does not resemble the exact geological dips and structures further processing like migration is required.

2.5. Seismic Migration

Migration is a step in seismic processing where the recorded seismic signals are moved to their correct position in time or space. Migration moves a dipping reflector to its true subsurface position and collapses the diffracted energy, which results in an increase in spatial resolution and provides a more realistic subsurface image. The main purpose of the migration is to stack the data according to the subsurface geologic cross-section either in time or in depth along the seismic traverse or volume. Mostly, the migrated seismic section is displayed in time because correct depth requires an accurate velocity model, which is not always available. The other reason is that it is easy to compare the stacked and time migrated sections before and after migration and it is easy for interpreters to better judge about the subsurface structure through the seismic section. In case of poor information of sub-surface velocities, it is preferred to keep both sections in time to get better comparison.

The migration which gives the output seismic section in time is known as *time migration* as in Figure 2.5. This figure gives the general conceptual idea of how migration works, and how the events are moved during migration. It is always important to have a clear strategy before applying migration. For every type of data and subsurface, there are different migration tools, and different migration algorithm works better for different types of subsurface structures. A strategy for migration also includes the choice of prestack versus poststack migration or time versus depth migration. Also, there should be appropriate parameters for migration

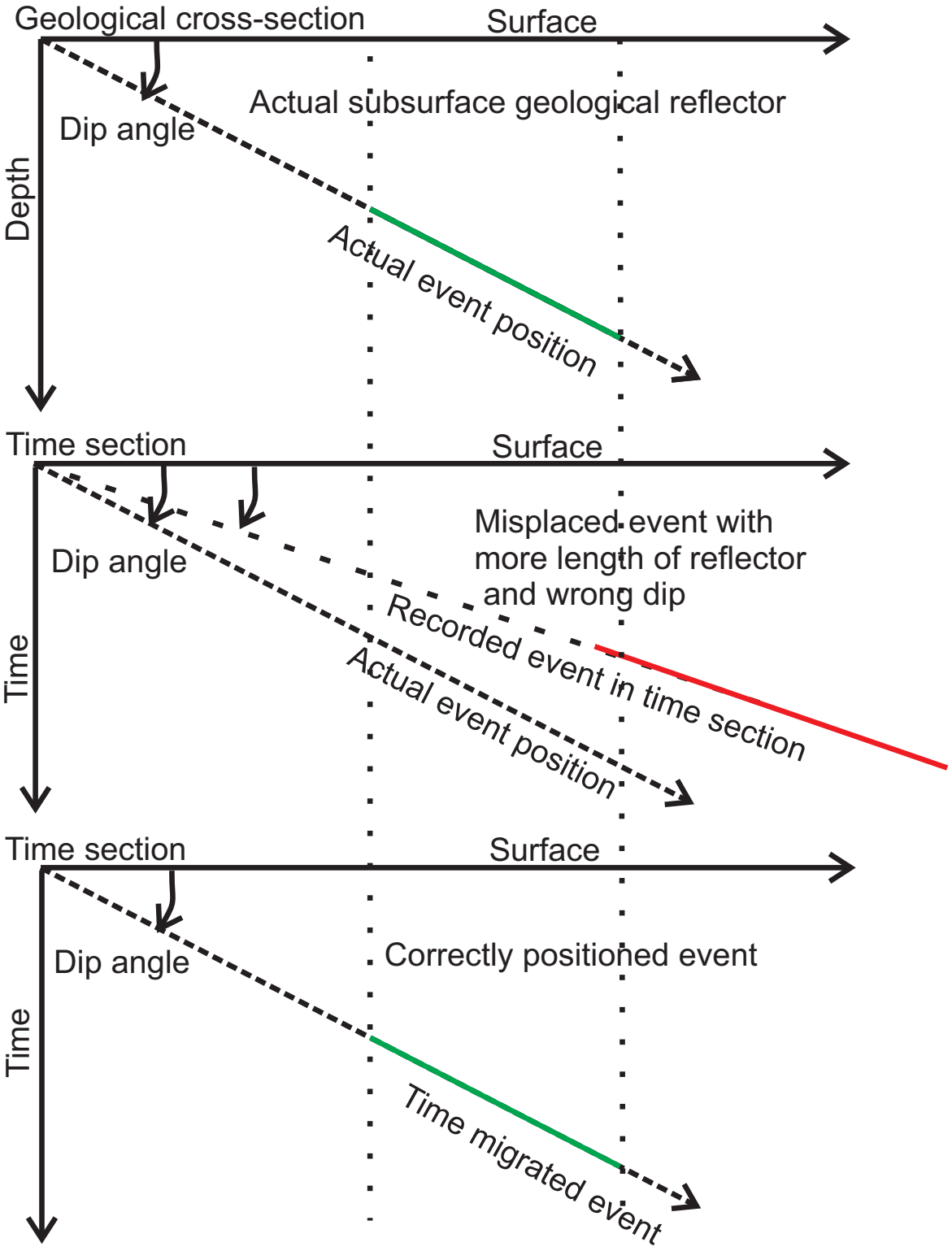

Figure 2.5.: Time migration principle, (1) the upper part shows the normal geological event position (as cross-section) where it is in the subsurface, (2) middle part shows event position (displaced) in seismic acquisition (before migration), and (3) lower part is the time migrated event to its correct geological position.

algorithm to work properly. Another important factor in migration is the migration velocity model which should be accurate. If the velocity function has errors, it could lead to wrong placement of the events and could end up in a mis-migrated seismic sections or volumes. Suppose if there is an error of 20% in the velocities, then the event may be misplaced by the error of 44% (Yilmaz, 2001) like shown in Figure 2.5.

Migration results in :

* moving the dipping events to updip,
* focusing diffractions from faults, pinch-outs, edges and discontinued reflectors,
* removes the effects of reflector curvature such as increased anticlines, decreased synclines and "bow-ties" (triplication) (Stolt, 2002).

Migration Algorithms

Migration algorithms are mostly based on the scalar wave equation which are common in use. These algorithms handle the reflections and multiples as seismic signals. Any such kind of energy like noise, surface waves, and multiples are considered as the primary reflections. Migration algorithms are considered into certain categories which are based on:

* integral solution to scalar wave equation,
* frequency-wave number representation,
* finite difference solution.

But, no matter which migration algorithm is used for data from hardrock environments, it should fulfill the criteria:

* handle the steep dipping events accurately,
* be able to handle the lateral and vertical velocity variations,
* should be robust and efficient,

∗ should be easy to implement.

There were three main era's in the history of seismic migration. First, in historical time before computer age, the first technique was developed which is known to be semicircle superposition method. Then there was a development of other technique known to be the diffraction-summation technique. The migration which moves dipping events by summation of diffractions is well known as Kirchhoff Migration. Kirchhoff Migration is the most flexible migration algorithm and can be easily implemented and used in 2D and 3D, prestack and poststack and as a time or depth migration. Kirchhoff migration can also be implemented and used to migrate shear and converted waves, apply a dip filter, interpolate the input data and cope with spatially aliased data. Kirchoff migration is commonly used. Kirchoff summation was introduced by Schneider (1978), which was already in use before, during the times of diffraction summation technique with added amplitude and phase corrections applied to the data before summation (Yilmaz, 2001).

Another migration technique for zero offset data (Claerbout and Doherty, 1972) is based on the idea that a stacked section can be modeled as an upcoming zero-offset wavefield which is generated by the exploding reflector. By use of this model of exploding reflector, the migration concept is considered to be the wavefield extrapolation in the form of downward continuation followed by imaging. Downward continuation of wavefield can be used conveniently using the finite difference solutions to the scalar wave equation. The migration which is implemented based on such type of solutions is known to be the finite-difference migration (Claerbout, 1985).

(Stolt, 1978) introduced another method of migration which is based on the Fourier transform. This method involves the coordinate transformation from frequency to vertical wavenumber axis while keeping the horizontal wavenumber unaltered. Later Stolt and Benson (1986) gave practical implementations together with theoretical lessons in field of migration with emphasis on frequency wavenumber methods.

One more way to express the frequency-wavenumber migration is the phase-shift method which is purely based on downward continuation to a phase shift in frequency-wavenumber domain (Gazdag, 1978).

Out of all of the migration algorithms, none of them meets the criteria which fully cover the problems of the industry in migrating the data. So, the industry has to depend on different algorithms according to their needs and requirement in

handling their problems to resolve. Like one algorithm which is based on integral solution of scalar wave equation which is known to be the Kirchoff time migration. This is able to handle the steep dips up to 90° angle.

Other algorithm known as finite-difference time migration algorithms can handle all types of the velocity variations. But they have a certain limit in handling the degree of steepness of the dip of a seismic reflector.

In the end, the frequency-wavenumber algorithms have limited ability in dealing with the velocity variation especially in lateral extent. So, as a result, none of the migration algorithm in particular is able to cope with all types of problems.

Reverse time migration (RTM) (Levin, 1984) propagates the source wavefield through the model and back-propagates the measured receiver wavefield as a new source wavefield. In most of the cases, the ability to make use of these complex wave field models allow imaging of events of the subsurface that otherwise have poor direct illumination. This migration is the most expensive method of all other migration algorithms but provides superior images.

Migration parameters

After the decision of migration algorithm to be used, the geophysicist need to set the appropriate parameters for the correct migration, like the Kirchoff migration. A proper aperture size matters a lot. If the aperture is smaller, then it can result in the removal of steep dips in output migrated seismic sections. Also smaller aperture create the undesired horizontal events with the random noise in migrated seismic section.

In downward continuation migration algorithm, the depth step size is an important parameter in finite difference methods. Its setting is dependent on the dip, velocity, spatial and temporal sampling and frequency in the wave field.

In Stolt or phase shift migration, the stretch factor is important. If the velocity is constant, then the stretch factor is considered to be 1. In general, the larger the vertical velocity gradient, the smaller the stretch factor is needed.

Requirement for the data

For migration input section, there are requirements depending upon the desires by the interpreters. Various aspects include :

* length of seismic line or volume of seismic line,

* signal-to-noise ratio (S/N) of input,

* spatial aliasing,

If the subsurface contains steep dipping reflectors, then the line length must be long enough to let the steep dipping event to migrate to its actual true subsurface position. If the recording length is short, then it will lead to erroneous migrated results. In case of 3D, the surface area in x,y direction should be larger then the target depth of the subsurface structure (Yilmaz, 2001).

Migration velocities are very important as well as the aperture size. As the velocity increases with increasing depth, the deeper parts are more likely to be error prone then shallow parts. Another important point is that, the steeper the event, more appropriate migration velocities are needed to migrate that event, as the migration displacement is proportional to the dip of the event.

Theoretically the diffractions extend to infinite time and space. In practice, it is different and the amplitude is finite and the aperture is chosen over which the summation is done. The aperture may be measured in distance or traces and should be large enough to include the largest lateral movement from the highest velocity and steepest dip in the section. Insufficient aperture will cause dip limitation. Too wide aperture may slightly increase run time and may introduce noise. If the stationary point is known the optimal aperture is the size of the first Fresnel zone.

Kirchoff time migration can handle steep dipping events. The events with dip up-to 90° is also possible to migrate. In special cases, in Kirchoff depth migration, even the option of turning rays is possible to incorporate for migration.

The 3D Kirchoff time migration is used to migrate the 3D seismic data from Schneeberg crystalline rock environment. The main reason of choosing this migration is that, this can handle most of the problems in migrating such dataset. However, there was no proper migration velocity model available for migrating this

dataset and this algorithm can handle the migration with constant velocity when there is are lateral velocity variations. This tool is not as expansive as RTM and gives the reasonable migrated output.

Since CRS processing is heavy in computing times some optimizations were introduced into the computer code. This is discussed in the next section.

3. Optimizing by hybrid MPI and OpenMP

3.1. Why Optimization?

3D CRS processing has many problems in terms of efficiency. It is expansive when 8-parameters search is performed. The code used in this work was initially written by (Müller, 2003). This code, however, was not suited to handle the big data volume. This is because of the reason that it is not well written for efficient performance and better memory usage. These all together make the data handling and processing difficult for seismic data processor. To resolve this issue, it was an experimental trial to optimize the code to make it run faster for processing big dataset. To implement this optimization, concurrent programming and hybrid (MPI + OpenMP) was introduced in the code where it is necessary. The most cost effective routine in the code is semblance search routine, which is utilizing more then 90% of the CPU time. The concurrent programming routines were applied at some routines to the data input and output and the hybrid optimization approach to the semblance search.

3.2. Concurrent programming

Concurrency is the property of the system in which two or more processes are occurring simultaneously, interacting with each other. In terms of computers, it means different independent activities are performing on a single system simultaneously instead of sequentially or one after each another. In the past, there were computer systems which only had a single core or processor which only allows a single task to be performed. Now-a-days, most of the systems are equipped with multi-processors, i.e., they have more then one CPU and can perform more then one task at the same time. Such type of machines are able to perform multiple tasks simultaneously on different cores. The procedure which handles different tasks is known as task-switching. Performing more then one task on these processors is

called multi-tasking.

Computers with multiple processors have been used as servers and clusters for high performance computing (HPC) tasks for a number of years. These machines have multiple cores on chips which are used in multi-tasking. Such like (multi-cores) more then one core on the single chip is also becoming common in small machines and desktops these days. Whether the machine has multiple processors or multiple cores on single processor (or both), such machines are capable of running multiple tasks in parallel. This type of concurrency is known to be hardware concurrency.

In computer machines, a thread is the smallest executable programmed instruction which can be performed independently on the operating system scheduler according to the programmed task. Figure 3.1 shows two types of tasks on different hardware to explain concurrency. One part (a) describes the concurrency in single core and (b) describes multiple tasks on multiple cores. On single core machine, task switching is done and chunks from different tasks are interleaved. On a dual core machine or with more cores/CPUs, each task can be executed on its own core. Although the availability of the concurrency in the hardware is obvious with multi-core systems, these days, some processors are available which can execute multiple threads on a single core. This is important to consider those hardware based threads which can measure how many tasks can be executed in parallel with the hardware. Task switching in this case is also easy, but parallel execution is more robust and efficient (Williams, 2012). In workstations and desktops or laptops with single cores, there are several tasks running even when the machine idles. This is because of the task switching.

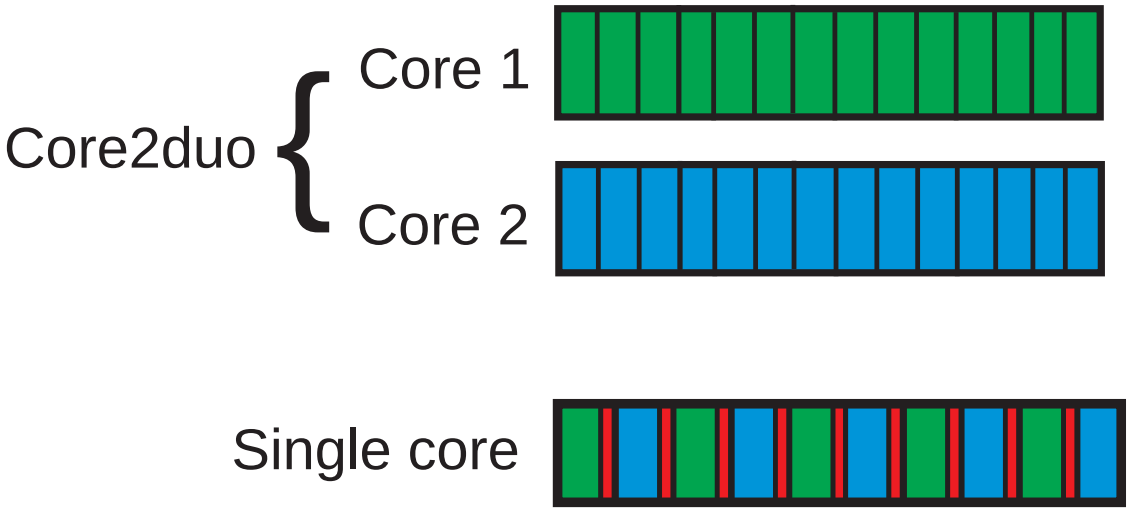

Figure 3.1.: Multi-tasking on single core and dual core machine.

Concurrency with multiple processes

Before going into the concurrency of programming, the most important point is to evaluate the program and try to identify which parts need the concurrency (if the program is already available). Then one has to analyse which parts of the program can be parallelized and which need task switching. This makes easier to move towards the solution to the problem of writing a concurrent program. The first way to make the program concurrent is to divide it into separate multiple single threaded processes that are executing and running concurrently at the same time. These threads could communicate with each other and with the main thread of the program. There is one weak point in this threading that they can execute simultaneously and interfere each other if not well programmed. This can make the process slow or even can halt the machine.

Concurrency for performance

Machines with multiple cores are existing for many decades, but in that time, they were available only in supercomputers, mainframes and large server systems. These days, 2, 4, 8 and 16 cores processors are easily available on a single chip and manufacturers are improving performance daily. As a result, multi-core systems are available as desktops, laptops and other small machines having a single chip with multiple processors, which are able to execute multiple tasks in parallel. If a code needs to take advantage of this multiple cores processors, they have to execute the tasks in parallel concurrently. There are two different ways to achieve concurrency. One is to divide the task into small parts and run those in parallel. This is known as task parallelism. It is quite complex and tricky. Different factors are kept into consideration while dividing the tasks into parallel threads. There is another way in which the code performs the same work on different parts of the data. This is known as data parallelism. The codes which are able to perform such tasks of parallelism are called parallel tasks.

Concurrency in coding

In order to get the code optimized and concurrent, programmers should have the complete knowledge of code. Be aware of the parts of the code which have to be parallelized and which should not. In some cases, its simple but sometimes, it is complex to dicide which parts should be parallelized. If the complexity in programming is high, it may end in bugs or hangups of the machines. Mostly concurrent code is not easy to understand and to deal with. Sometimes, its cost to

convert from sequential to parallelized code and to run the code exceeds then the performance increment of output. The performance may not be as efficient according to expectations. One of the reason is that the task run generates too many threads, then it consumes the resources of machines and can result in making the whole system to process slower. This can exhaust the available memory and space for the process because threads require certain space for execution and communication.

The use of concurrency for performance is just like any other optimization strategy, where it has great potential to improve the performance of the code/application. On the other hand, if it is done wrong, it can lead to the complication of code which is harder to understand and the chances of bugs increase depending upon the code complexity. Therefore, it is only worth-wile when applied to the critical parts of the code for performance gains which need to be designed to optimize.

3.3. Concurrency and threading in C++

In 1998, the C++ standard does not acknowledge the thread's existence. So, it was not possible to make any thread execution in that compiler until 2000. Now, C++ standard is fully equipped with the thread generating libraries as well as memory models on which the threads are dependent. Supporting concurrent programming is one of the changes C++ compiler has in it new standards. There are different types of compiler these days which are advanced and can deal with the parallel tasking better.

A *compiler* is a computer program (or set of programs) that transforms source code written in a programming language (either C/C++, Matlab, Java, Fortran, or any other etc) into binary language which is machine readable to make the source code executable. When running the compiler for building the executable, the compiler first parses (or analyzes) all of the language statements syntactically and critically one after the other and then, in one or more successive stages or "passes", builds the output code, making sure that statements that refer to other statements are referred to correctly in the final code. The output code is the object code which is executable. The object code is machine code (binary language converted which can understand the code in terms of machine language) that the processor can process or "execute" one instruction of code at a time.

Efficiency in C++ threaded library

One of the important aspect for developers is that C++ libraries provide facilities of performance based efficiency of programing routines. It gives reasonably comprehensive facilities for concurrency and multi threading. Every given platform has its specific routines to go beyond those for implementation. It is necessary to understand what the standard libraries provides with its facilities.

For the simple case, how to generate a simple thread with a small program example, lets have a look at the simple code written below, which shows how to incorporate the threading in simple programs. Below is one example in which the idea is given how to include the thread library in a simple code. As normal routine programs, its included in header. The program shows how to generate a single thread in simple program. The program shows that there are thread libraries in C++ compilers which if we include library in our program and then we can assign the task to generate threads at certain level, and then they can perform multi-tasking.

```
#include <iostream>
#include <thread>
void crs()
{
  std::cout<<"CRS Express\n";
}
int main()
{
  std::thread t(crs);
  t.join();
}
```

3.4. Thread Management

In concurrent programming, threads will be used to make the code working with an optimal performance. So, the first point is how to generate the thread. This can be perform easily in C++ with its standard library like below given when including in the header of a standard program:

```
#include <thread>
```

This will make the program able to incorporate the threads if inside the threads "call" is implemented. The thread call is a trigger to generate thread by calling it while executing program.

Basic thread management

Generally every C++ program is running on at least a single thread which performs its task, and which is started by standard C++ run-time : main(). But the program can generate threads in addition to this. This thread can run concurrently with the main thread. The program exits when it completes the task or the thread.

Launching thread

Threads are launched by constructing the "std::thread" object that defines a task to perform by thread. If the thread is simple, then it performs tasks easily and it does not need returning. But in complex programming, it also needs some additional routines and parameters. In the complex case, it has to perform certain different tasks independently through some communication system between the thread systems to perform a number of tasks assigned to threads. Once the thread is launched, it stops when it joins back or becomes single, or orders to stop. The C++ thread library boils down in construction of std::thread object:

```
void semblence_search()
std::thread my_thread(semblence_search);
```

For thread, it has to be decided in the start whether to wait for it to finish by joining, or to leave it to run on its on by detaching it. If one does not decide before the thread is destroyed, then the program terminates. It is of vital importance to ensure that the thread is joined or detached correctly. Another worth-wile point to note is, if the thread is not finished before it joins or detached, it runs for a long time after the object of the program is destroyed. If we don't wait for the thread to finish, then it should be ensured that the data accessed and processed by the thread is valid available unless the thread finishes the program and tasks to complete.

Multithreading in C++

There are two important components in parallel programming. One is Message Passing Interface (MPI) and other is OpenMP.

3.5. Message Passing Interface (MPI)

Message Passing Interface (MPI) is a standard portable communication system designed by researchers to apply for parallel tasks on a wide variety of computers. The first MPI standard was presented in "Supercomputing conference 93" in November 1993. It is a language independent communication protocol which is used to program parallel computing systems. The goal of MPI is to provide high performance computing (HPC) and concurrency. It is the most dominant platform used for high performance computing in super computers and clusters these days. MPI implementation comprises of different set of routines which can be directly called from C, C++, Fortran, and Matlab and certain other languages. It has been implemented for different memory architectures. Its implementations are optimized routines in different sets of hardware.

Working with MPI

The MPI interface is meant to provide a synchronized path and optimized communication between the set of processes, which are directed to nodes, clusters, servers or computers independent of the language in which the task is programmed. Optimally for high performance, while using MPI, every single core or node should be assigned different independent tasks. For MPI tasks to be performed in a code, a library known as "mpi.h" needs to be included in the header when MPI routines are called in the program. MPI multi threading follows the distributed memory architecture as shown in Figure 3.2. The figure illustrates the general idea of the distributed memory architecture in which each CPU or node is assigned the specific amount of memory known to be RAM which is used during the multi-tasking. The data processed by each CPU is dealed on its specific assigned memory part. Each CPU or node is connected with separate physical memory where the data comes and tasks are performed. *Node* is the group of different CPUs e.g., 8/16/32.

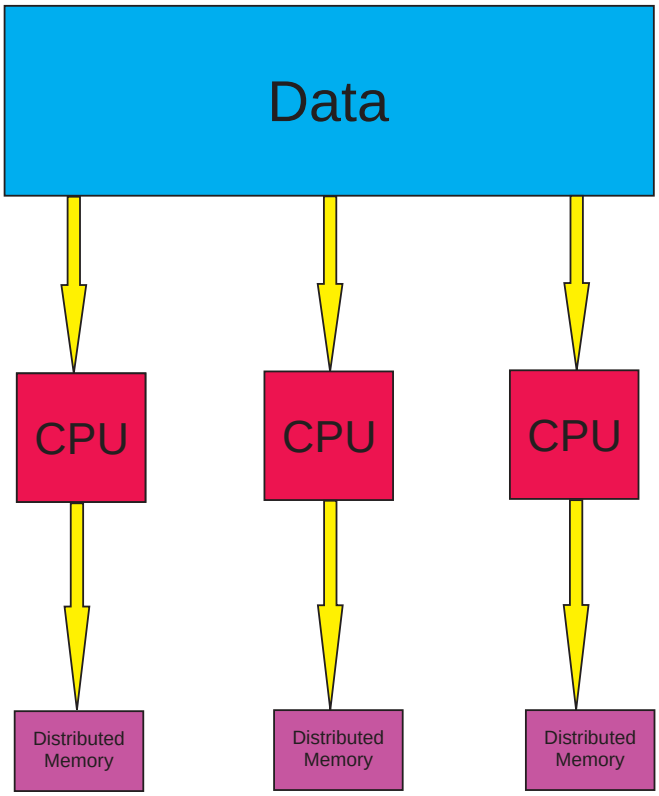

Figure 3.2.: Distributed memory architecture of machine.

MPICC compiler

mpicc is a program which helps the programmer to use a standard C/C++ programming compiler together with Message Pass Interface (MPI) libraries.

3.6. Open Multi-Processing (OpenMP)

OpenMP (Open Multi-Processing) is an application program interface (API) that is developed to support shared memory architecture for parallel programming. It supports different platforms in shared memory environment based on multi-processing programming in different languages like C/C++ Fortran, Matlab etc on variety of architectures of computational units. OpenMP is a portable synchronized model that gives the programmer an ideal environment for developing the applications for different routines from normal desktops, laptops to rack servers, clusters and clouds. The aim of OpenMP is to provide parallel applications of many disciplines in an easy way.

The thread is a run-time entity that is able to execute independently a stream of tasks. OpenMP is a platform that provides the opportunity to generate multiple threads from an existing main thread. It is a method of parallelizing with multi-threading where the master thread (main thread) forks out into different slave threads in a parallel fashion as given in Figure 3.3. The figure shows the shared memory architecture, in which all the CPUs or nodes are connected to a single shared memory. So, while performing the tasks, the CPU brings data to a shared memory platform where all other also performs tasks at the same shared memory.

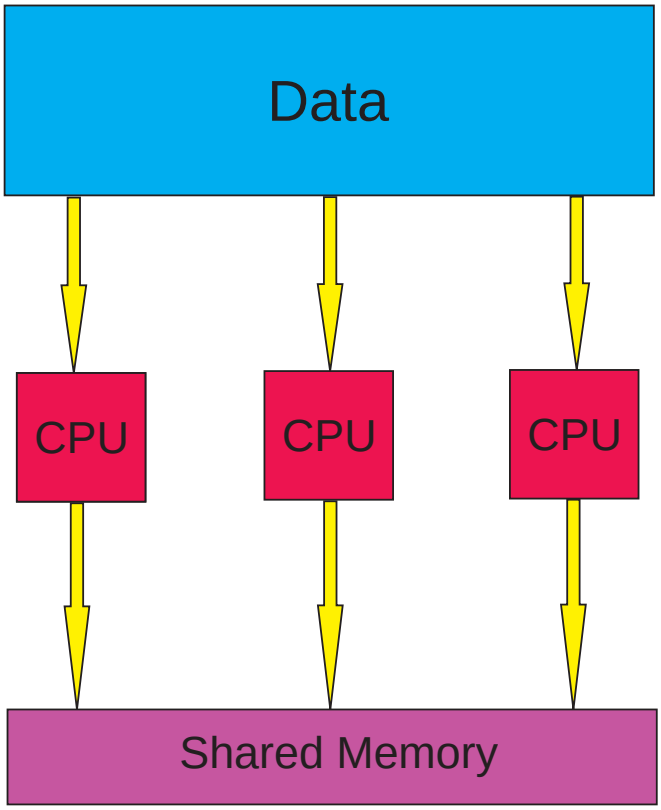

Figure 3.3.: Shared memory architecture of machine.

Fork-join model of OpenMP

In the OpenMP environment, multi-threading can be executed simultaneously on an individual single core or single processor. It is portable in use and provides the opportunity to the programmer to avoid the number of potential programming errors while making it executable for multi-tasking. It follows the Fork-Join model which is also seen in Figure 3.4. Under the umbrella of this OpenMP, the program starts with a thread known as master thread or initial thread. When OpenMP parallel construct is encountered by a thread while executing the program, it generates a

series of threads, concurrently, called as "fork". This becomes the master of the threads and collaborates with other thread members with coordination. At the end of the program, the full stream of threads join with the original or master thread of the team. All members of the threads terminate at the single main thread which is the master thread, and this is known as 'join' as shown in figure.

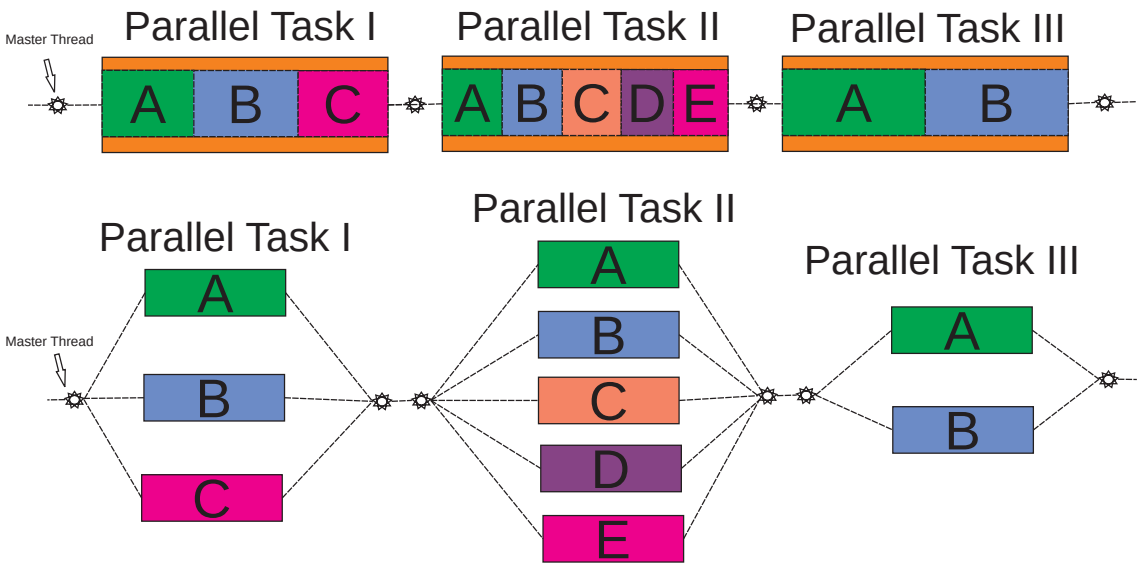

Figure 3.4.: Generation of threads with OpenMP.

Working with OpenMP

It is not difficult to parallelize an application with OpenMP. The impact of this optimization is localized on small portion of the program in a way that modification in original program is only needed in few places. The main advantage of parallelization of the source code with OpenMP is that the original sequence of the program is preserved. In order to work with OpenMP threads in a code, there is special library 'omp.h' which is called in the header of the program. This is called in any program as given below.

```
#ifdef _OPENMP
#include <omp.h>
```

In C/C++, the pragma are provided with OpenMP application program interface (API) to control the parallelizm. A *pragma* (pragmatic information) is the standard comment style which has a specific meaning to the compiler or to some program. In computer programming, a directive pragma (from "pragmatic") is a language

construct that specifies how a compiler (or assembler or interpreter) should process its input. Directives are not part of the language, they are not part of the grammar, and may vary from compiler to compiler, but instead function either as an in-band form of a command-line option, specifying compiler behaviour, or are processed by a preprocessor. In OpenMP, these (pragmas) are called compiler directives. They start with #pragma omp followed by the key to identify the directive. A large number of applications can be parallelized by using few compiler constructs or one or more functions like :

- Parallel construct
- Work-load sharing construct

These constructs decide what should be done by parallelization of task (Chapman et al., 2008). Suppose if a programmer has to generate some threads at some task inside the program, then the programmer has to instruct to initialize some parallel threads. It is not difficult to handle this situation, as a programmer can easily control the threading during programming. The threads depend on demand, either can be maximum possible, or one can define the number of threads to generate at the task level. For a small program it can be done like :

```
#pragma omp paralel
{
  printf("CRS_Express %d\n",
  omp_get_num_thread());
  }
} /* -- End of Parallel route --*/
```

The important point is that if the specific task in a code is executed in parallel fashion, then the parallel construct should be closed at the end when that task is completed.

3.7. Hybrid approach for optimizing common-reflection-surface-stack (3D CRS)

In a hybrid approach, OpenMP is used together with a MPI implementation to accelerate the processes. The accelerated version of the hybrid 3D CRS is named as *CRS express*.

The original 3D common-reflection-surface-stacking (CRS) code by Müller for 3D volumes takes a lot of time in processing. Almost 94 % of the time is consumed in calculating the semblance during the search process. The idea is to accelerate the computational process in terms of time with same available resources and with the same output. Addition of concurrent programming at some routines and OpenMP are incorporated in the MPI based 3D CRS code. This optimization is done in some routines without changing the actual structure of the code. At some parts, parallel threads have been generated to optimize the tasking in parallel fashion. This is an easy task to implement. The process is robust and works better while utilizing all available resources of the machine. It is more efficient in the shared memory architecture compared to parallel memory based units. Some initial tests show that, the processing is 10 times faster then the original 3D CRS code in terms of efficiency. The observed progress is shown in Figure 3.5. In ideal conditions, when libraries are more suited for compiling the program, the code works even more than ten times faster then the original version as shown in the graph.

Test analysis of hybrid implementation

In order to check whether this implementation is successful and perfectly working for the seismic data processing, some initial tests have been performed on synthetic data set. For this, 2D Sigsbee 2A seismic data has been used to compare results of the original code with the hybrid CRS express code. In this test, not only the time comparison has been checked, also the quality of the output of the seismic dataset has been observed in detail.

3.8. Practical application (Synthetic data example)

For analysis of the hybrid CRS, different tests have been performed first on synthetic dataset. For this purpose, 2D Sigsbee 2A has been used to check the reliability of the performance of the code and the quality of the output.

Sigsbee 2A is a synthetic 2D dataset consisting of a single seismic profile. This is a marine dataset with a complex sub-surface salt body and some diffractions. For comparison, this dataset is also reliable to investigate the reflections and diffractions response. Although this is a 2D dataset, the code can handle both types of dataset (2D and 3D) for processing. The main reason of testing the hybrid 3D CRS code

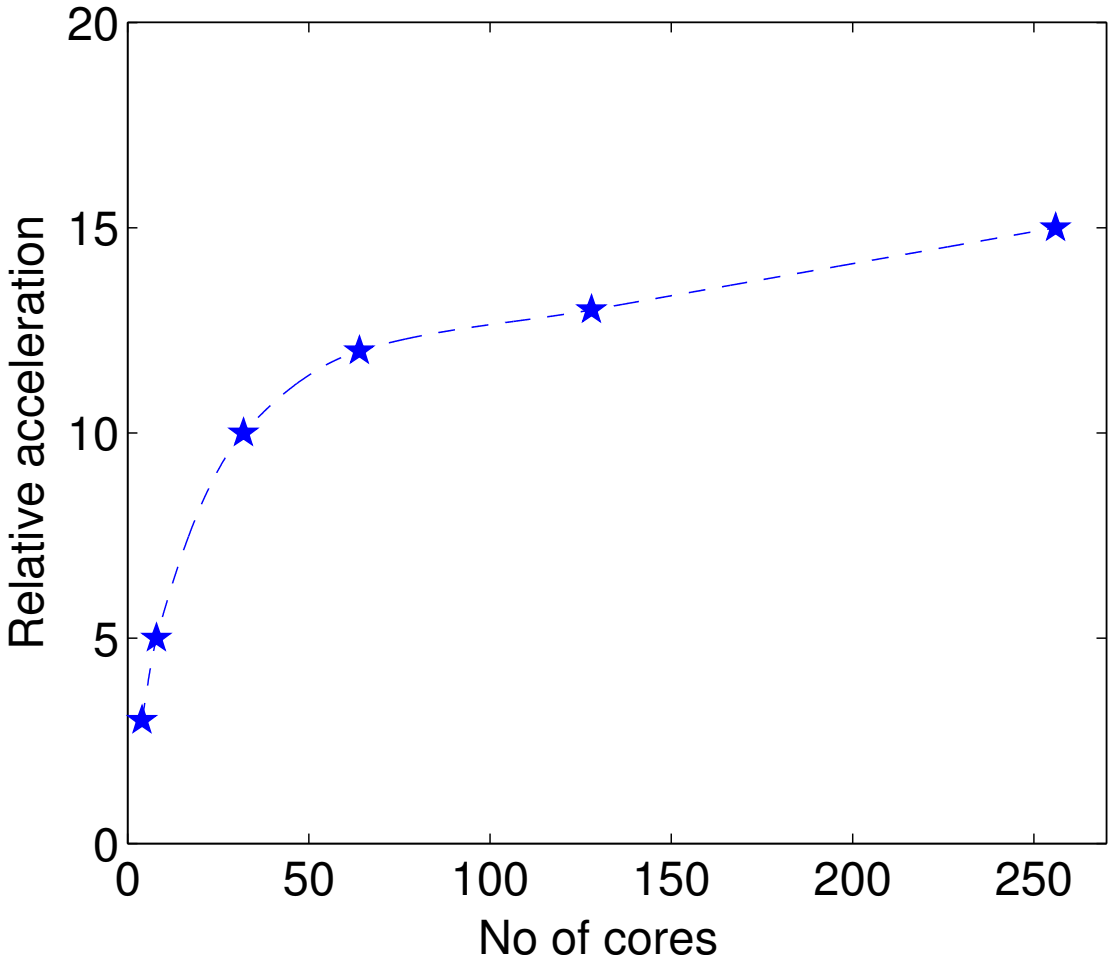

Figure 3.5.: Graph showing the 3D CRS (express) processing with time. (relative acceleration of the hybridized MPI+OpenMP 3D CRS implementation as a function of number of cores)

on Sigsbee 2A dataset is that, this is a well known dataset and if there is any flaw or defect in the output, then it could be easily detected.

For test analysis, the complete procedure of CRS stacking was performed with the CRS express code to check the attribute calculations and parameter estimations, and to test whether it works similar to the original code. Both codes are tested on the same machine, on the same dataset, on same the number of cores with the same parameters. The process of CRS is performed in sequence. The resulting output shows that the attributes computed by the hybrid code are the same as the attributes computed with the original code. The resulting cpu time is at least 10 times faster then that of the original code.

If we compare the CMP stack of the original code with the hybrid code, we cannot distinguish noticeable difference in the output in Figure 3.6 and Figure 3.7 . The most important point is to have a similar output of the attributes. So, while comparing the difference between the output of the original and hybrid CRS code, a closer look is done for different attributes. Starting from the Figure 3.8 and Figure 3.9 which show the radius of curvature of normal incidence point wave. Both in this plan shown the same output result. The other main attribute is the angle which is in Figure 3.10 and Figure 3.11. Here in these two figures, we see that there is no difference at all in terms of reflections and diffractions. Similar conclusions apply for other attributes like curvature of normal wave in Figure 3.12 and Figure 3.13.

One of the outputs provided by this code is the coherence which is an important ingredient of the CRS workflow. If we compare the coherence of the original code in Figure 3.14 versus the (later used) hybrid optimized code in Figure 3.15, then both are same and there is no difference in the output section of either of them.

The last comparison is in the final output the CRS stacked section. Figure 3.16 and Figure 3.17 gives a clear indication that both results look similar. So, this means that the output of the CRS stack with its attributes is same in the hybrid optimized output compared to the original code. Direct comparison of the results of output from both codes (original and hybrid) show very little or almost negligible difference in output.

3.9. Discussion and conclusion

In this hybrid optimization, the important target was to accelerate the code in order to be able to work on a bigger scale. The whole effort to work on the acceleration is to optimize the code so that it should be able to deal with the industrial scale dataset in an academic environment on the small computers. The results in output shows that the optimized output is not only similar compared to the original code, but its computational cost is 10 times less. For big Tera-byte dataset, this effort helps to get the results by saving several days of CPU time.

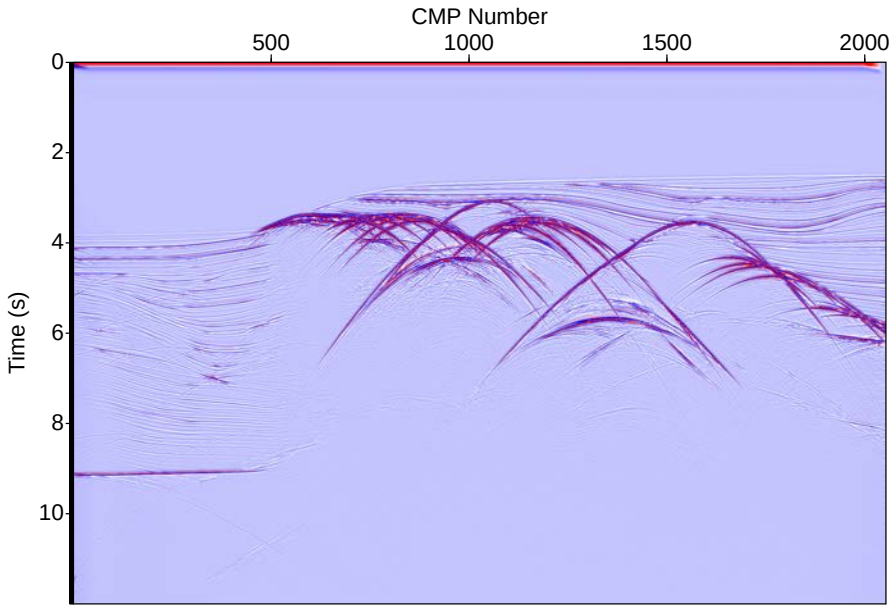

Figure 3.6.: CMP stack section of original CRS code.

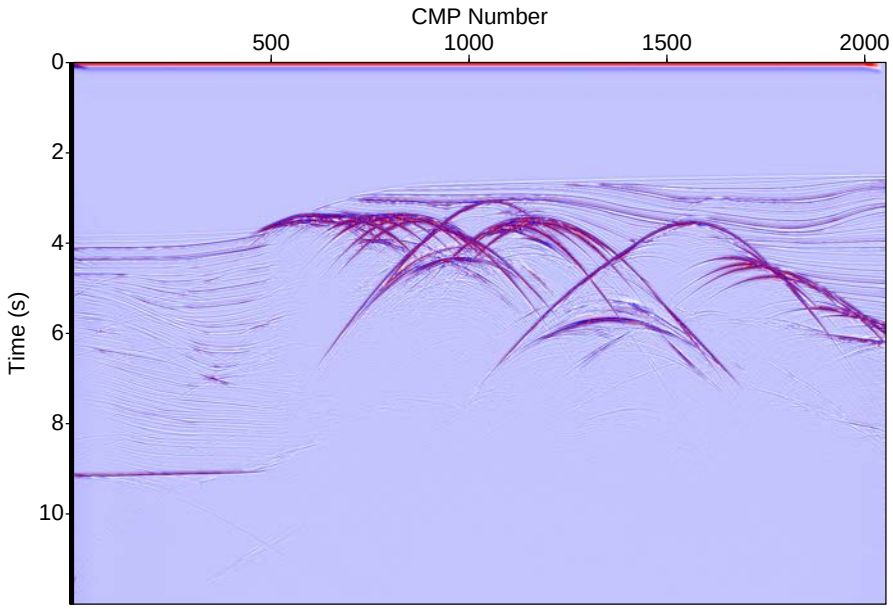

Figure 3.7.: CMP stack section of hybrid CRS code.

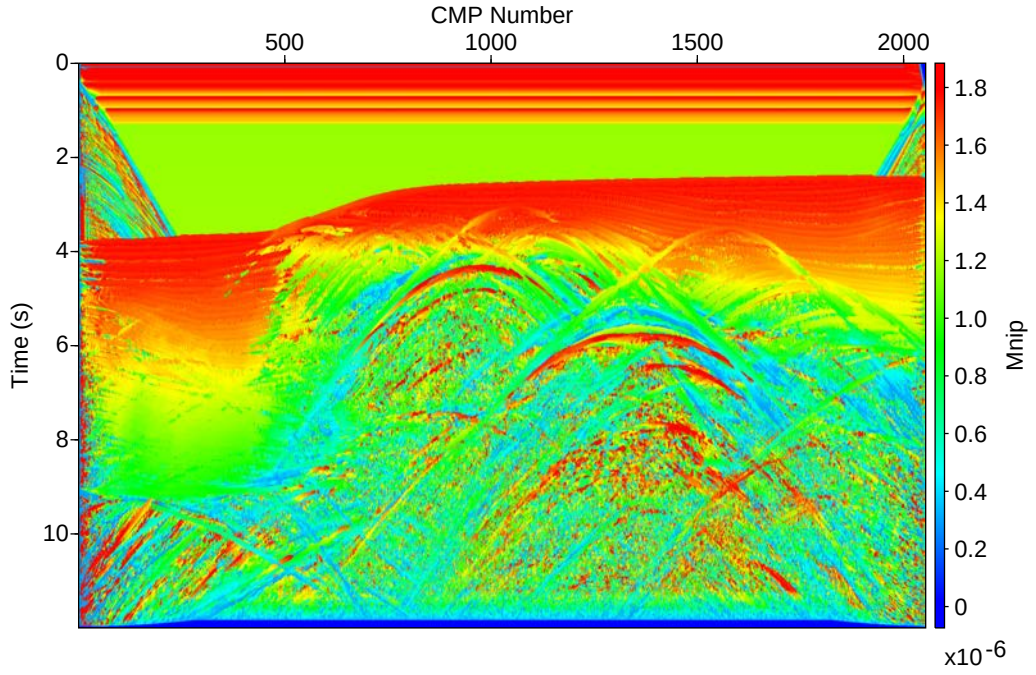

Figure 3.8.: NIP wave radius determined by the original CRS code.

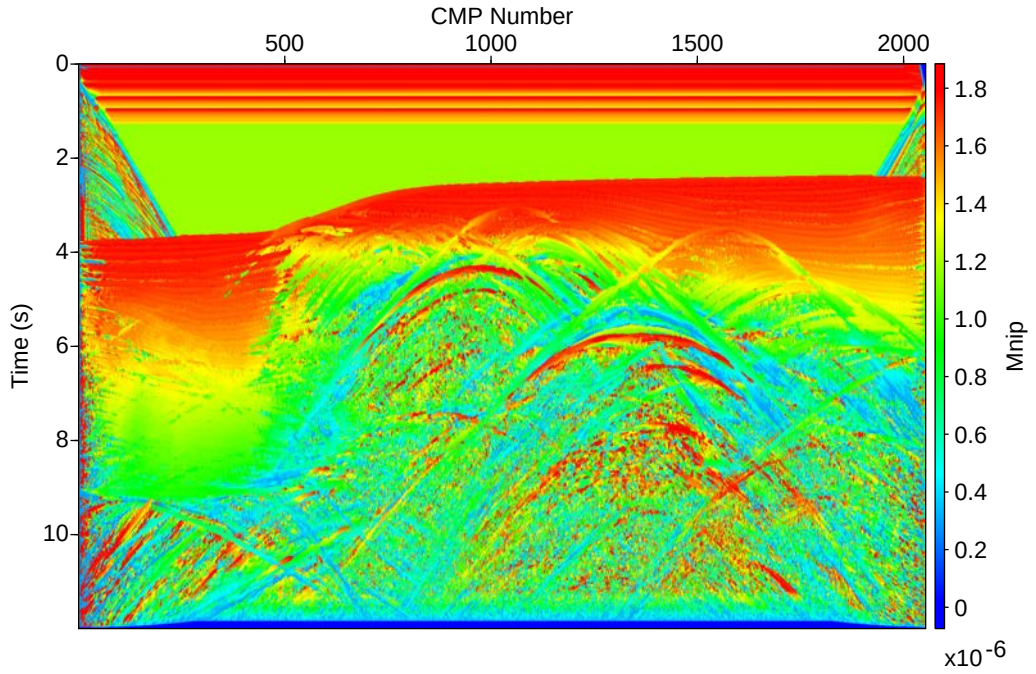

Figure 3.9.: NIP wave radius determined by the hybrid CRS code.

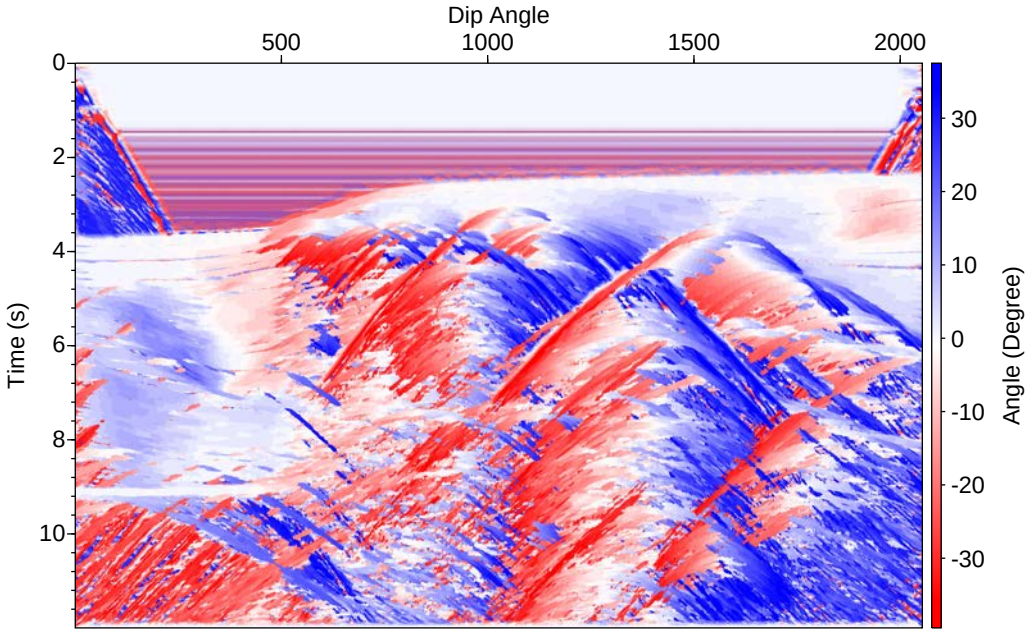

Figure 3.10.: Angle α determined by the original CRS code.

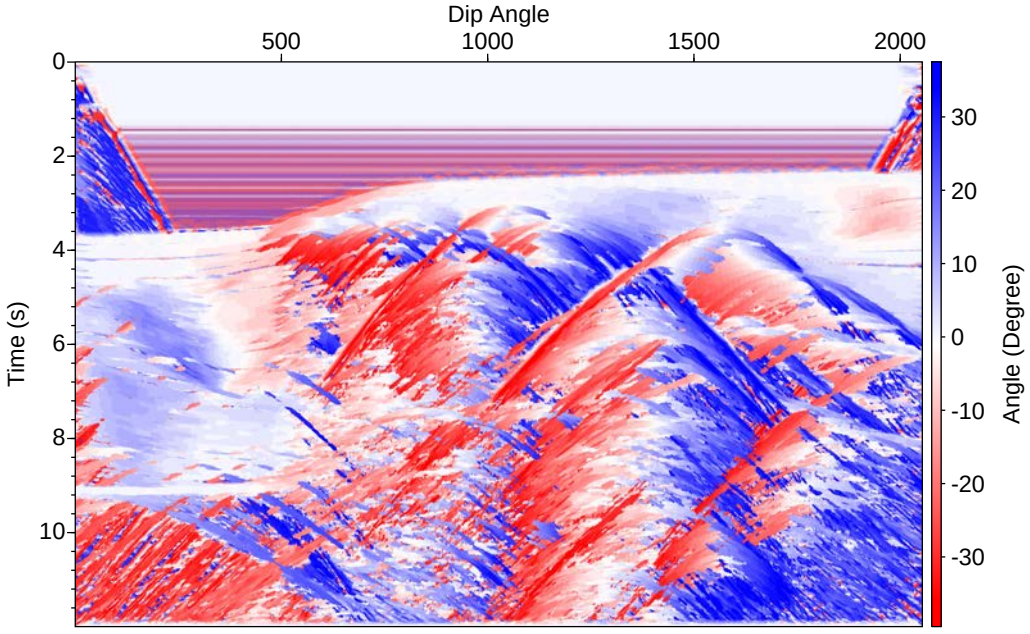

Figure 3.11.: Angle α determined by the hybrid CRS code.

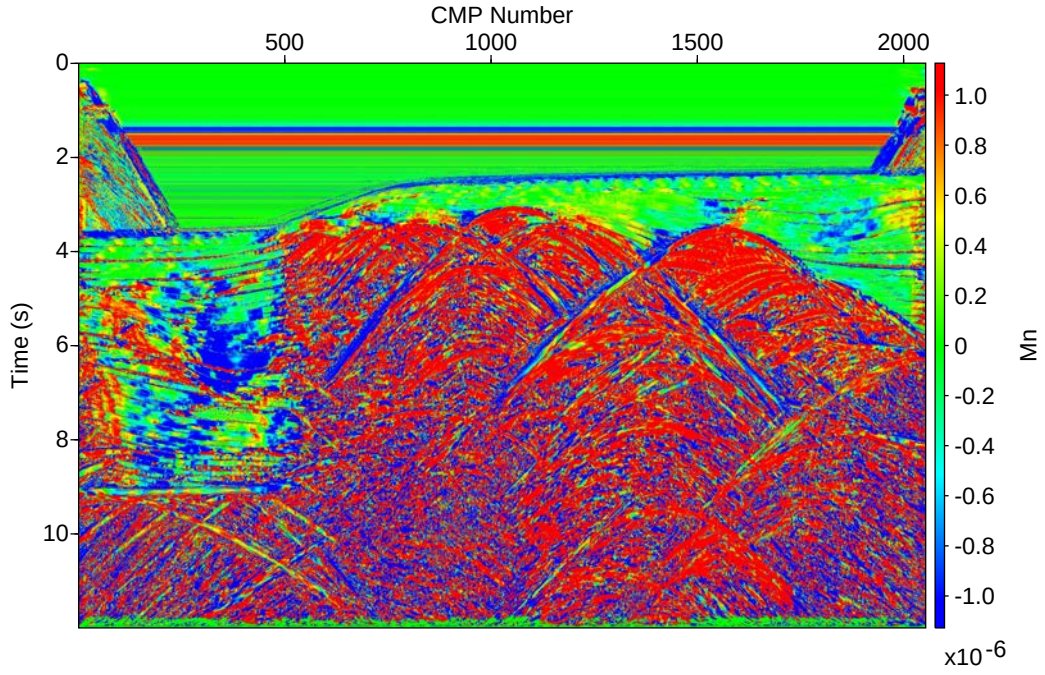

Figure 3.12.: N wave curvature determined by the original CRS code.

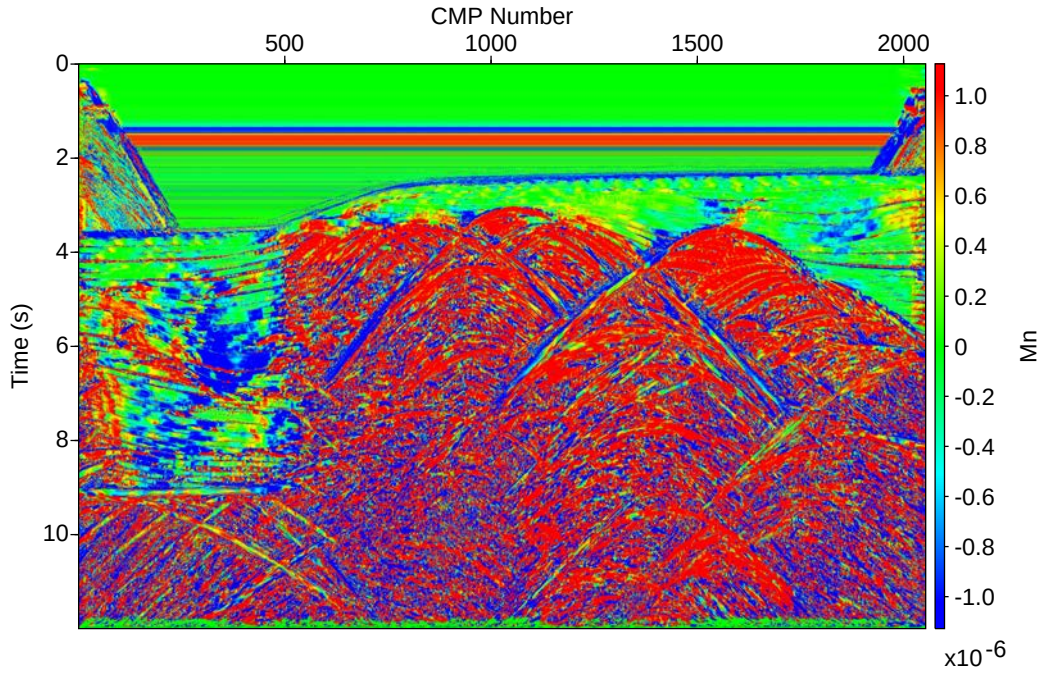

Figure 3.13.: N wave curvature determined by the hybrid CRS code.

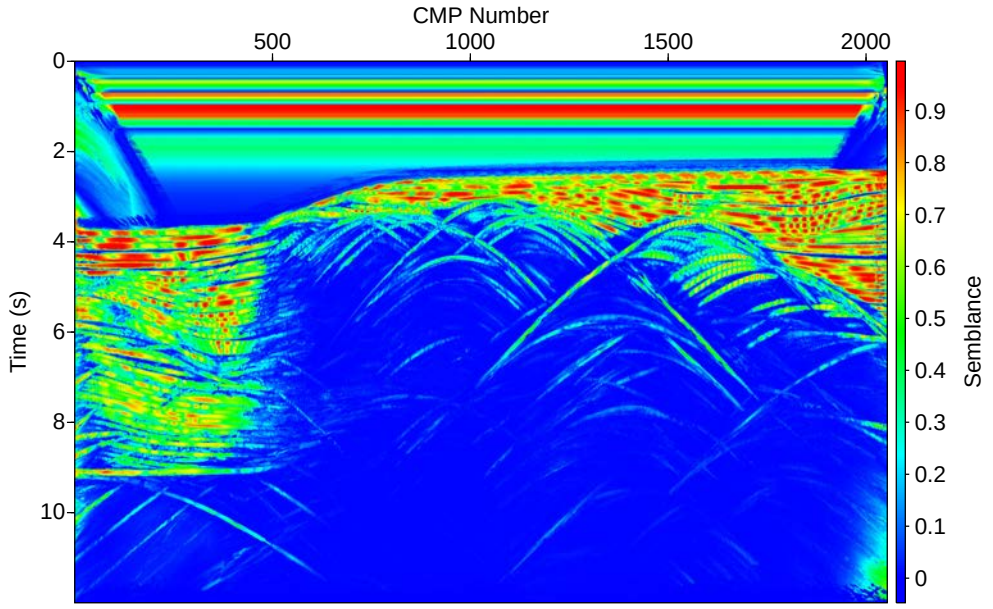

Figure 3.14.: Coherence determined by the original CRS code.

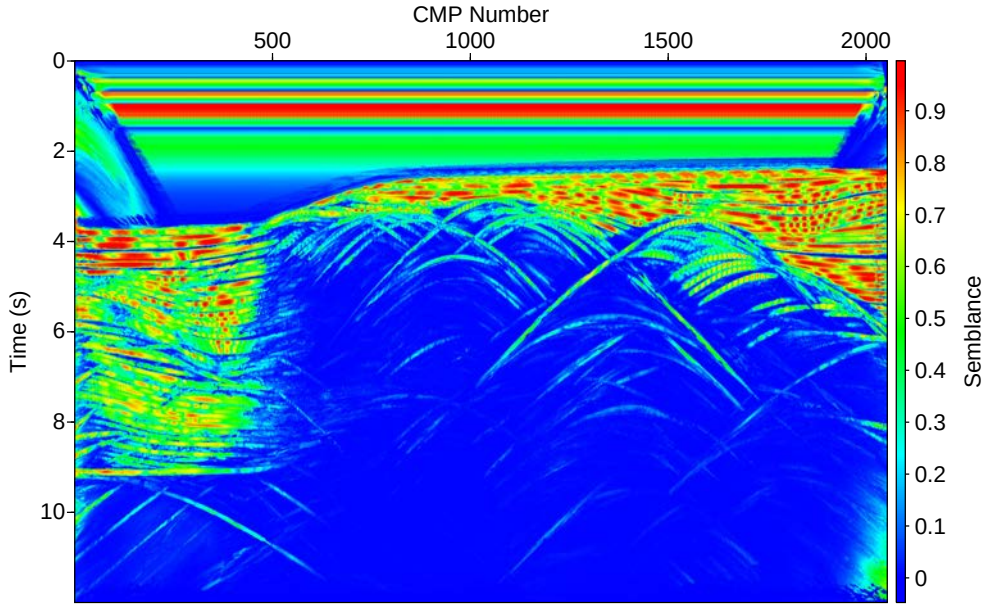

Figure 3.15.: Coherence determined by the hybrid CRS code.

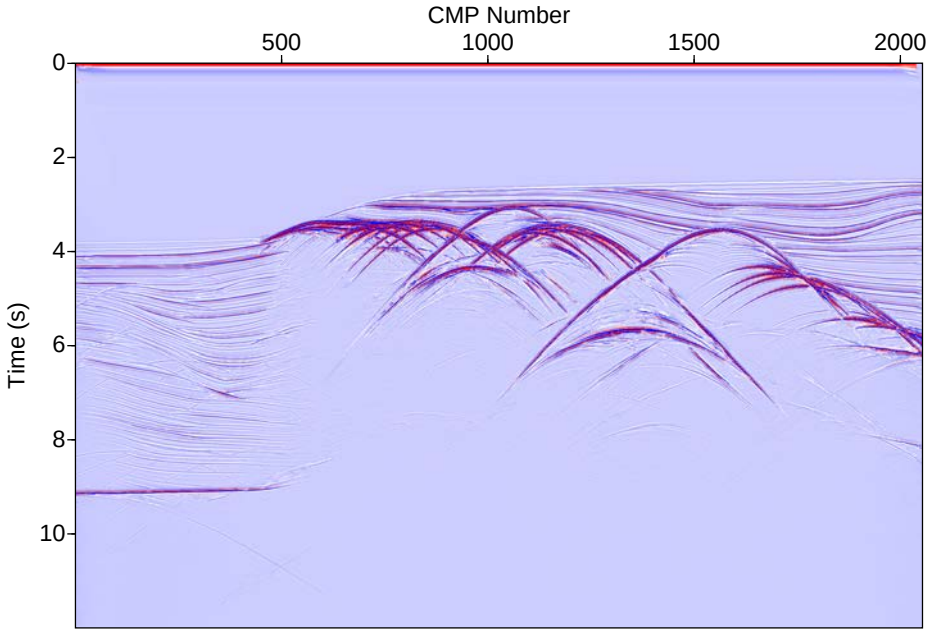

Figure 3.16.: CRS stack section obtained by the original CRS code.

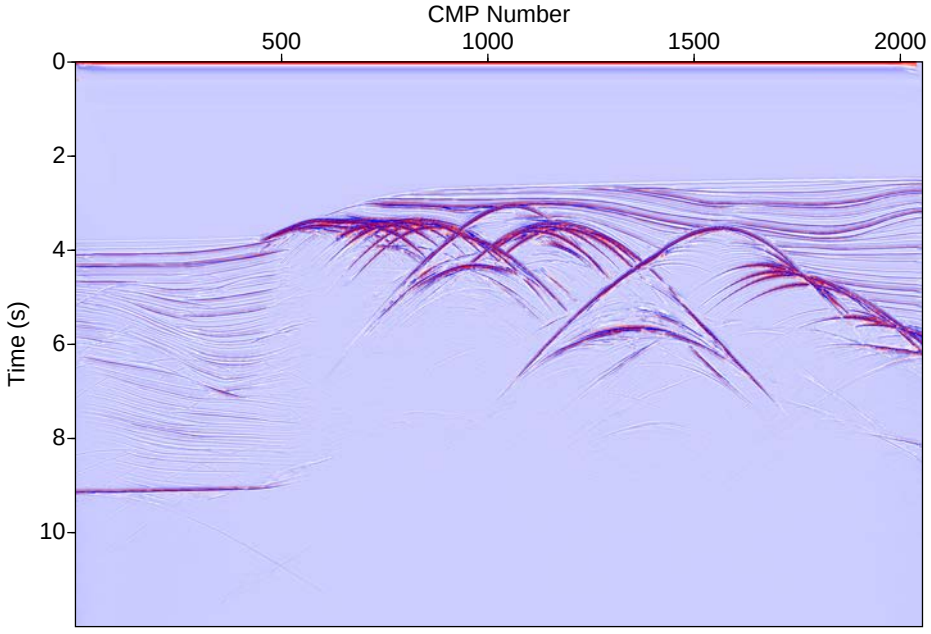

Figure 3.17.: CRS stack section obtained by the hybrid CRS code.

4. 3D Seismic imaging in crystalline rock

4.1. Study area (Schneeberg, Germany)

The Schneeberg study area (Figure 4.1) is located in the south-east of Germany near the Czech Republic border. At the north-east side is the Poland border. Population of Schneeberg is very low, and most of the cities were established due to the mining history of the area. Schneeberg is a small town with some earth science importance because of the regional and local tectonics. In the past, the activities were linked to the mining occupation. The region is under the eyes of explorers because of geology and geomorphology of the subsurface. There was mining in the area until the late 1980. The study area is shown with red star in geographic map in Figure 4.1.

The Schneeberg is the part of Saxo-thuringian Zone which is quite complex in geology, structure and tectonics (Linnemann and Romer, 2010). The subsurface is a rich geological environment which acts as an important reservoir. This area was subject of intensive uranium mining (e.g., Berger et al. 2011). One reason for targeting this region for geothermal exploration is prior geological information on the subsurface because of the mining history. Other reason is that according to the geologists and geophysical experts, it is a prospective zone for the petrothermal energy exploration. *Petrothermal* resource is the energy of the "hot dry rock" inside the earth. The main concept is that there are regional faults and some small conjugate faults which are cross-cutting each other generating a natural fracture system for exchange of heat if cold water is injected. This means that less fracing is needed and water will flow along the natural fracture system. This super heated water is then used to run turbines to produce electricity and other energy. Feasibility studies have shown that, the area is ideally suited for the petrothermal reservoir exploration (Berger et al., 2011).

In Germany, exploration for hydrothermal energy is a common practice for about a decade already. They include Bevaria and the Molasse basins which has a

Figure 4.1.: Study area located on geographic map.

temperature gradient of about 30° Celsius per km of depth increase (Lüschen and Schulz, July-2014). Heat sources in sedimentary environments contain the hot water forming hydrothermal reservoirs like in the Molasse basin carbonate aquifer. In this case, water is pumped to 3-4 km depth and hot water is used to drive turbines and to provide that to local households. Later the cold water is re-injected for heating and reuse.

In the case of Schneeberg, the granite intrusion is a dry hot rock in the subsurface and acts as petrothermal reservoir. The water is injected for heating by the dry hot rock. This hot water is pumped to the surface to provide heating energy to customers and to run turbines for electricity generation. Petrothermal reservoirs hold a much greater hydrothermal potential in Germany then the conventional geothermal reservoirs because these reservoirs are constrained only in small areas (Paschen et al., 2003).

4.2. Geology and tectonics of area

Schneeberg is a part of Saxo-Thuringian Zone which has a special position (e.g., structure and tectonic, mining exploration). The area is under keen observation of geologists because of the regional tectonics. This zone has been variably affected during the Variscan Orogeny. Some parts are vanished significantly in Variscan deformation and metamorphism (Allochthonous Domain), whereas other parts have been strongly preserved in orogenic belts in the form of nappe zones (Emmermann and Wohlenberg, 1988). This clearly shows the compressional regime and thrust tectonics of the area. The two domains are separated by the SE Wrench and Thrust Zone that predominantly includes rocks of the Autochthonous Domain (Kroner et al., 2007). In the tectonic map of Figure 4.2, the study area is shown in a red square. The complexity of the tectonic regime is visible from the map. The major upper top lithology comprises Devonian rocks with some sandstone (Harjes et al., 1997). The lower part is completely dominated by crystalline rocks specially with granitic and metamorphosed rocks. The NE part is dominated by Permian sediments in the upper area. In the NW and western part, younger plutonic rocks are present which are also in the southern parts. The regional fault Roter Kamm which is shown in the geological profile (Figure 4.4) outcropping at several places in Schneeberg area. This fault is approximately 70° in dip. In the lower part of this study block, through which the Roter Kamm passes comprised of older granitic rocks. The metamorphosed rocks are lying inclined above this granitic body as shown in the cross-section. The subsurface except the upper few hundred meters, is completely composed of granite. Tectonically this block is in the compressional regime, so it is heavily fractured (Linnemann and Romer, 2010).

In the NW direction, there is a red coloured intrusion which is the younger granitic body. The cross-section geological profile (Figure 4.4) is reflecting the subsurface structure and geology near by in-line 660. The distribution of in-lines and cross-lines are shown in Figure 4.3. The in-line number 1 starts from the NW and ends with in-line number 712 in SE. The cross-line 1 starts from SW and ends at cross-line number 868 in the NE. The position of the profile is shown by a white bold line in the geological map (Figure 4.3). The fault line Roter Kamm strikes from NW to SE. Its position is shown in the geological map by an arrow. This continues through the whole volume striking from SE to NW direction and dipping in the NE direction. Greenish blue colour is the metamorphosed rocks overlying the granites which is also visible in the profile. The yellow coloured lithology reflects the clayey schist with quartzite which is dominated in the south-eastern part and goes deep inside the earth inclined in the NW direction. The yellow coloured intrusion indicates the high grade metamorphic rock.

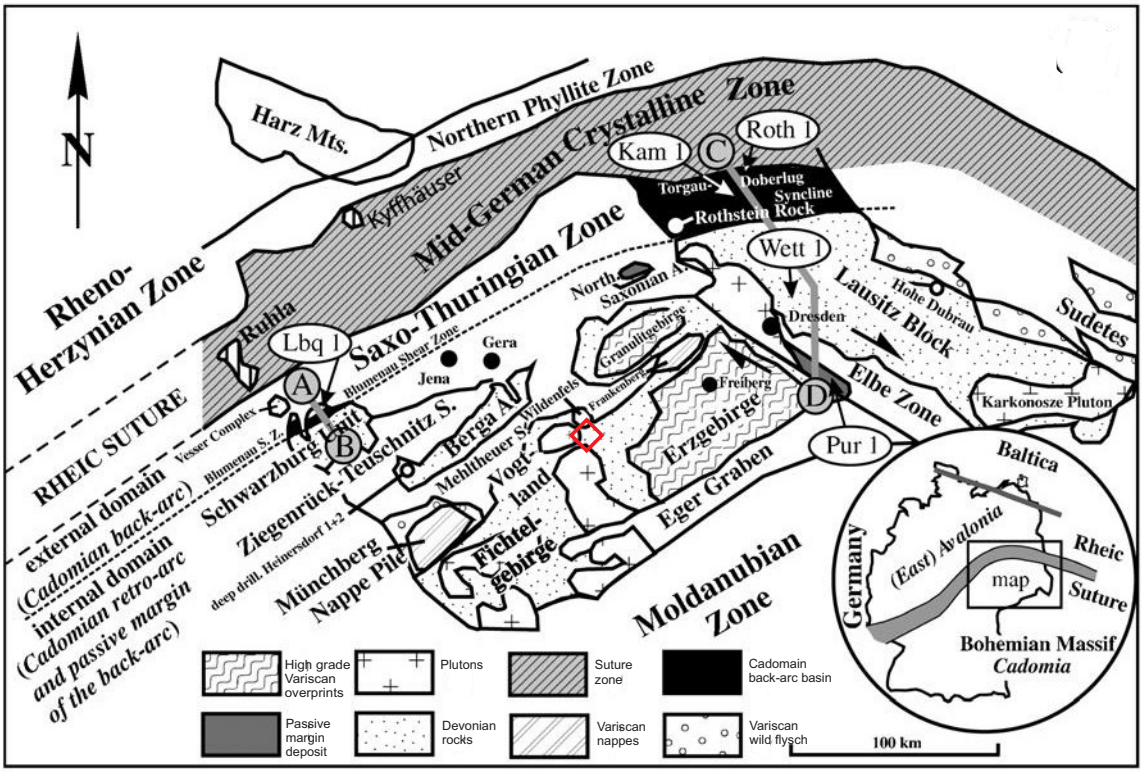

Figure 4.2.: Regional tectonic map showing Schneeberg study area (Linnemann and Romer, 2010).

Conjugate faults are present dipping perpendicular to the Roter Kamm as shown in geological cross-section. The inclined overlying layers of rocks are metamorphosed rocks which are present on top of the granitic body. The conjugate faults cross cut the metamorphic rocks. Conjugate faults terminate at the Roter Kamm.

In this geological map of Schneeberg, there is a brown coloured area in NE part. This area was exposed to mining on a large scale in the past. Still in some parts mining is continued till today.

4.3. Seismic acquisition (Survey design)

In this 3D seismic acquisition, vibroseis is used as the energy source for generating seismic waves. The study area comprises 140 km^2 with northening from 5602955 to 5619705 and eastening from 4538275 to 4555025. The planing projection of the

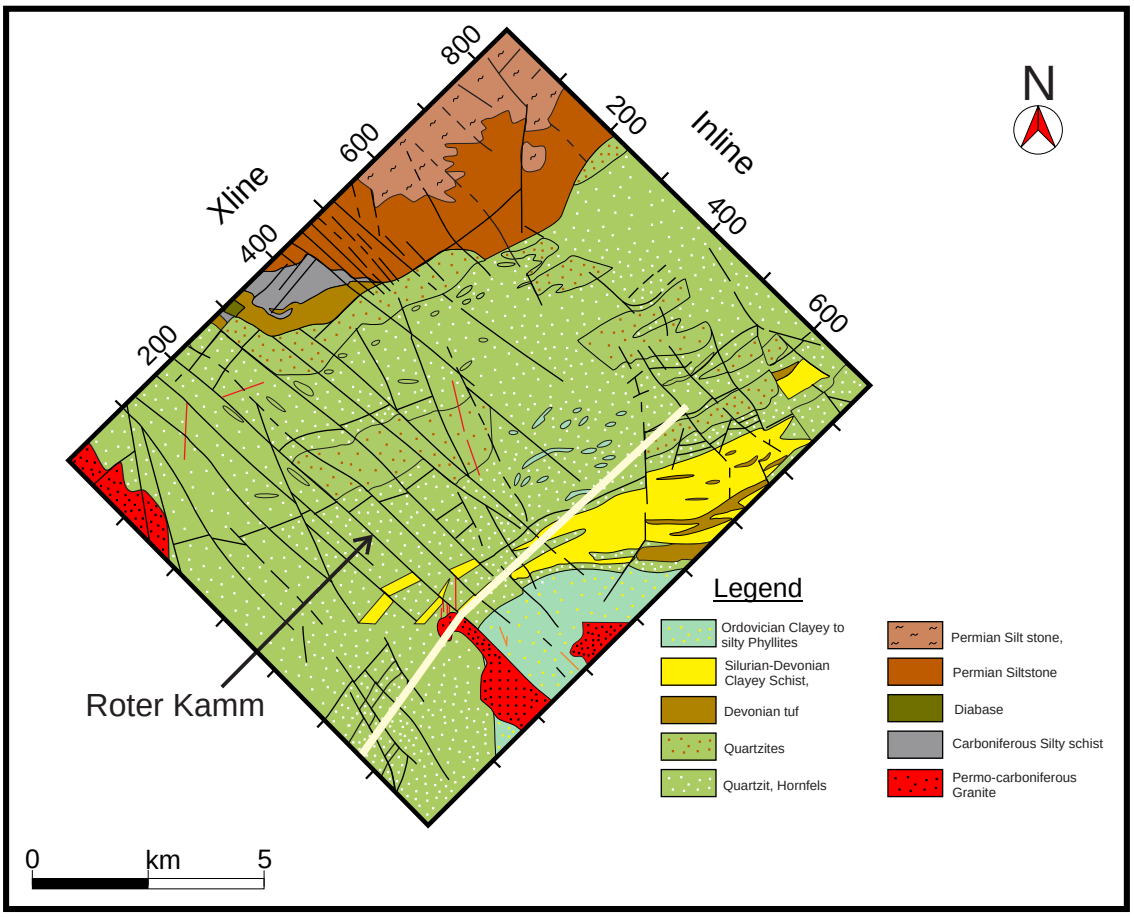

Figure 4.3.: Geological map of Schneeberg study area. Coordinates specify in-line and cross-line locations. (modified after (Berger et al., 2011))

seismic acquisition is shown on the geographic map of Figure 4.5.

Seismic acquisition

The 3D seismic survey was carried out by DMT GmbH & Co. KG, Germany. A 3D seismic survey has been done in this study area in order to understand the detailed sub-surface structure and geology. Before the seismic survey, previous studies of gravity and magnetic surveys were interpreted to design the seismic survey. The results of gravity and magnetic anomalies helped to design the survey and set the layout plans for the acquisition lines and source receiver positioning, and azimuth etc. In the start, the survey was planned as a 10x10 km grid as shown in Figure 4.5. But, when the survey was assigned, there was an area inside the planned acquisition

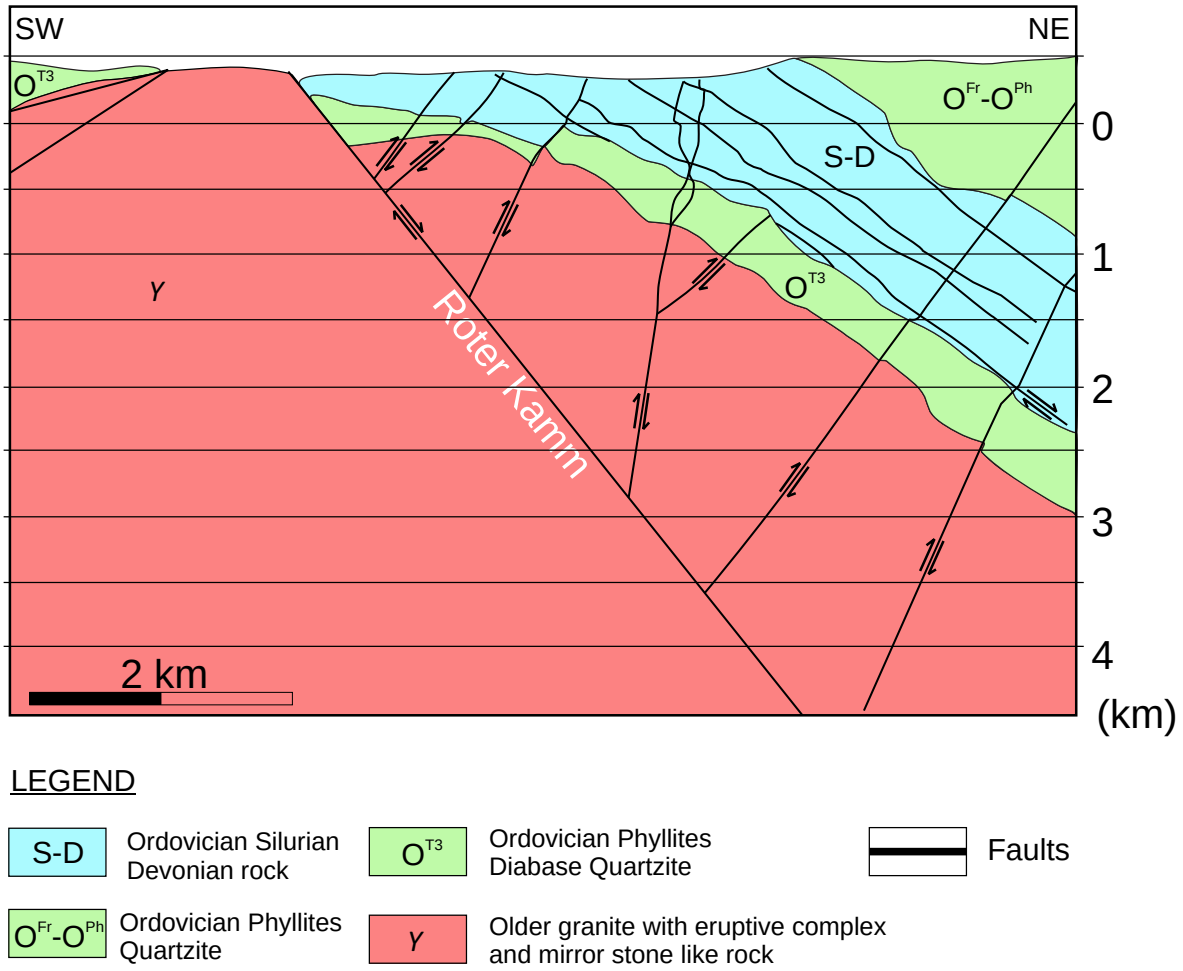

Figure 4.4.: Cross-section of Schneeberg study area passing near in-line 660. (Berger et al., 2011)

grid, which was not permitted to be surveyed by authorities. Due to this reason, the survey plan was changed and extended from 10 km to 13.5 km in the north-eastern part. The non-permitted area is shown in Figure 4.6 as a purple patch. This does not allow continuous coverage of the seismic survey. The acquisition team had to plan the extension of the grid for the seismic survey to obtain the maximum possible coverage of the subsurface signal in the area of interest. The extended new survey plan is shown in Figure 4.6. DMT has done the acquisition of this area. The acquisition was done with the azimuth of 45° from North. The data acquisition was completed in November, 2012. The fold density map is shown in the Figure 4.7

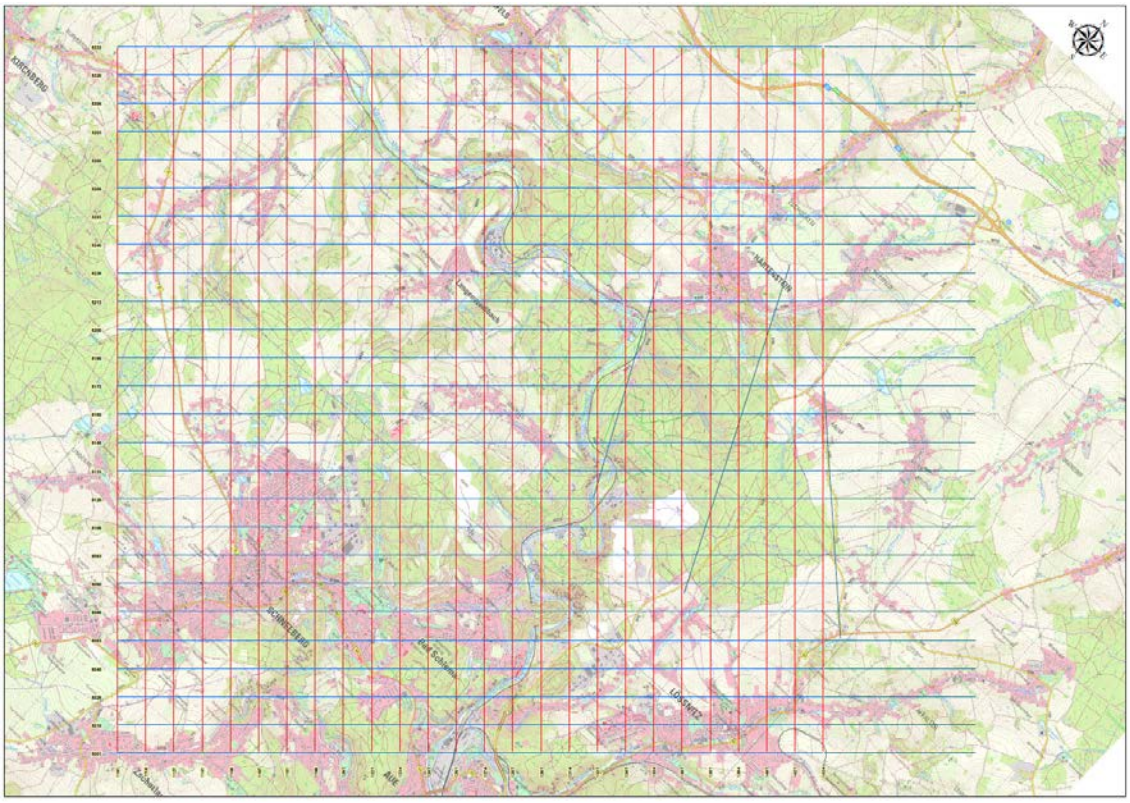

Figure 4.5.: Planing of acquisition lines (courtesy of LIAG, Hannover, Germany).

4.4. Acquisition parameters

For seismic acquisition, vibroseis was used as source. A *vibroseis* is a device that generates controlled seismic energy to perform both the reflection and refraction seismic survey. Normally it is mounted on a truck. This is used for the onshore seismic data acquisition. The source and receiver lines were not straight due to the constructed sites and different landscapes. The non-permitted area is the cause of the zig-zag acquisition in that region. The acquisition parameters are given in Table 4.1 .

Seismic pre-processing

First stage pre-processing and QC steps are done in the field during seismic data acquisition. Important pre-processing routines are performed after the field work is finished. This has been done by the Leibniz-Institut für Angewandte Geophysik (LIAG) Hannover. SeisSpace Promax by Halliburton Landmark has been used for

Parameter	Value / Unit
Seismic source	Vibroseis
Sweep length	10 sec
Frequency content	12 Hz - 96 Hz
Geophone content	1 C
Acquisition area volume	140 sq km
Recording time	10 sec
Time sample rate	2 ms
No of channels	6000
No of receivers	8146
No of source points	5348
Source interval	30 m
Receiver interval	30 m
Source line interval	400 m
Receiver line interval	400 m
Maximum offset	14000 m
No of in-lines	712
No of cross-lines	868
No of CMPs	617651
No of traces	31198591
Max no of fold	150
CMP bin spacing	15 m
Spacing between in-lines	15 m
Spacing between cross-lines	15 m

Table 4.1.: 3D seismic data acquisition parameters.

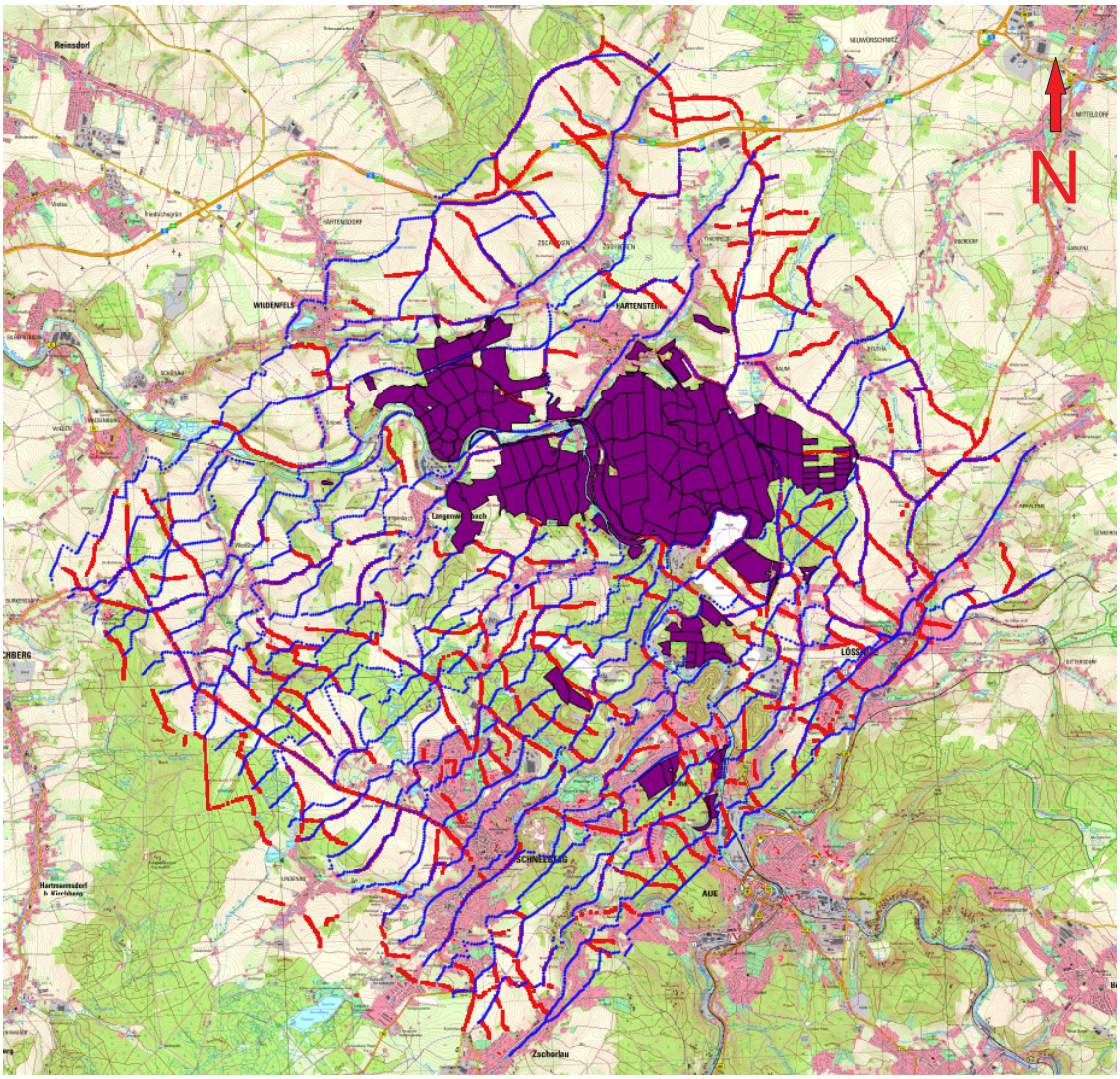

Figure 4.6.: No-permit area indicted by purple colour. (courtesy of LIAG, Hannover, Germany).

pre-processing. Some pre-processing was also done at the University of Hamburg. Details are given below. The most essential pre-processing steps are:

* Static correction: Static corrections were applied with the Promax software.

* Trace editing: In the QC of the data, it has been observed that many traces are of poor quality. Almost 2 million traces were found with bad quality signal. These traces were removed to increase the signal-to-noise (S/N) ratio.

* Top mute: The upper 500 ms (TWT) display a low quality signal. This portion of the data was muted with a top mute. Seismic Un*x was used for this process.

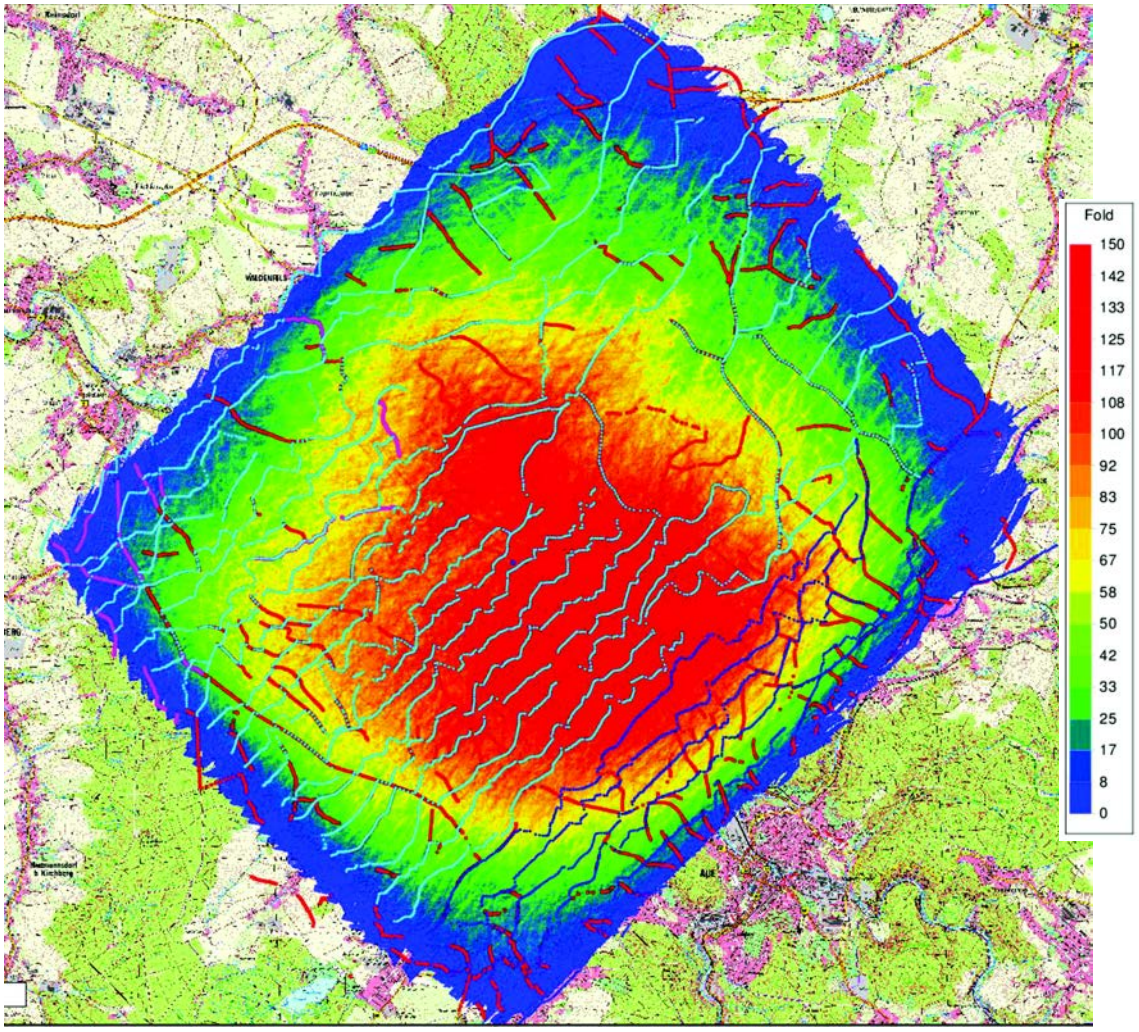

Figure 4.7.: Map of fold density of Schneeberg reflection data (courtesy of LIAG, Hannover, Germany).

After this pre-processing, the data was ready to be stacked as a 3D volume. A shot gather of the 3D dataset is shown in the Figure 4.8. This is a comparison of the hardrock dataset with an ordinary sedimentary environment dataset. The difference is quite clear and shows that hardrock data have a poor S/N ratio. The difference is to show the problem and difficulty to image the hardrock and how the data looks like compared to the sedimentary seismic data. It is a challenging task to process such type of data to get the clear subsurface structure and tectonic model. For this case, 3D CRS stacking has been applied to get improved results.

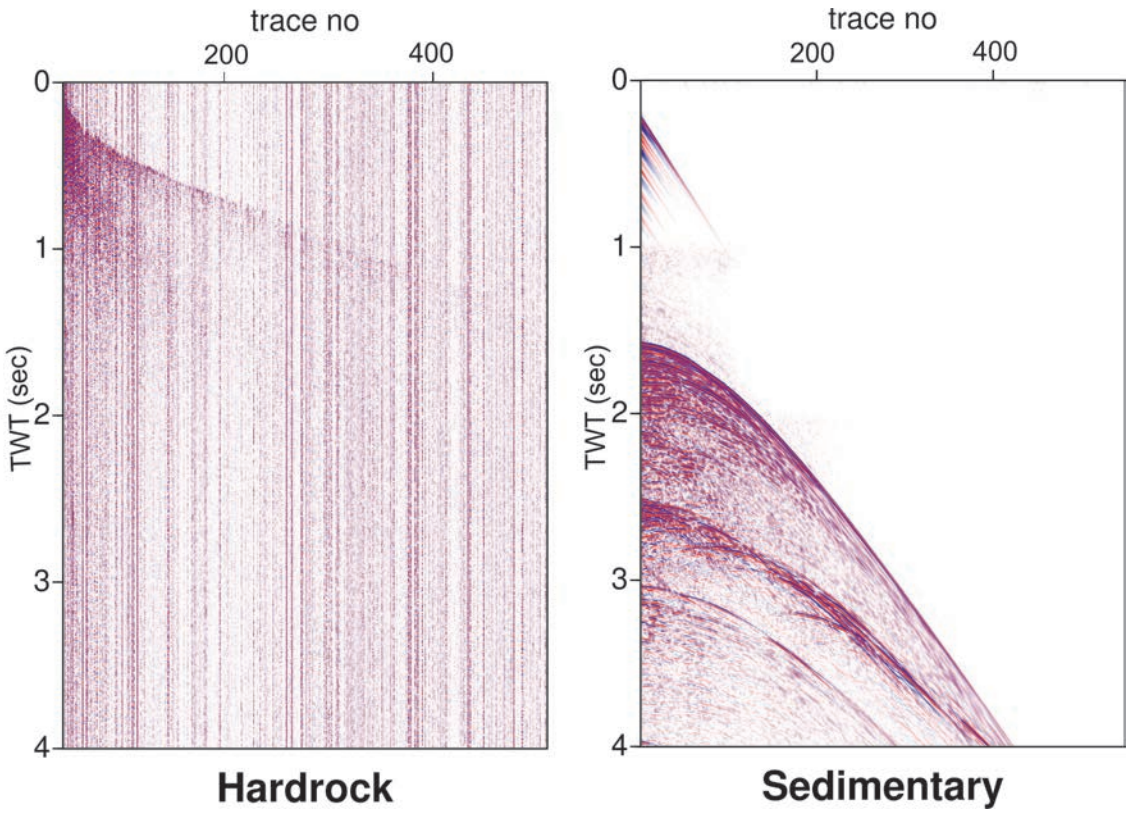

Figure 4.8.: Shot gathers of hardrock (Schneeberg area, Germany) and sedimentary rock (TGS Levantine basin, Mediterranean Sea).

Seismic processing

Because of the poor S/N ratio of the Schneeberg data, the 3D CRS workflow is applied as given.

4.5. 3D CRS processing

The data are recorded over a complex crystalline subsurface structure and display a very low signal to noise ratio. The application of CRS to these data is motivated on previous research which proved that CRS leads to better results from low signal-to-noise data when compared to the conventional CMP processing. A 3D CRS workflow was applied to get the optimal image quality. The common-reflection-surface (CRS) workflow represents such an alternative processing path of reflection seismic data from time to depth (Baykulov et al., 2011).

Parameter	Value / Unit
Surface velocity	4000 m/s
Maximum dip angle	80°
Offset aperture (min)	1000 m
Offset aperture (max)	4000 m
Midpoint aperture (min)	400 m
Midpoint aperture (max)	400 m
Azimuth	180°

Table 4.2.: Parameters used for 3D CRS stack.

3D CRS processing starts with the eight parameter search. The new and improved hybrid 3D CRS code is used to process the data. This makes easier to process large scale data. This saved lot of CPU time in days and weeks or even months. For processing the data, two super computers were used. One is a small cluster named as Thunder which is equipped with 64 cores and the other big cluster is called Blizzard comprising 8000 cores.

3D Automatic CMP processing (Brute stack)

Pre-stack pre-processed seismic data after static correction, trace editing and AGC is used for the automatic CMP search. Since, the Schneeberg block comprises mostly hardrock, the velocity is almost constant throughout the whole subsurface lithology. The automatic search estimates the best fitting stacking velocities from the preprocessed CMP gathers. The stacking velocities are expected to be high with very less variation about +/- 200 m/s. This brute stacking is done with a velocity of 6000 m/s.

Figure 4.9a shows the automatic CMP stack for in-line 390. The automatic stack is a part of the procedure to determine CRS attributes (e.g., Mann et al. 1999; Müller 2003) and represents the stack obtained after coherence-based determination of the CMP stacking velocity. The reason for choosing this in-line to observe more is that, it is located near the area of interest. The location and orientation of the in-line could be seen in the geological map (Figure 4.3). It can be described as an automatic way of velocity analysis for each ZO sample. The presented image can not be considered as the optimal result of a conventional CMP processing workflow. The output shows no significant event. Even with AGC applied, no events are detectable. The image is blurry.

The automatic CMP stack displays a poor S/N ratio and indicates that a multi-

parameter stacking method like 3D CRS involves more traces in the stack than the CMP method might provide an improved image. This was our motivation to apply the data-driven CRS workflow to the Schneeberg hardrock reflection data.

3D CRS Stacking

After automatic CMP stack, the angle and curvature of normal wave is calculated. This completes the 8 parameters attribute search. In this processsing, the angle search is performed in a wide range azimuth directions. The parameters for the 3D CRS search are listed in the Table 4.2.

It is well known that stacks represent an image and are the first step on the way to construct a geological model. It is, however, the only imaging result which is obtained in a purely data-driven fashion, free from any interpretation. In Figure 4.9b the CRS stack of in-line 390 is shown. Here reflection events are clearer, more continuous and easier to distinguish in comparison to the automatic CMP stack in Figure 4.9a. Note, that the color amplitude scales are not the same for both plots, since the CRS stack has higher amplitudes and dynamic range than the CMP stack. Many more traces contribute to the CRS image. Although the quality of the CRS-stacked section is already satisfactory because of the increased S/N ratio, we also considered the coherence as an additional imaging attribute. As mentioned above, this attribute is obtained in an objective data-driven way during the optimization procedure.

The coherence represents a low-pass positive definite version of the ZO stack image. It should display features very similar to the stack but with a decreased resolution. The coherence image of in-line 390 is shown in Figure 4.9c. Note again that, the color scale is different from the CMP and CRS sections in this figure, since the coherence is always positive and assumes values between 0 and 1. For data with a very good S/N ratio, the coherence section looks similar to a stacked section where absolute amplitudes are considered. For noisy data, however, the coherence section is the superior choice, since seismic noise does not stack destructively, if absolute amplitudes are used. In the coherence section it is obvious that the steep dipping continuous events crossing the whole section are of similar relevance as the events in the top left corner. This conclusion is not so easily derived from the CRS-stacked section (Figure 4.9b). Therefore, it is concluded that the coherence provides a suitable imaging attribute for the structural interpretation of this particular set of hardrock data. The coherence value directly reflects the physical relevance of the stacked event and may therefore be used as a weight to further decrease the noise level in the CRS-stacked section.

This weighting is performed in Figure 4.9d by simply multiplying the stacked amplitude with the respective local coherence. The S/N ratio of the weighted stack is considerably improved when compared with the unweighted CRS stack (Figure 4.9b). The prominent events present in this section are related to the reflections from the top of granite which is metamorphic rocks overlying and which could be the clayey schists which are present in the SE of the survey area (see geological map in Figure 4.3). Since the emphasize here is the application of the CRS method to hardrock data and the establishment of a data-driven workflow using various imaging attributes, no detailed interpretation of the images is given here.

Figure 4.10 presents the coherence section of in-line 369. The coherence section show many crossing events typical for hardrock data. Several NE-SW dipping structures are dominating the left part of the section. Between cross-line coordinates 200 and 500, strong events were observed for two-way-times larger than 2 s, which are not present elsewhere. This structure was called *Schneeberg body*. The Schneeberg body is a geological feature which represents the scattered energy below Roter Kamm at the position of xline 200 near 2 s time. On this in-line no obvious evidence of the Roter Kamm can be detected. The surface location of the Roter Kamm is at about cross-line coordinate 230 for this in-line section. Events attributable to Roter Kamm were actually only obtained on a few in-line sections. The seismic appearance of the Roter Kamm is characterized by a considerably smaller coherence when compared with the coherence of the conjugate faults. Conjugate faults are visible in the Figure 4.10 and 3D cube. On most in-lines the presence of the Roter Kamm in the study area is not expressed directly by a seismic event but by the fault throw of the conjugated faults or increased attenuation (Lüschen et al. 2015). In contrast to the geological model derived prior to the seismic experiment, the conjugate faults do not terminate at the Roter Kamm (Figure 4.4) but penetrate through it and extend considerably further SW.

4.6. 3D poststack Kirchoff time migration

To remove the imaging artifacts in the stacked volume, 3D Kirchoff poststack time migration is applied. Promax/Seisspace is used for this process. The parameters used for migration are given in the Table 4.3. As the data is big, the 3D migration is computationally expensive. One reason is that the events to be migrated are steep dipping and which needs large apertures for migration. The migration is done with a constant velocity of 6000 m/s since no significant lateral velocity variations are assumed. The variation in velocity is from 5800 m/s to 6200 m/s which is known from the mining information of the subsurface. The resulting output provides improved results and events are better focused in the 3D CRS stacked volume. The

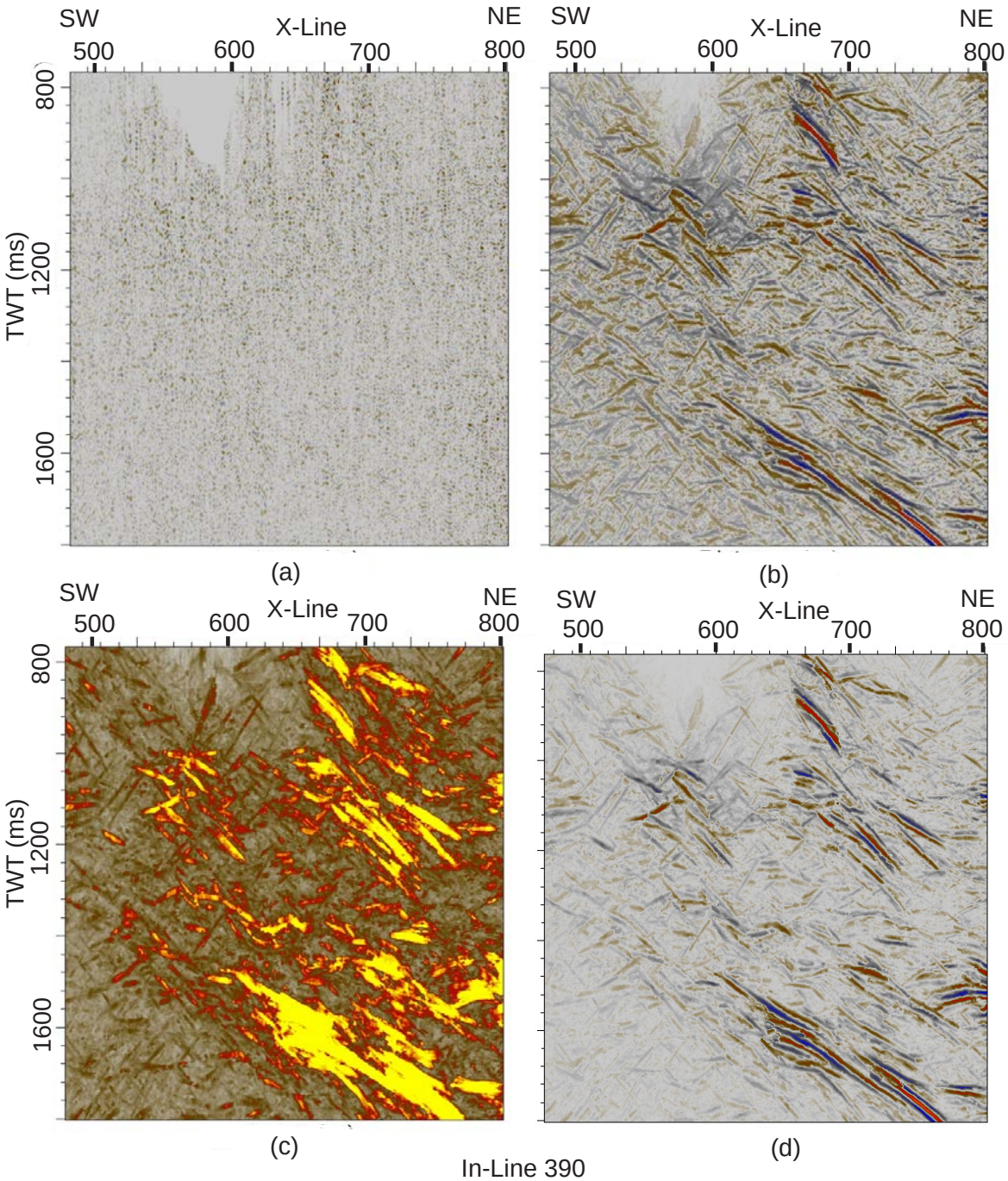

Figure 4.9.: Comparison of (a) (brute) CMP stack, (b) CRS stack, (c) coherence, and (d) coherence weighted stack (CWS) of in-line 390.

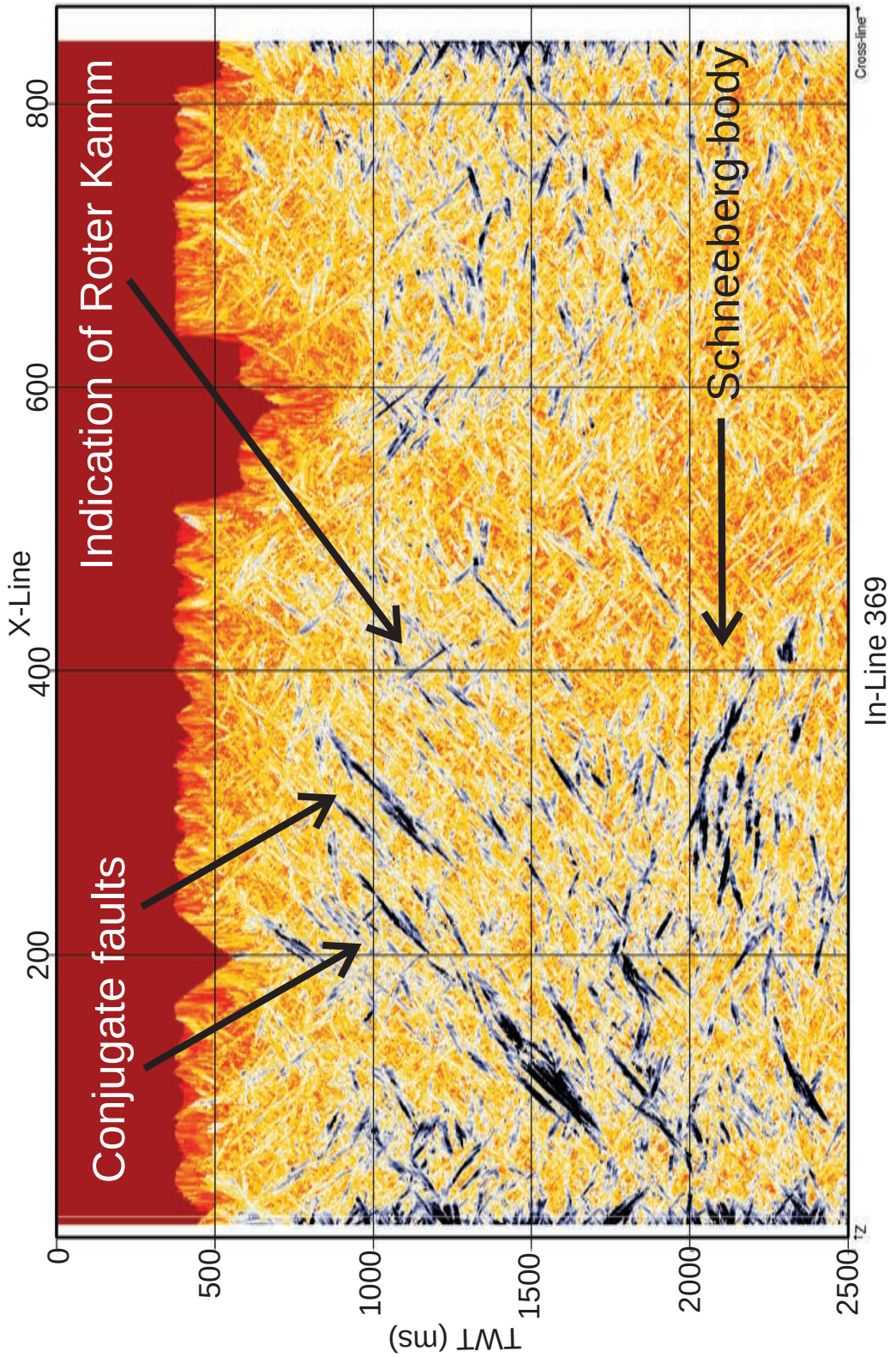

Figure 4.10.: Coherence section of in-line 369. Different features are pointed out with arrow which are observed in the subsurface.

Parameter	Value / Unit
Migration algorithm	Post-stack 3D Kirchoff Time Migration
Constant velocity for migration	6000 m/s
Maximum dip	70°
Maximum frequency	85 Hz
Migration aperture	6000 m

Table 4.3.: Parameters used for 3D Kirchoff poststack time migration.

top of granite is more prominent after migration.

There are some important features which are visible in the migrated seismic volumes. In Figure 4.11, in-line 290 is shown as migrated coherence. Several conjugate faults are visible in this migrated in-line. The faults are dipping SW direction. These faults start from the surface and terminate near 2200 ms TWT. But, there is also operator noise in the migrated coherence. The reason for this operator noise is the large apertures of the migration and the velocity errors. In the lower SW part of the coherence, there is some scattered energy near 2000 ms TWT. This scattered energy is because of the unexpected feature which is observed and was not recognized in the previous studies. In mutual understanding with the two operating partners Leibniz Institute for Applied Geophysics - LIAG Hannover and TU Bergakademie Freiberg, this scattered feature was named as the Schneeberg body. This feature was observed first time in the seismic studies and was a surprising (un-expected) result for geologists. This body is located just below the Roter Kamm near time 2000 ms close to the center of this study block.

The coherence weighted stack is also migrated which is shown in Figure 4.12. There are several conjugate faults better focused and resolved and with less operator noise. In this migrated section, S/N ratio is high. Subsurface structure is better interpretable. The top of granite in this migrated in-line is well imaged. To understand the subsurface structure and tectonics, this in-line is a good example. It resembles with the several features of the geological profile which is shown in Figure 4.4.

In the coherence weighted stack (Figure 4.12), the conjugate faults are visible as continuous events. The conjugate faults is visible which is cutting the top of granites and strikes the granitic body while obviously striking through the Roter Kamm which has no direct seismic expression in this image. Top of granite is also noticed in this figure. It seems that one or two of the conjugate fault strike deep and hit the Schneeberg body.

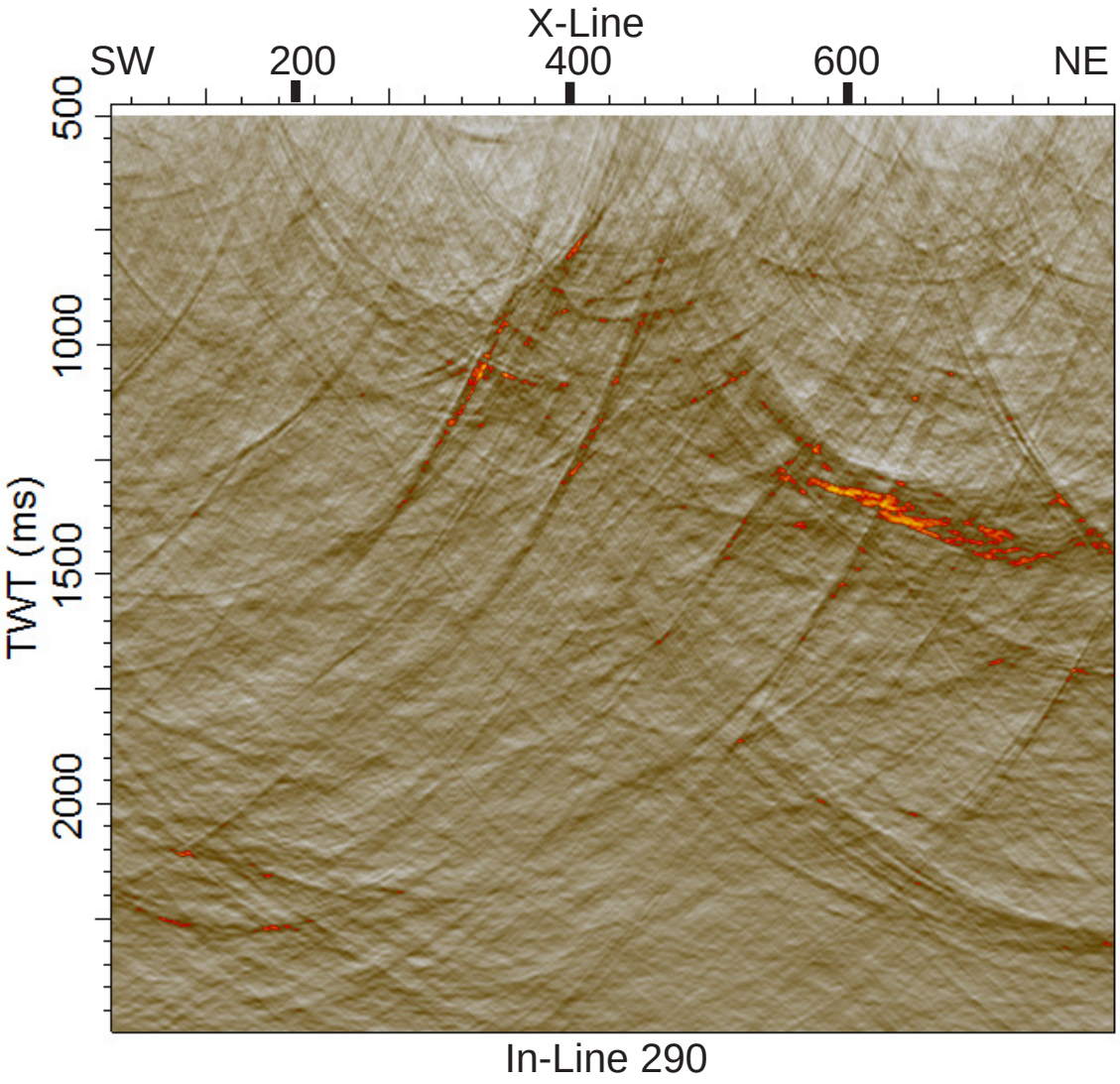

Figure 4.11.: Migrated 3D coherence in-line 290.

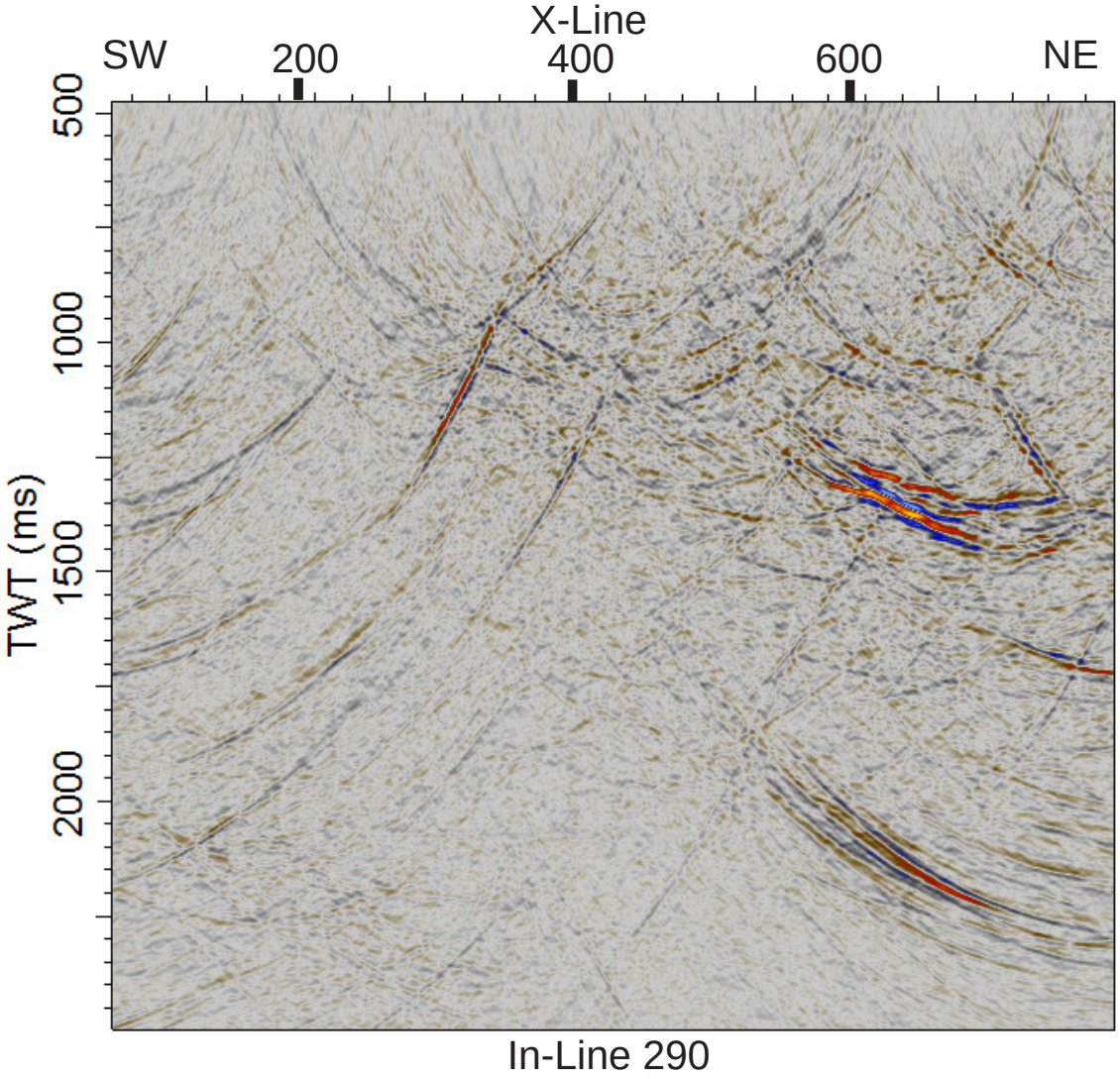

Figure 4.12.: Migrated coherence weighted CRS stack in-line 290. The features are better visible than in coherence.

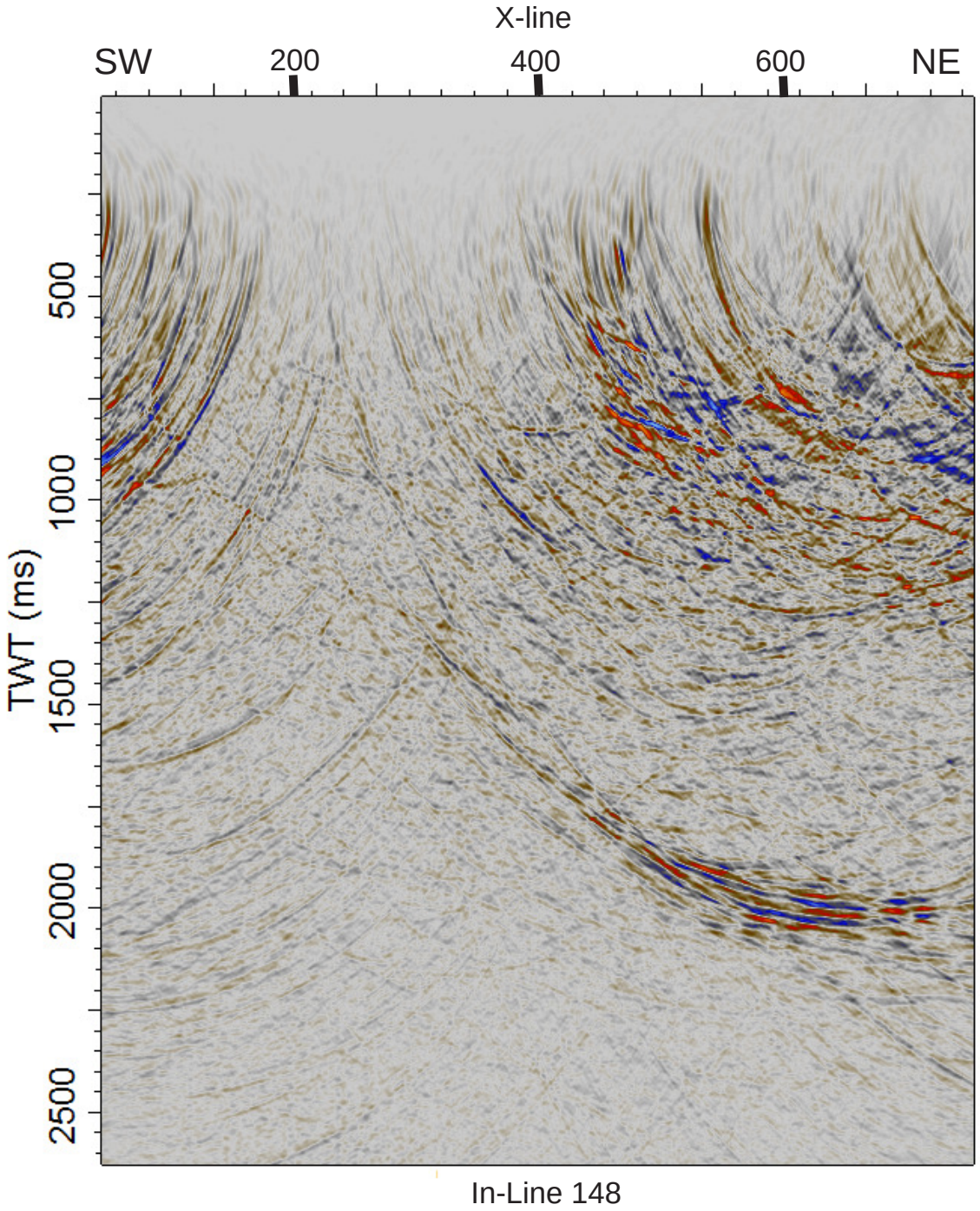

Figure 4.13.: Migrated 3D coherence weighted CRS stacked in-line 148. Starting from below x-line 200, slight hint of Roter Kamm with polarity reversal.

In the detailed study of the migrated stacked, migrated coherence and migrated coherence weighted stack, different features are visible in different in-lines and cross-lines.

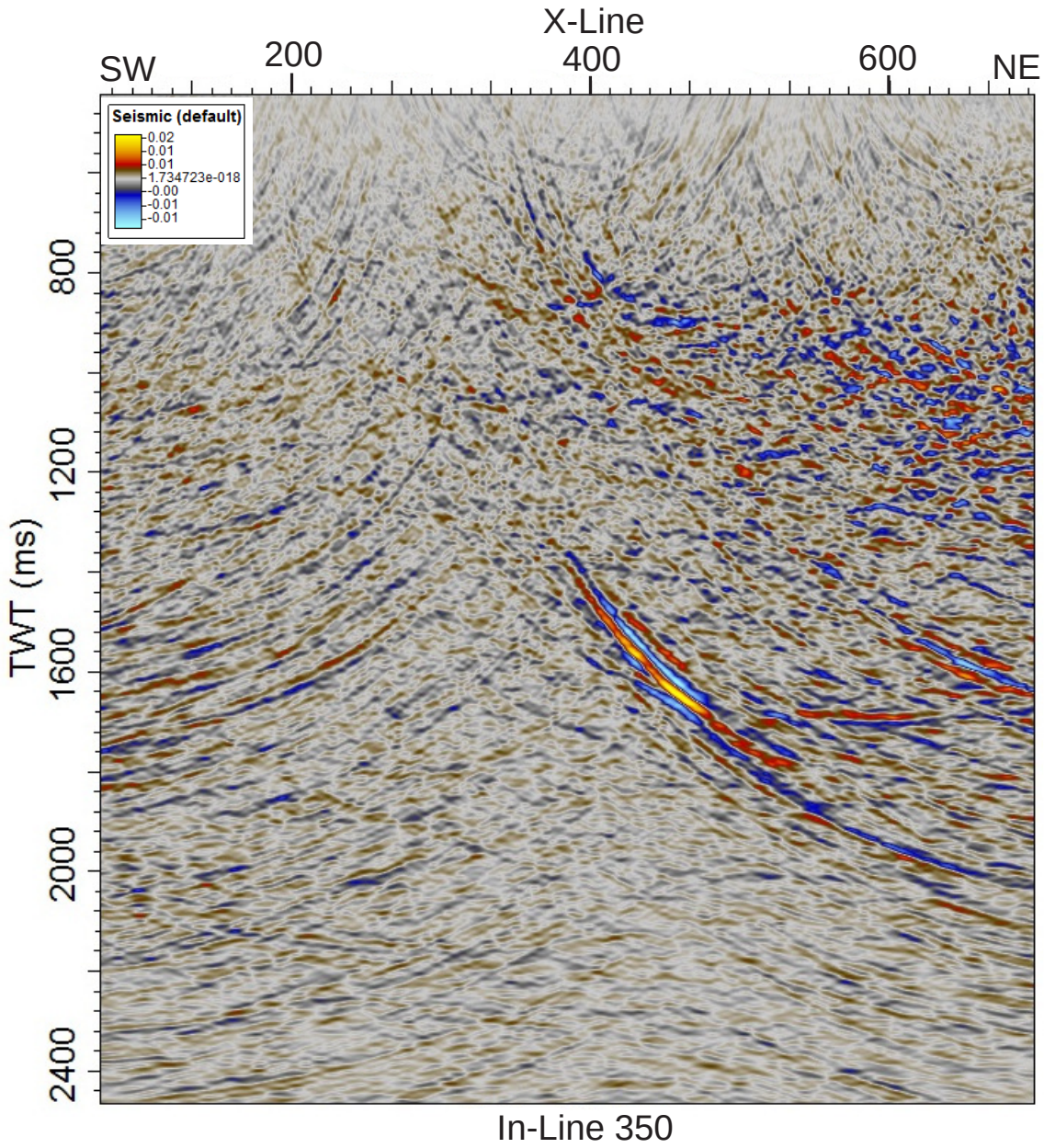

Figure 4.14.: Migrated 3D CRS stack in-line 350. In higher time 1600 - 2000 ms, the polarity reversal is strong. The legend shows the maximum coherence of 0.02.

In the migrated CRS stack of Figure 4.14, steep dipping fault is observed which passes through the center of the block. This can be interpreted as the major fault in this region, the so called Roter Kamm. In this section, the phase forms are studied. Standard seismic display of red, white and blue is used to observe the seismic

section. Red as positive and blue as negative is used as shown in figure. There are blue coloured negative amplitudes between two red coloured amplitudes in the continuous event of the fault. From this, it is concluded that, this fault has the property of polarity reversal. This can be interpreted that the fault is comprised of open fractures. The event is steep dipping and continuous until 2000 ms TWT. If the velocity in this medium is assumed to be 6000 m/s, then the depth of this fault is at about 6 km where it terminates in the subsurface. It is dipping approximately with an angle of 70°.

In Figure 4.13 the indication of the regional fault Roter Kamm is visible as slight indication (in blue coloured amplitude) just below the position of cross-line 200. There are migration smiles visible in imaging of this fault indicating the velocity and aperture issues. This fault is more clearly observed in the migrated coherence. It is important to note that the listric feature of the Roter Kamm is also noticed in the lower part of the fault in this figure where the fault terminates. In the upper right side of this profile, there is coherent diffracted energy visible which is concentrated at one portion. This is the area of mining activity in past decade. In the upper left corner of the profile, there are two inclined parallel events dipping in NW direction. These events corresponds to the younger granite and metamorphic rocks as visible in the geological profile cross-section.

In the Figure 4.15, which corresponds to cross-line 580, there are two steep dipping events. These events are dipping in the NNE direction. The steepness of the events is approximately 70° in dip. These events corresponds to the reflection of the rocks which are intruded in the sub-surface indicated by yellow colour lithology in the geological map. These are metamorphosed rocks comprising quartzite with clayey schist. The events are well visible as seismic reflections because of strong impedance contrast. The event is observed in the subsurface, starting from position in-line 600 until in-line 100 dipping to the north. The event is continuously visible in cross-lines starting from cross-line 430 to cross-line 700. The reflecting events terminate in the subsurface at time 2300 ms TWT. In the upper NE area, the coherent energy is corresponding to the mining area indicated by brown colour in the geological map of Figure 4.3. At time 2800 ms TWT, there is a small event in the center which is dipping north. This reflects a small scale feature in the deep subsurface. The dip of this event is not as steep as the upper two events (which start from the surface).There is a new reflecting event observed from 3200 ms TWT to 3300 ms TWT. This event is not observed in the migrated stack, but only in the migrated coherence weighted stack or migrated coherence.

Time slices of the seismic volume show features in map view. Events typical for

data are explained in time slice 1330 ms TWT Figure 4.16. In this figure, all those events are visible which are expected in the subsurface from the previous geological knowledge. The figure shows a time slice of migrated coherence. In the NE, the mining zone is visible due to diffracted events and criss-cross pattern. In the middle, the conjugate faults are visible which are indicated by arrows. In the SE, the two strips are steep dipping events from clayey schist and quartzite which are also observed in the cross-line directions. The green coloured arrow shows the direction of north in the time slice.

Deeper parts of this data show more features then expected and which are not seen in the geological map. The evidence of the Schneeberg body start near the time 2000 ms TWT. In the time slice of Figure 4.17, the Schneeberg body can be seen in SW close to center. This body is observed continuous throughout some slides. Figure 4.18, Figure 4.19 and Figure 4.20 show that there is continuity of this Schneeberg body with increasing time. In the start of the project, there was assumption that, the Schneeberg body might be an artifact caused by the acquisition foot print. However the continuity of this feature in some time slices with the symmetry raises the argument that this body could be physically existing in nature (subsurface) with the specific pattern as observed. This gives the answer of that question with the strong evidence in the time slices of migrated coherence section. The Schneeberg body could be evolved due to the conjugate faults that strike inside the granite body. The crossing pattern of Roter Kamm and conjugate faults play major role in making the fractured zone. This makes the intersection of two fracture systems at the Schneeberg body.

From the observations of the in-lines and cross-lines, it was assumed that the Schneeberg body is just a body acting as a cause for diffracted energy here. But, the time slices starting from 2000 ms TWT to 2500 ms TWT show that, this body has some symmetry in it. The Schneeberg body seems to be in a pattern of alphabet X. It seems that two events are crossing here in this sequence perpendicular to each other. The strong coherent symmetry is striking from SE to NW direction. The other coherent body which is striking from NE to SW direction cross cuts the first event.

Comparing to the time slices of migrated coherence with the time slices of coherence weighted stack (CWS) the later images are cleaner with higher signal to noise ratio. The signal is more pronounced as shown in Figure 4.21. The steep dipping events and the pattern of conjugate faults is more clearly visible. Each time slice has its own eatures, but the structure of either the steep dipping events, the Schneeberg body or the conjugate faults, they are visible throughout some of the time slices.

The time slice shown in Figure 4.21 shows most of the features which are indicated by the geological map. The time slices Figure 4.22 shows the conjugate faults. The Permian sediments are observed in the north-eastern part of this cube. In Figure 4.23, the steep dipping events start to be visible. Down in the cube in time, the steep event is more strongly noticed as observed in Figure 4.24 and Figure 4.25 respectively. The strike of this event is from east to south-west. In the Figure 4.26, at the position where the in-line 400 and cross-line 300 cross each other, there is a pattern of scattered energy. This is Schneeberg body. In the migrated coherence time slice, this structure was strongly imaged, but in CWS the S/N ratio is not as good. This shows the pattern like two perpendicular fracture systems are crossing each other. Similar behaviour is noticed near 2100 ms TWT (Figure 4.27) and 2150 ms TWT (Figure 4.28). Some other intruded features are noticed at 2700 ms TWT as shown in in Figure 4.29 in north-eastern part near position of in-line 400. These events are deep and no interpretation has been made yet about these events.

Figure 4.30, represents the 3D (migrated coherence) overview of the sub-surface features of this study area. The block shows the in-line 130, cross-line 600 and time slice of 2110 ms TWT. The continuity of the events can be observed where the in-lines and cross-lines cross each other. Figure 4.31 showing in-line 148, cross-line 650 and time slice 2700 ms gives another view with the CWS. A slight indication of Roter Kamm is observed between the cross-line number 200-300 for in-line 148. Figure 4.32 with in-line 369, cross-line 650 and time slice 2150 ms indicates the position of Schneeberg body in 3D which is visible in in-line and also in the time slice. The inclined clayey schist is also strongly observed in the cross-line. The complexity of the subsurface structure is visualized in these 3D cubes. Figure 4.33 gives the sub-surface overview of migrated coherence in transparency to get an idea of subsurface structure in 3D. Only the strong coherent events are displayed. The 3D transparency view allows to observe the nature of these events as structure and tectonics in three dimensional view. The chosen threshold allows us to see only the signal and unwanted noise is removed to see only structure and get the idea how it looks like 3D in the subsurface. There are few video animations available with the thesis as electronic supplement in a DVD. The detailed information is available in the appendix.

4.7. Conclusions

Application of a 3D CRS-based workflow to the Schneeberg 3D hardrock reflection seismic data has shown the surprising results. As the S/N ratio of these data is low, the automatic CMP stack showed no significant evidence of any event. The multi-parameter stacking operator provides an alternate approach to the conventional processing of the hardrock data. The data consists of diffractions and steep dipping structures. The 3D CRS has provided improved images of the sub-surface. The coherence which is an output of 3D CRS workflow has low resolution but, it gives more information of the structure and tectonics particularly for these data. Although the coherence has low resolution, it is considered as an alternate imaging attribute. This is helpful in imaging the hardrock data which is dominated by the diffractions. Weighting of the coherence (coherence multiplied with stack) further improved the resultant image which helped in the interpretation of the images. The most prominent feature of this data is the steep dipping reflection from clayey schist. The conjugate faults are mapped in the migrated coherence and CWS. Rother Kamm reflected only faint hints from the seismic signatures and this behaviour of Roter Kamm was unexpected for the geologists as it was expected to be the most prominent feature of this area. The coherence of Roter Kamm is less then the conjugate faults. Two fracture systems are imaged which are well observed in the time slices of coherence. Some features are still not interpreted like the reflections from the higher times more then 2700 ms TWT. Migration needs to be updated with the proper velocity model.

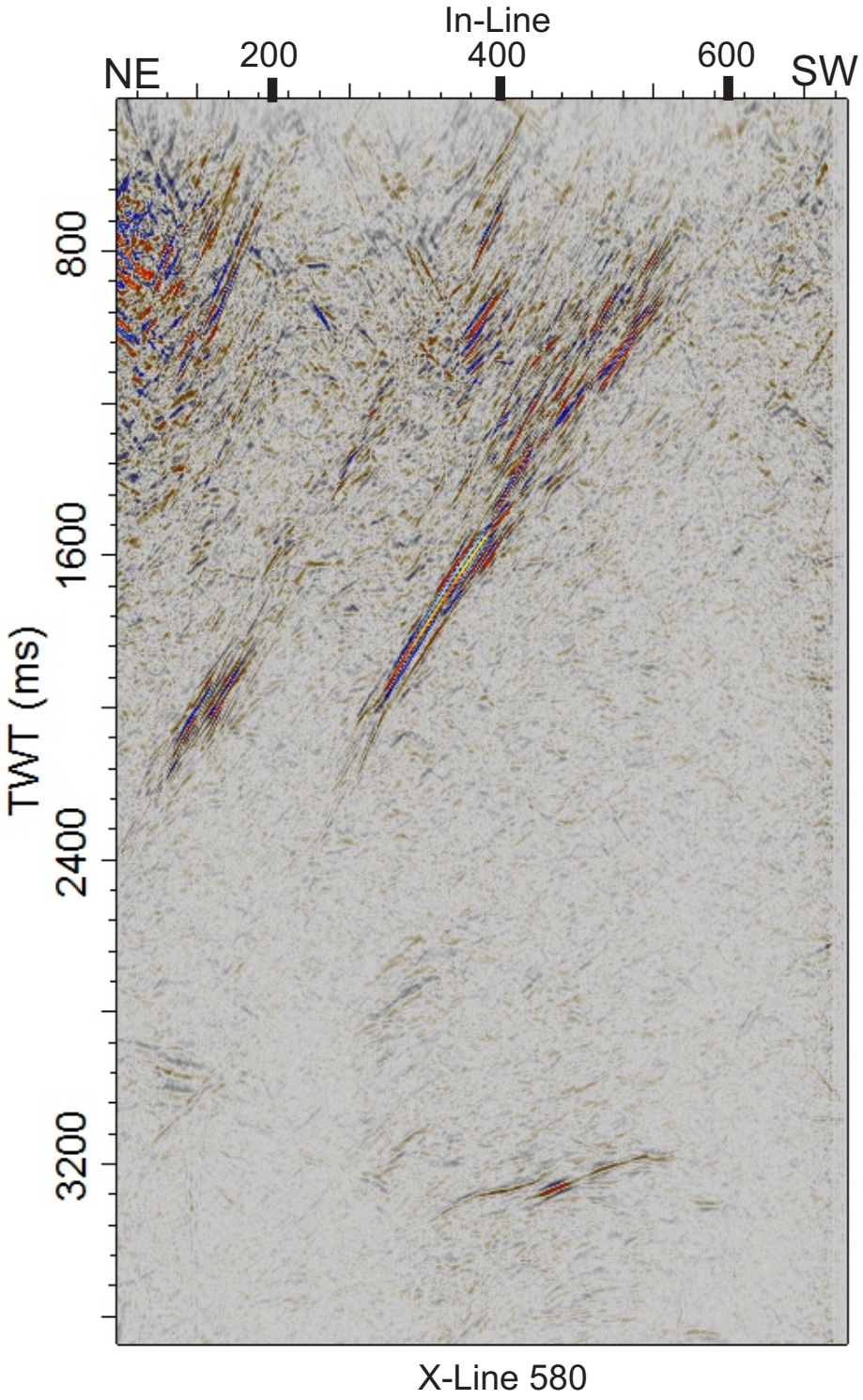

Figure 4.15.: Migrated 3D stack weighted CRS stack cross-line 580. Steep dipping NE clayey schist is strong event in this section. Event nearly below in-line 350 at time 2800 ms is also noticed which is small and dipping in north. Strong reflection from higher time near 3200 ms is also observed.

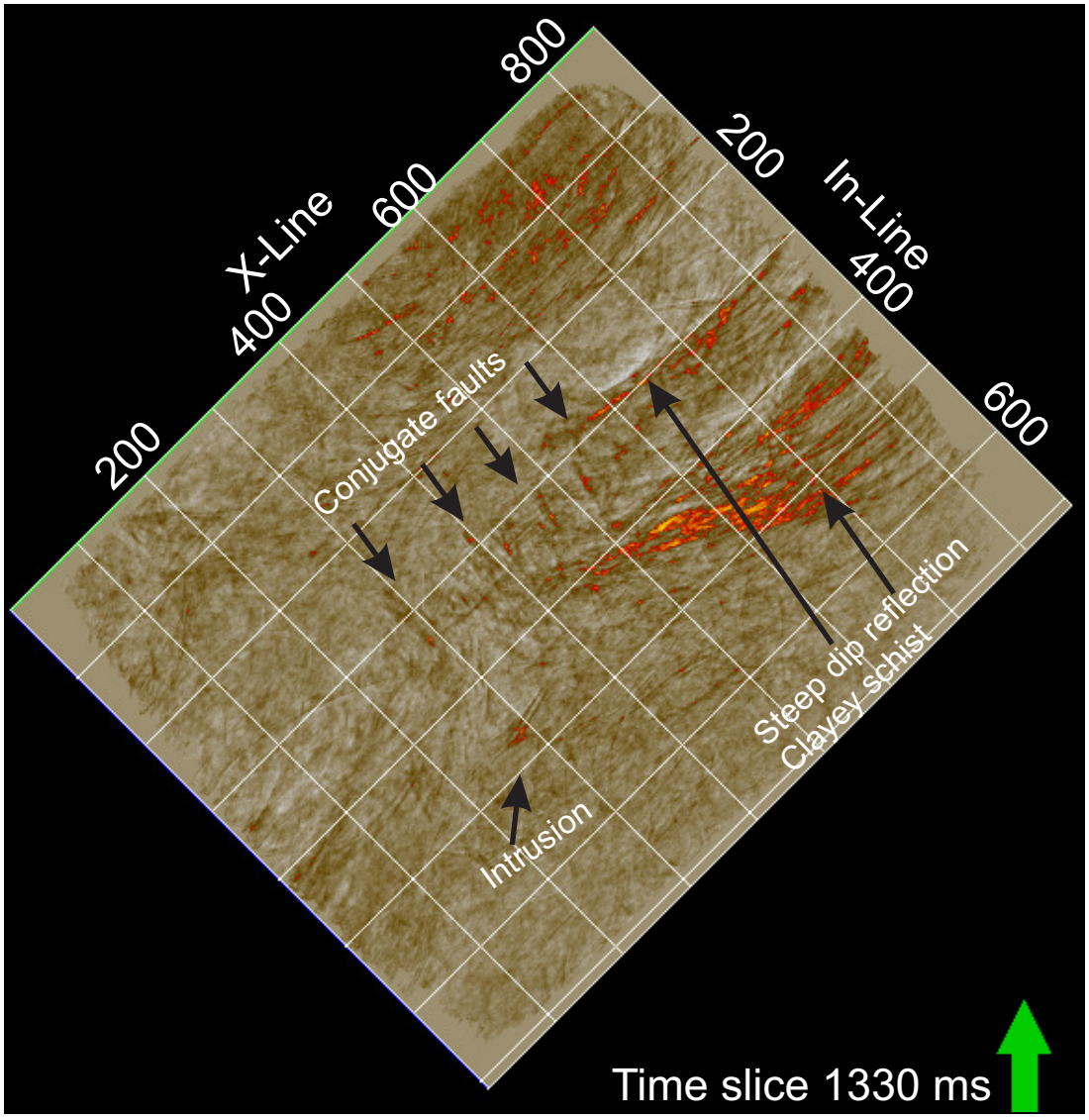

Figure 4.16.: Migrated coherence time slice 1330 ms.

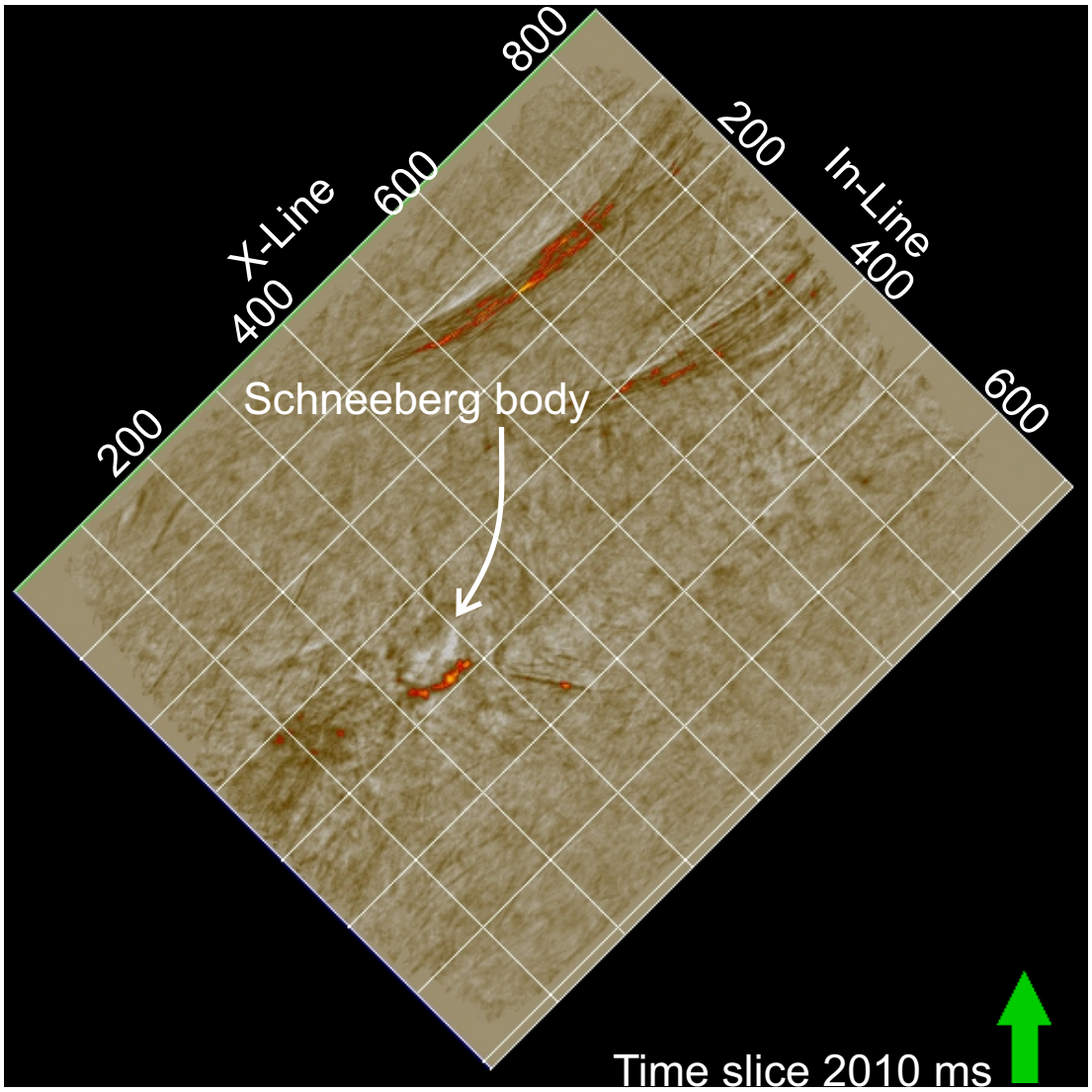

Figure 4.17.: Migrated coherence time slice 2010 ms.

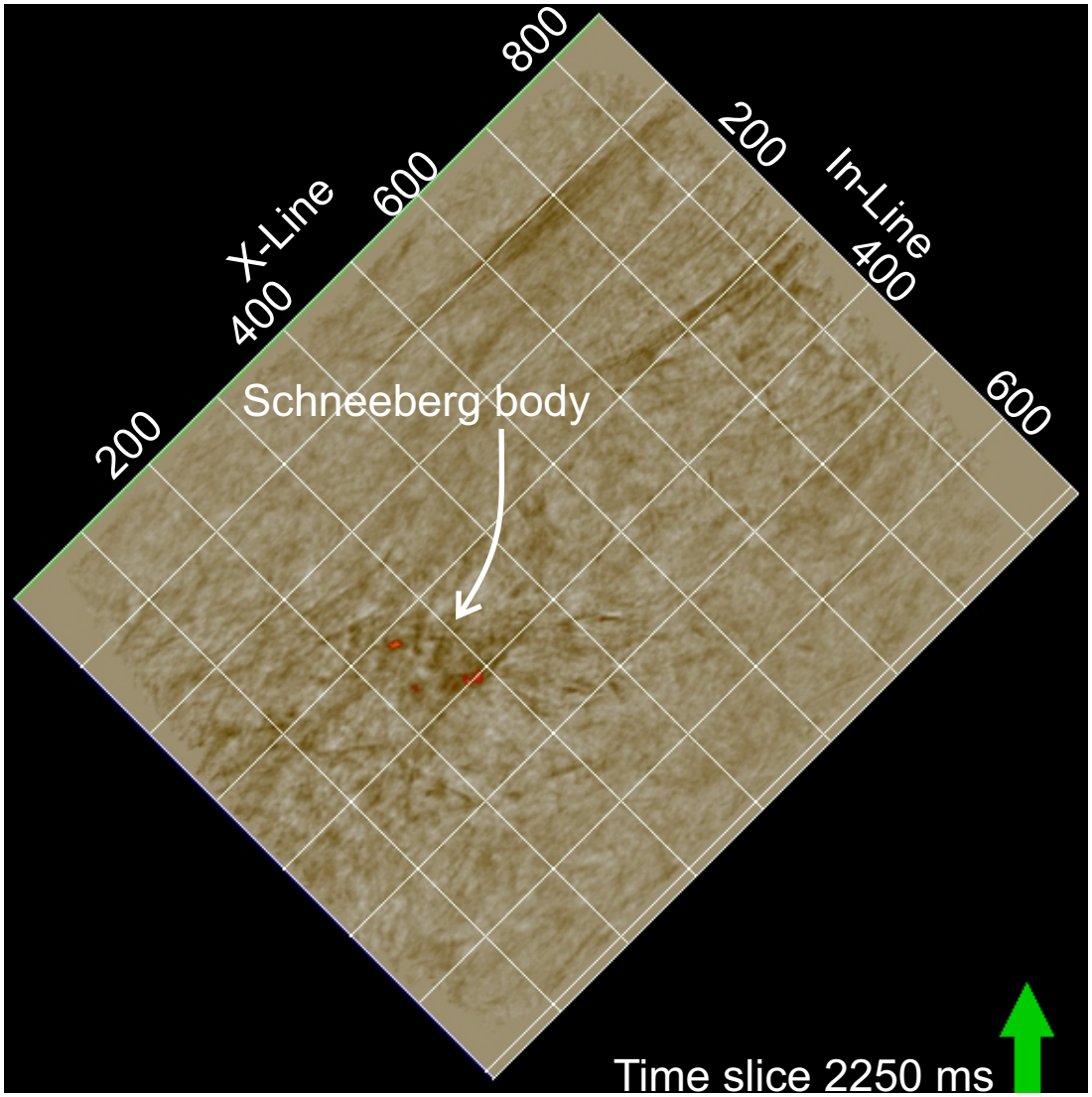

Figure 4.18.: Migrated coherence time slice 2250 ms.

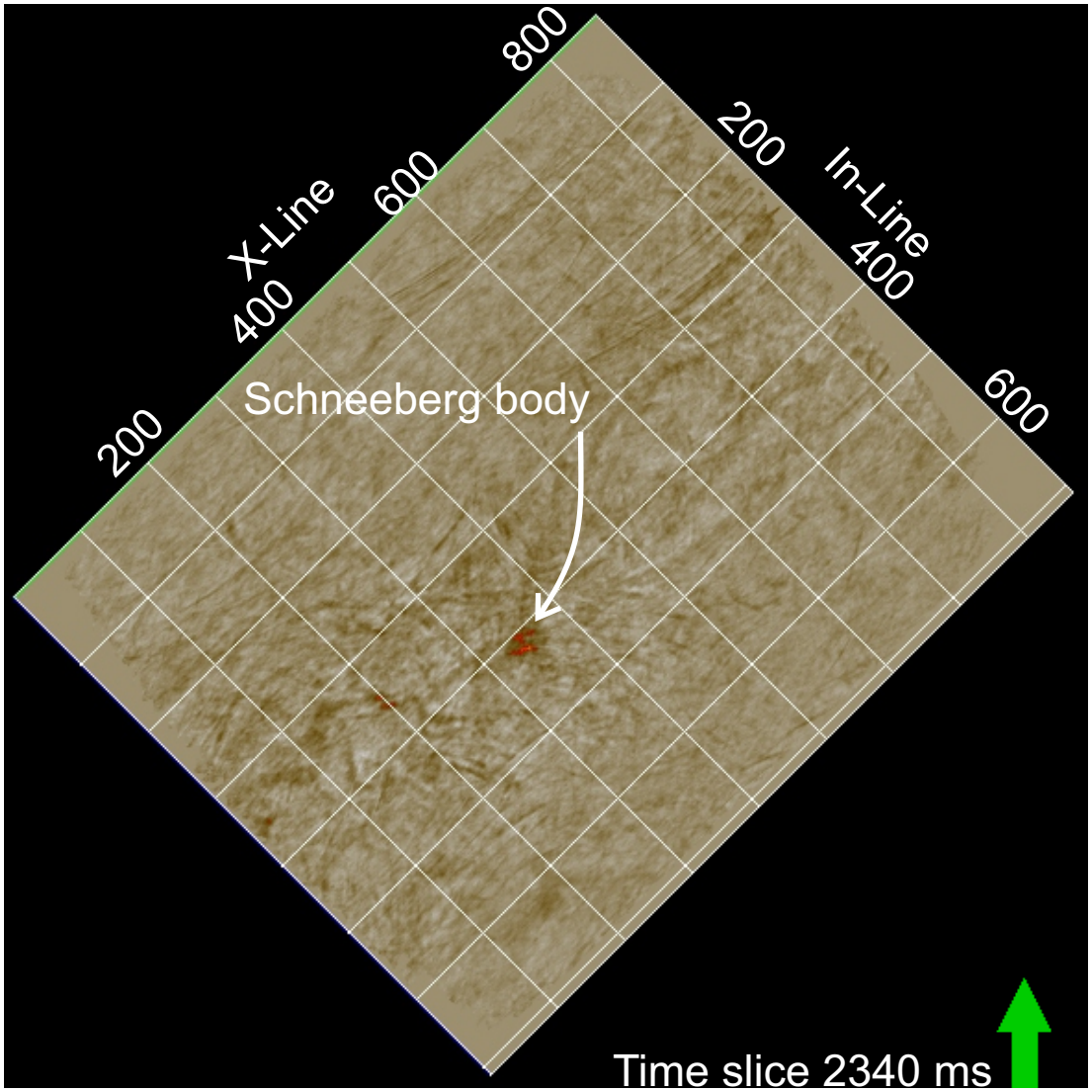

Figure 4.19.: Migrated coherence time slice 2340 ms.

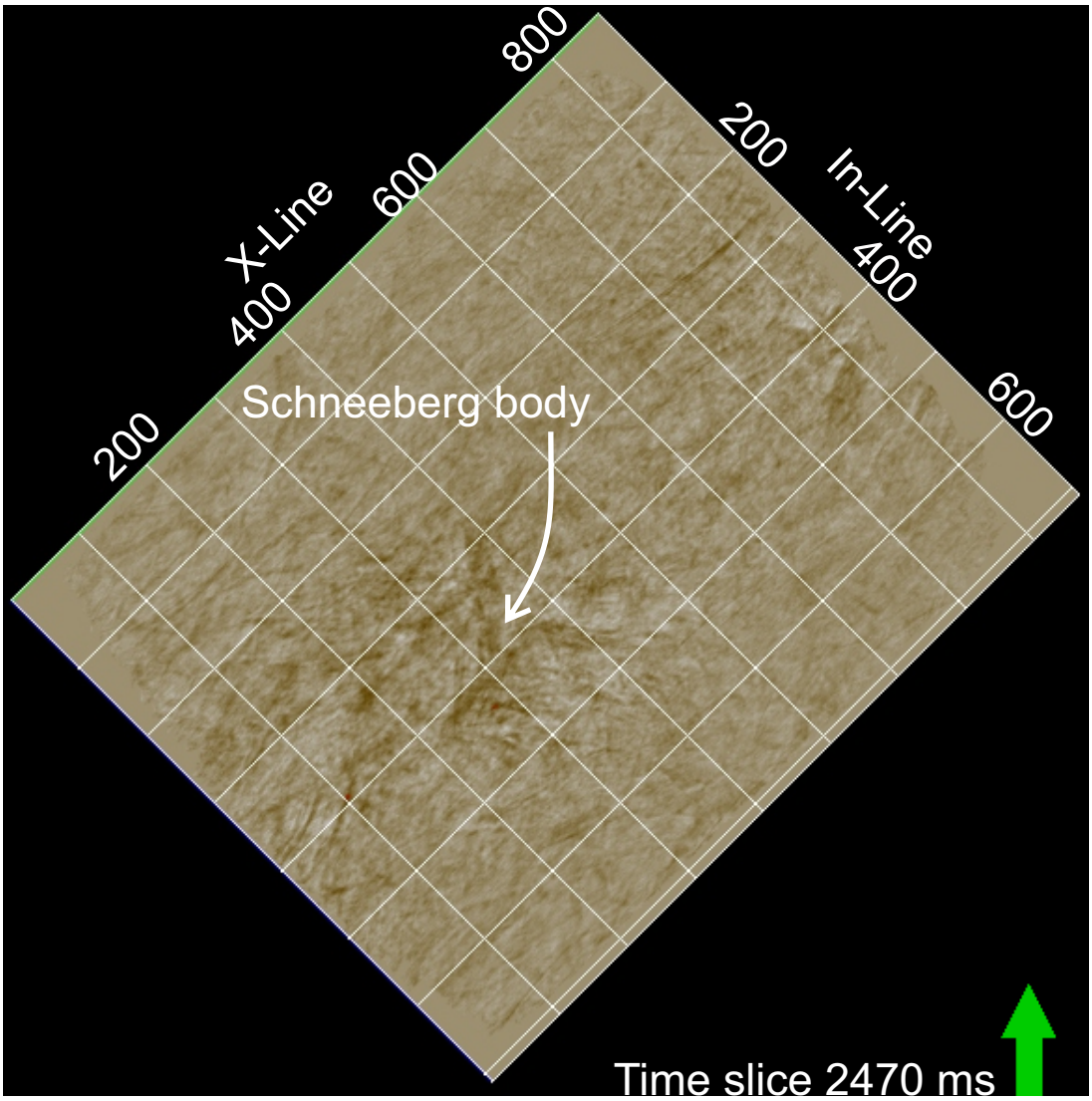

Figure 4.20.: Migrated coherence time slice 2470 ms.

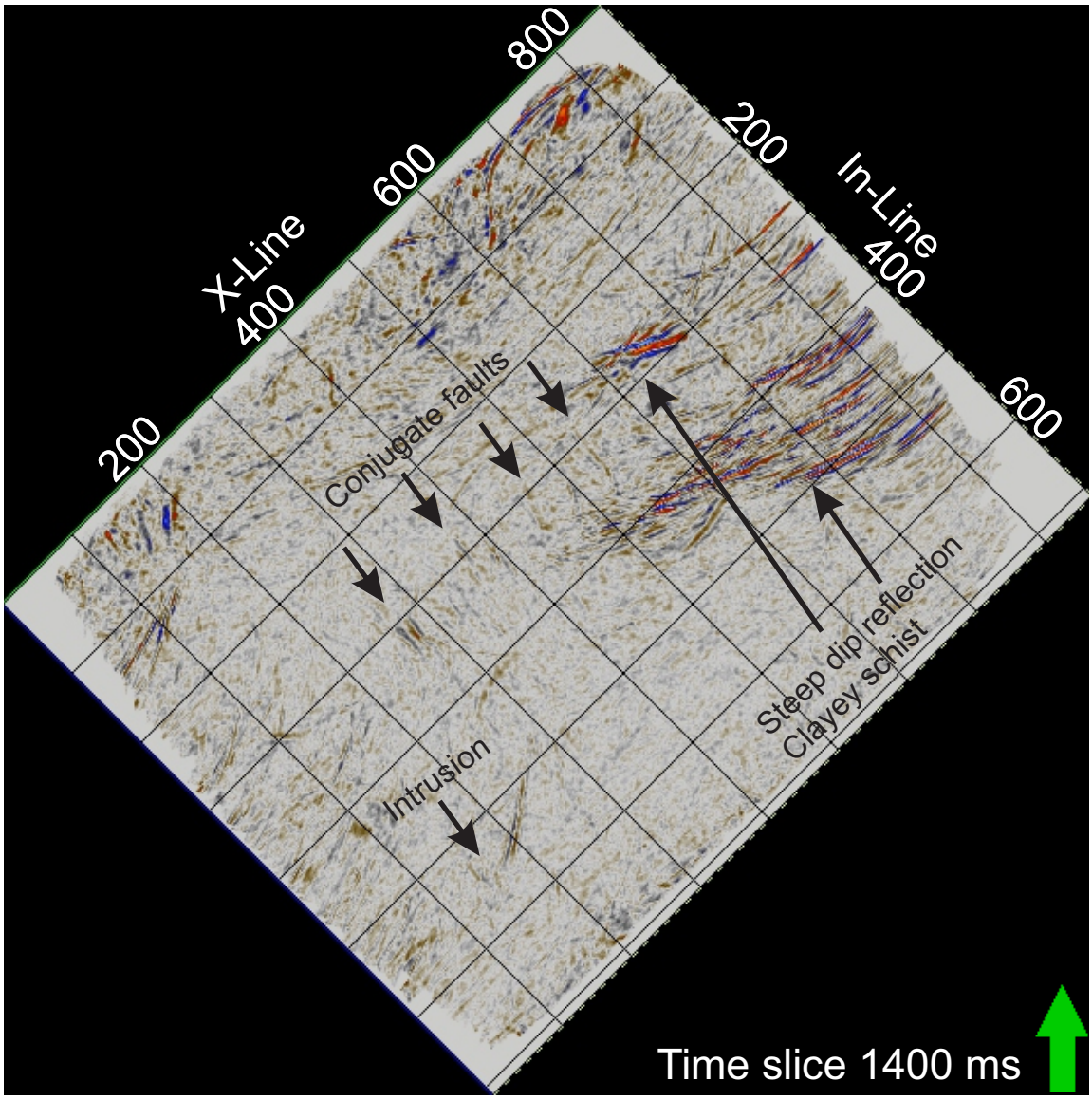

Figure 4.21.: Migrated coherence weighted stack time slice 1400 ms.

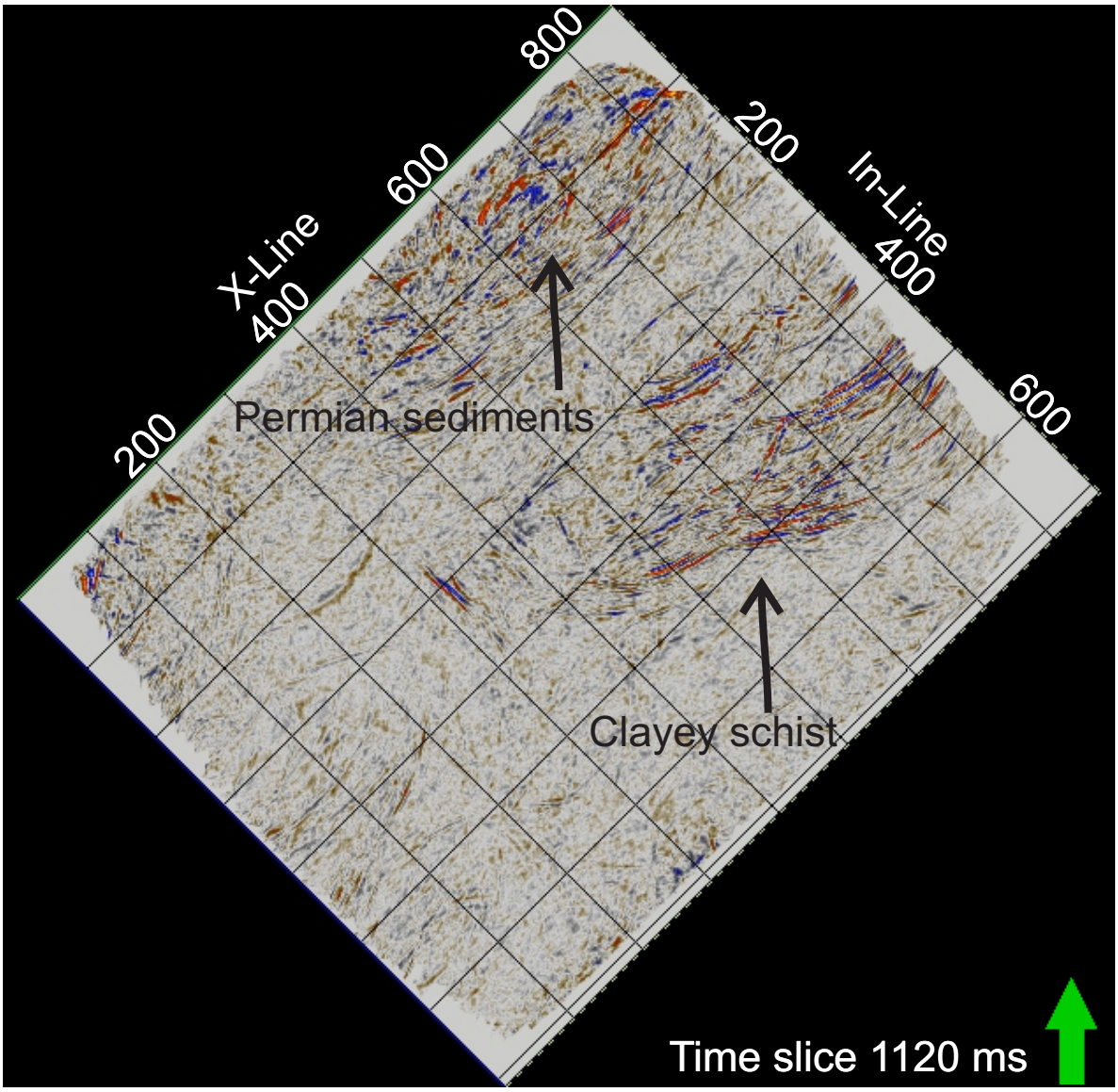

Figure 4.22.: Migrated coherence weighted stack time slice 1120 ms.

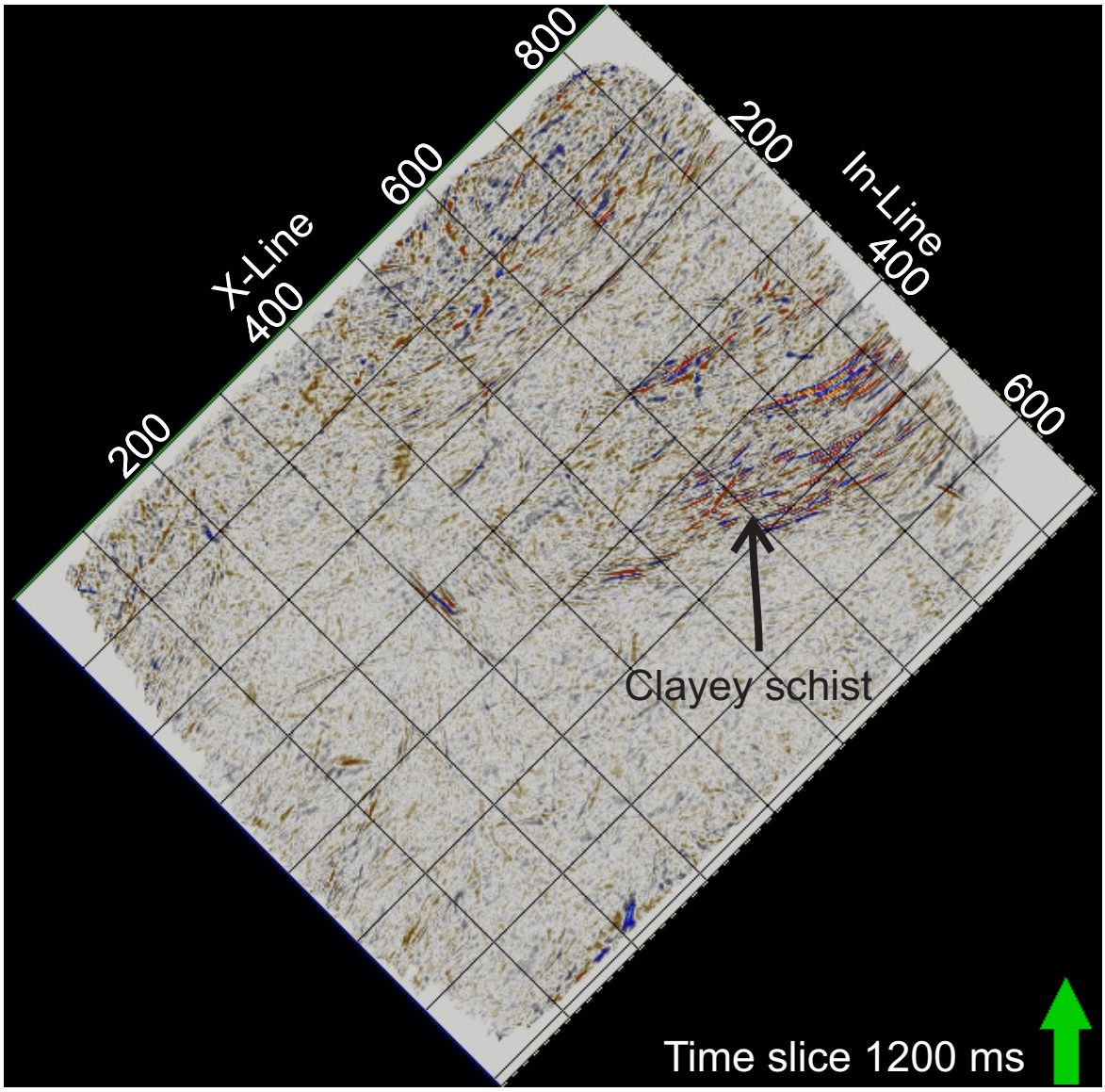

Figure 4.23.: Migrated coherence weighted stack time slice 1200 ms.

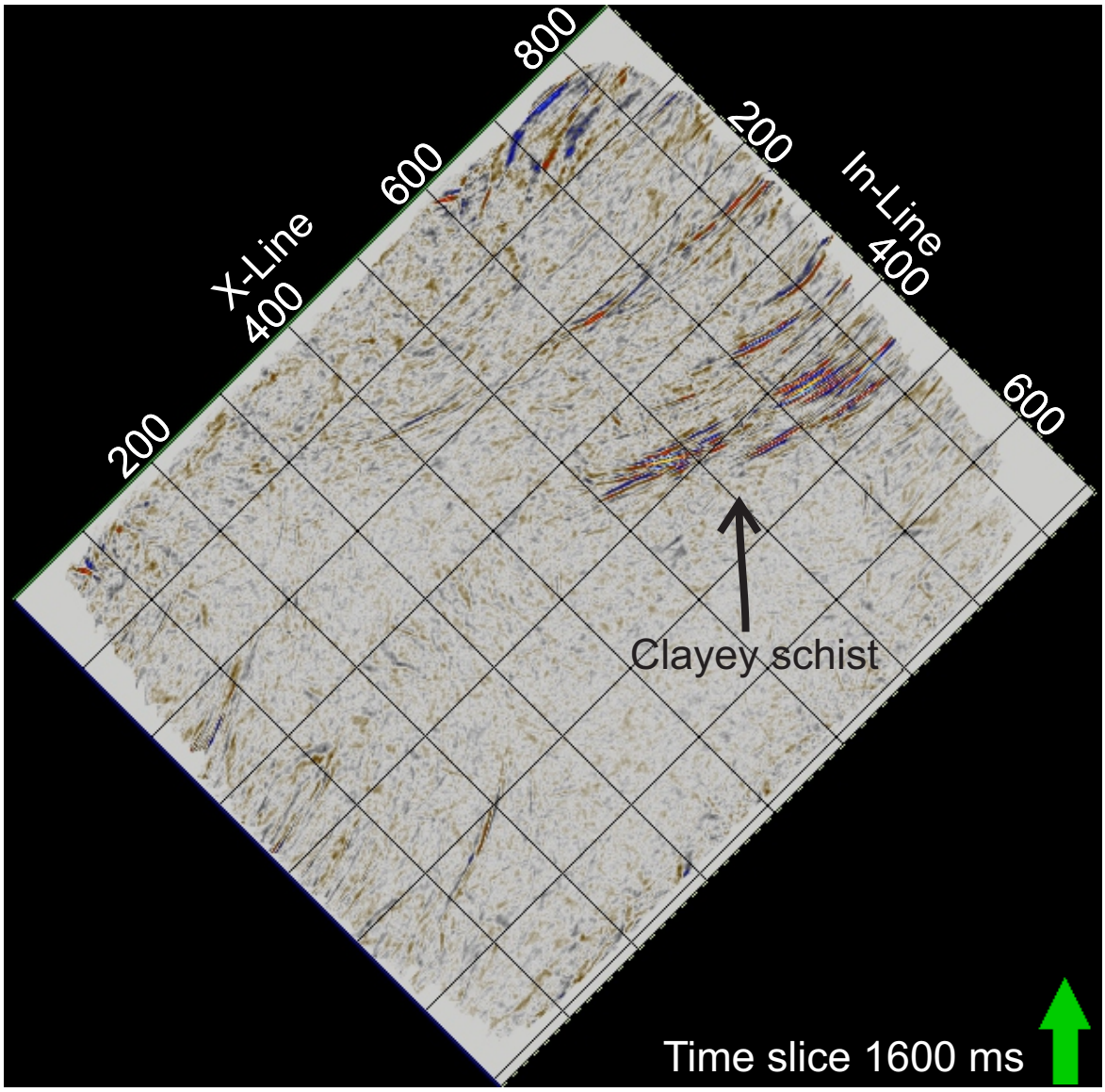

Figure 4.24.: Migrated coherence weighted stack time slice 1600 ms.

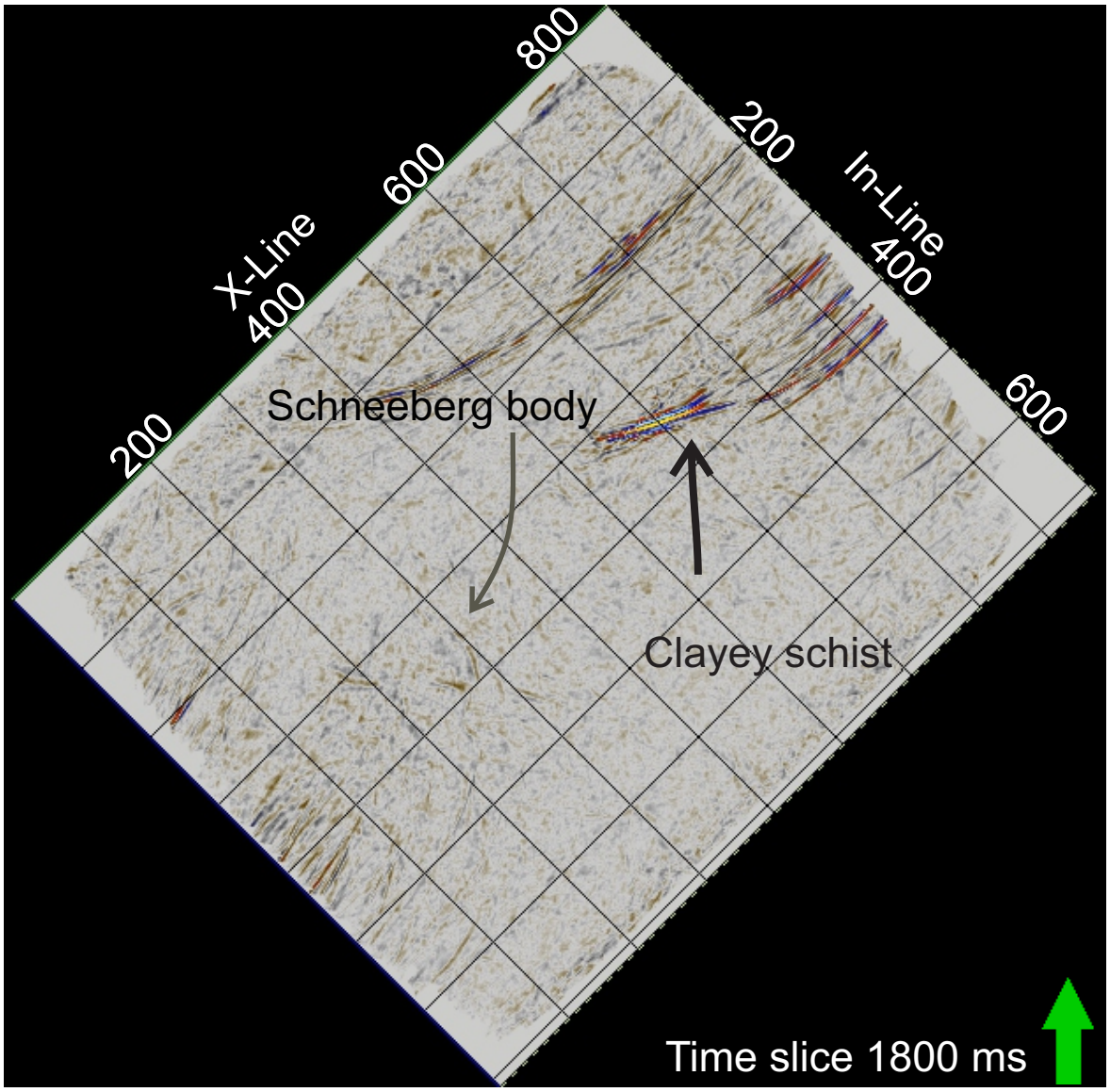

Figure 4.25.: Migrated coherence weighted stack time slice 1800 ms.

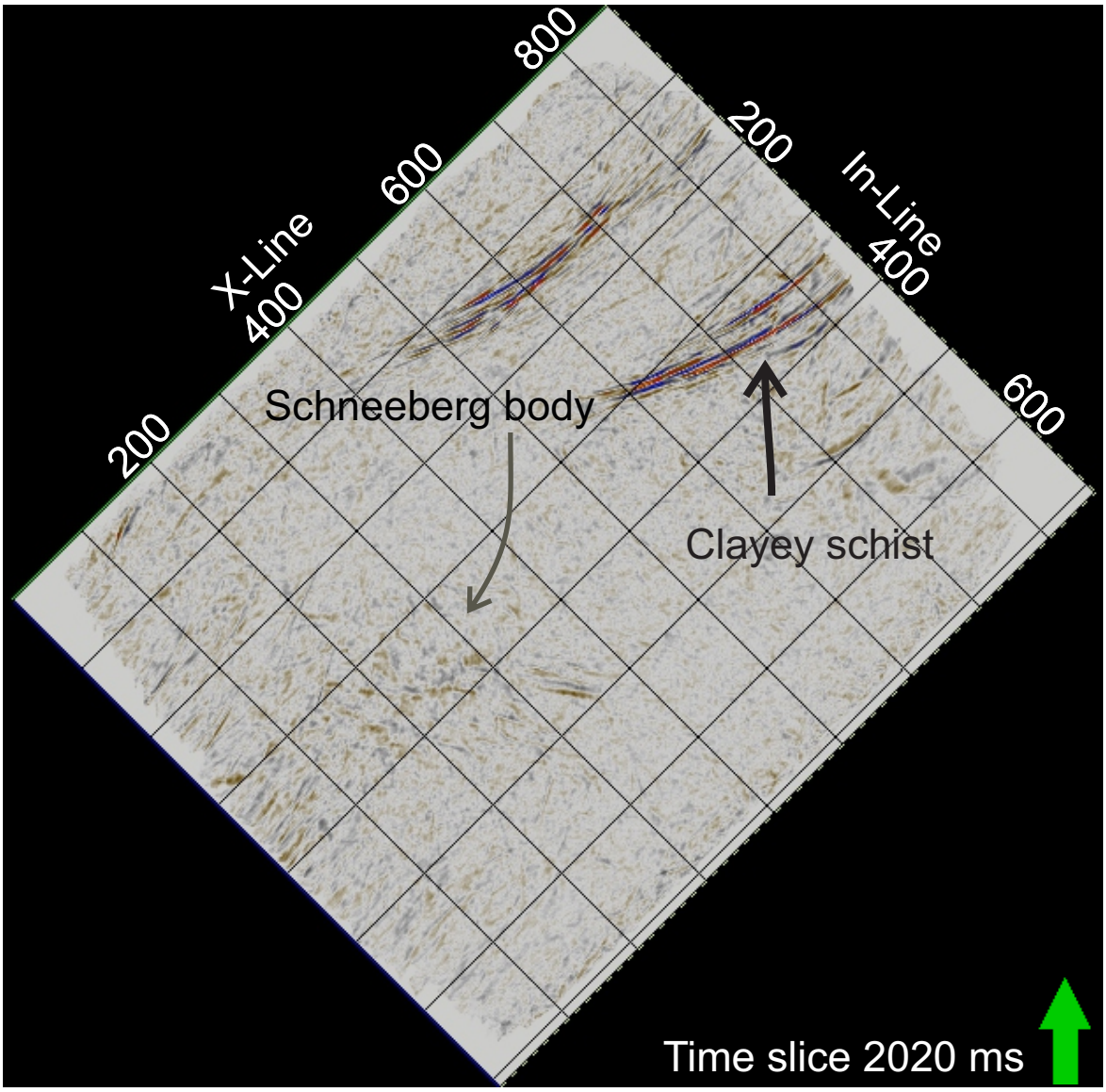

Figure 4.26.: Migrated coherence weighted stack time slice 2020 ms.

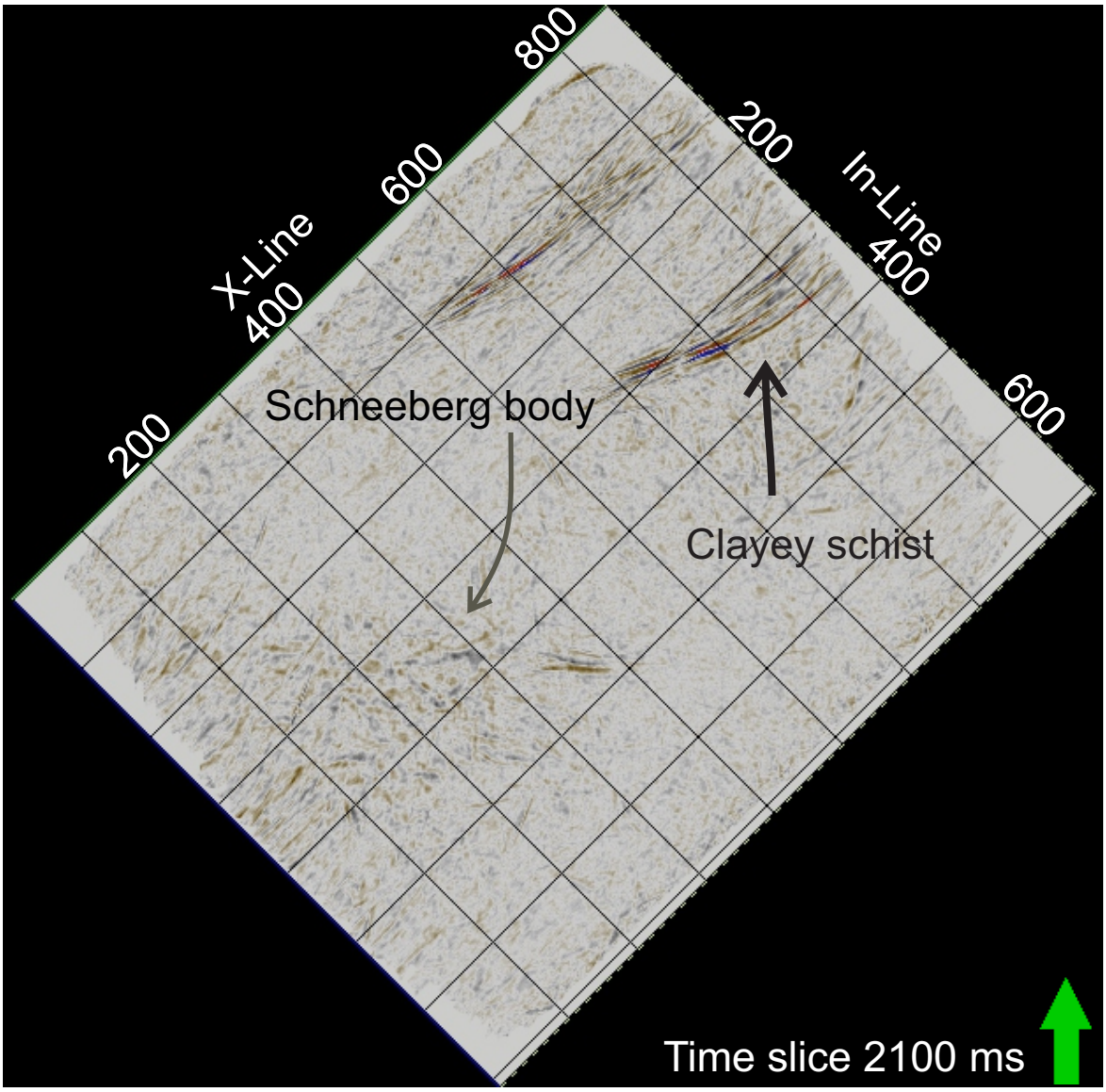

Figure 4.27.: Migrated coherence weighted stack time slice 2100 ms.

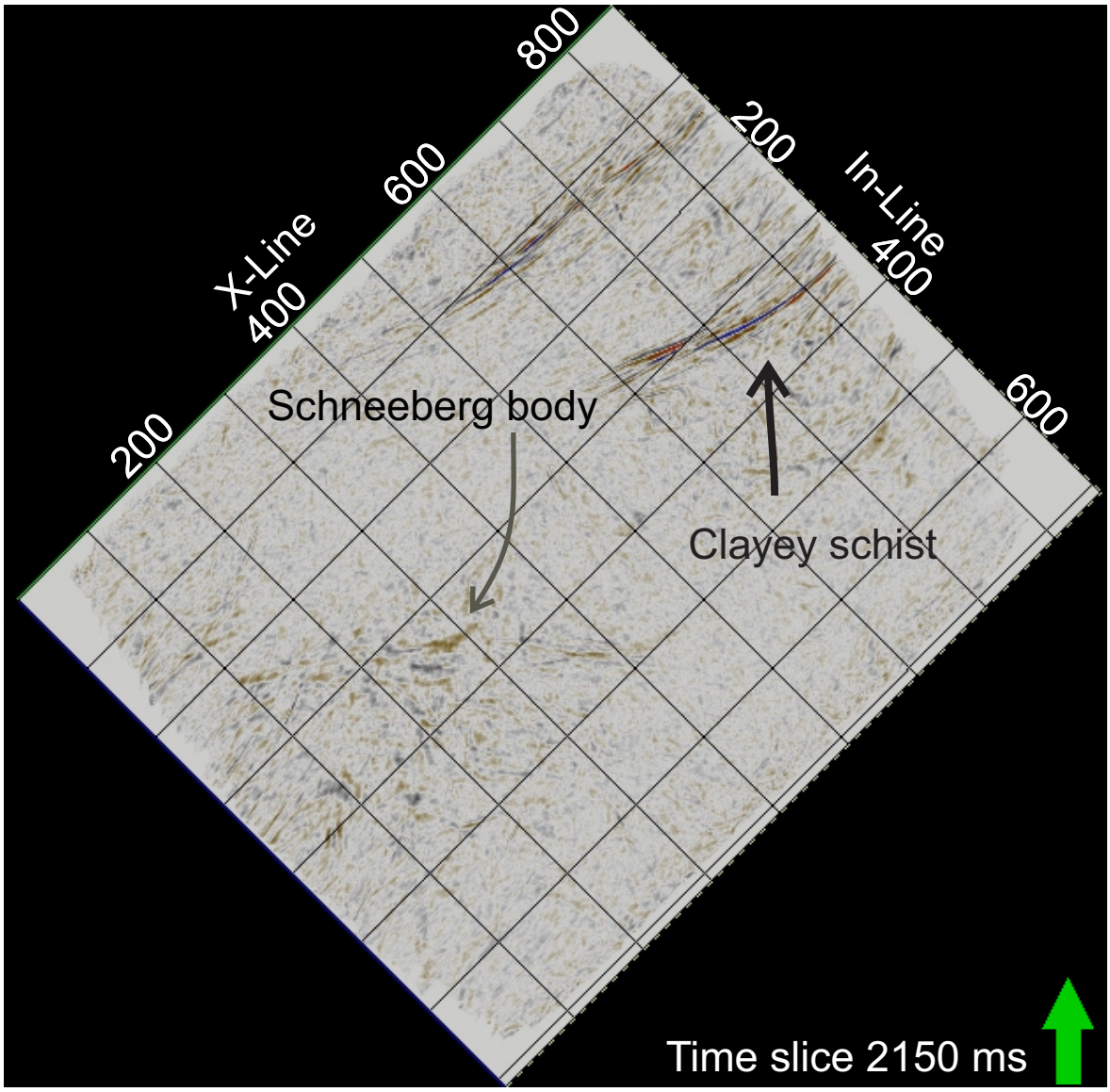

Figure 4.28.: Migrated coherence weighted stack time slice 2150 ms.

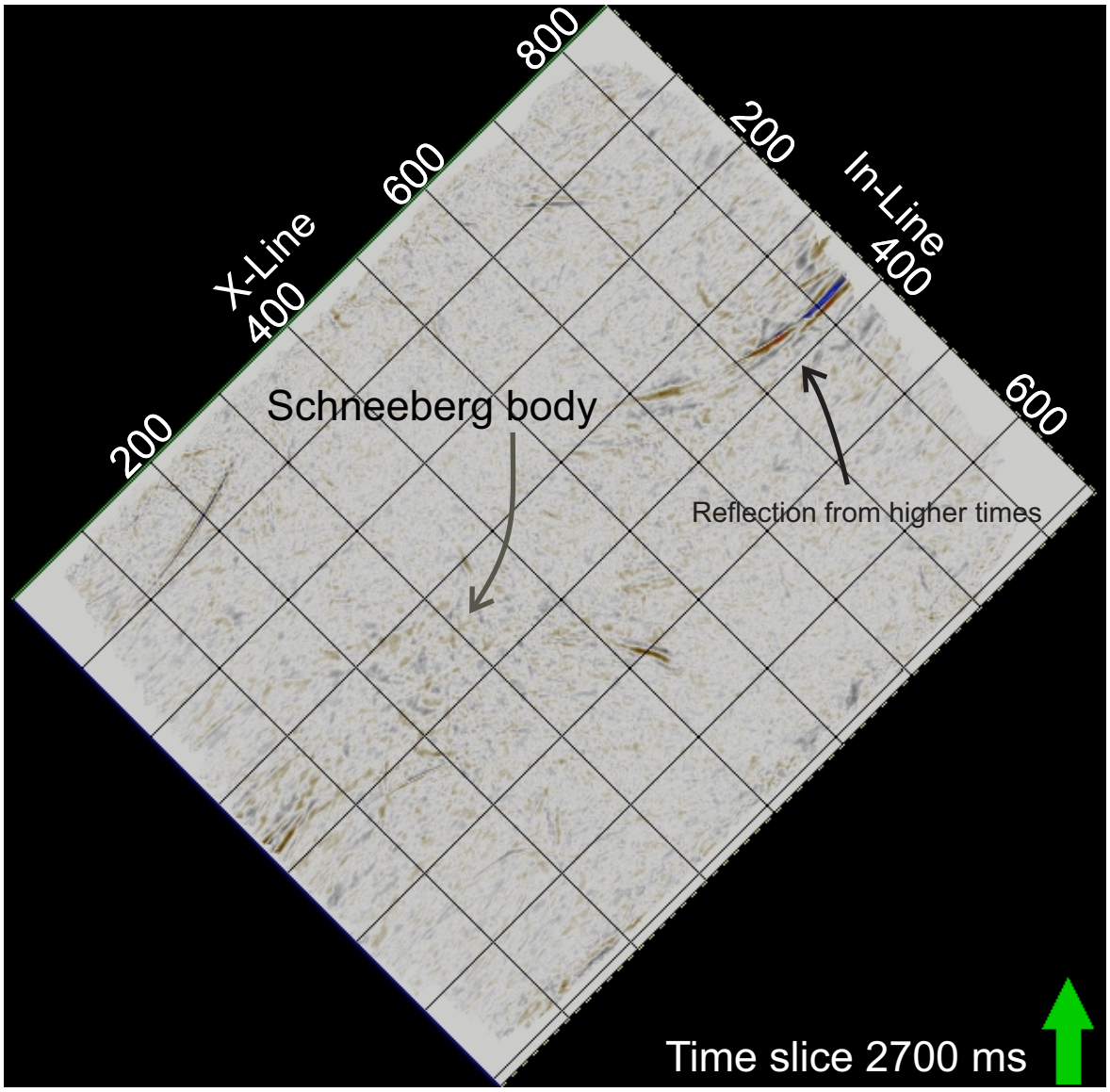

Figure 4.29.: Migrated coherence weighted stack time slice 2700 ms.

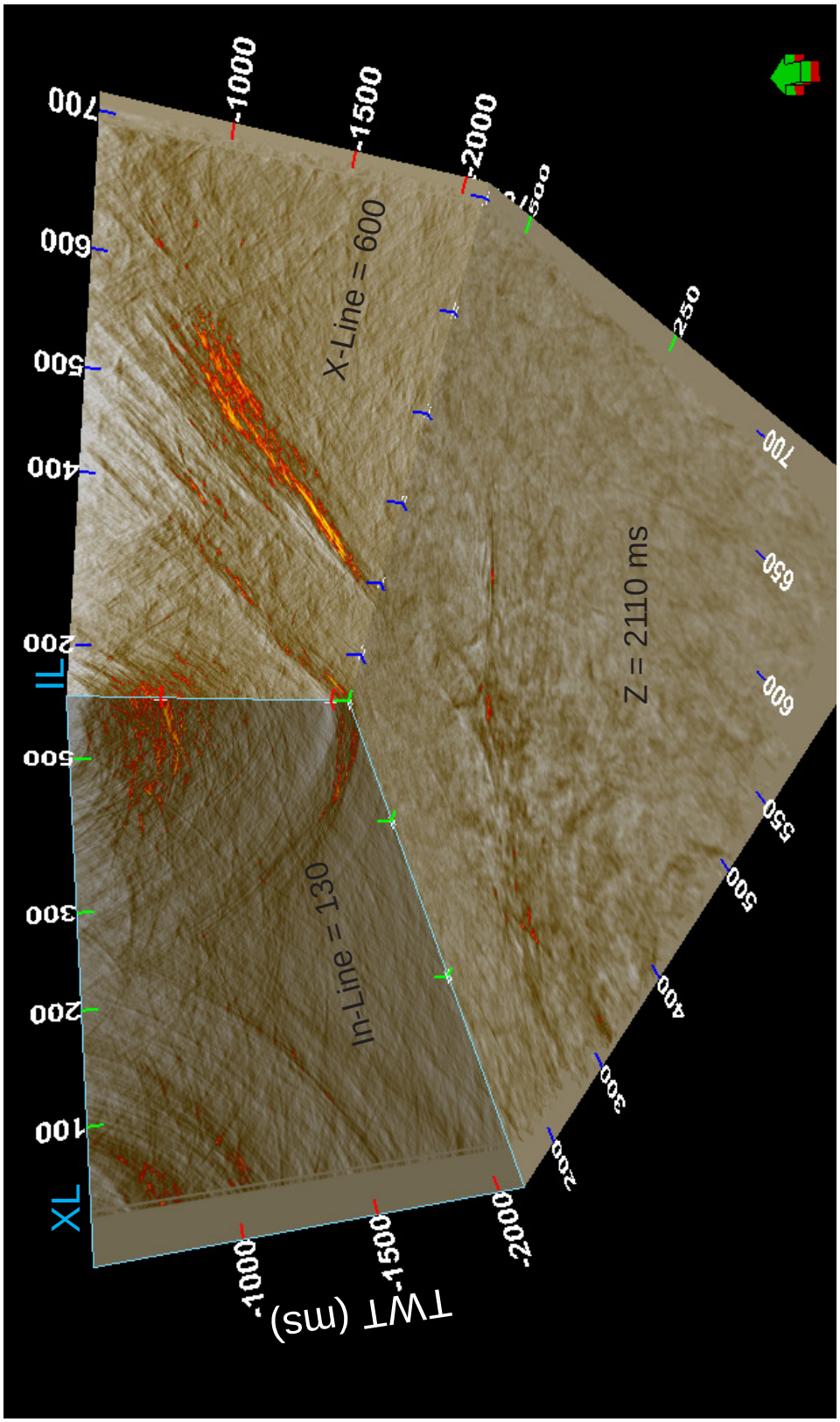

Figure 4.30.: Migrated coherence volume (inside structure).

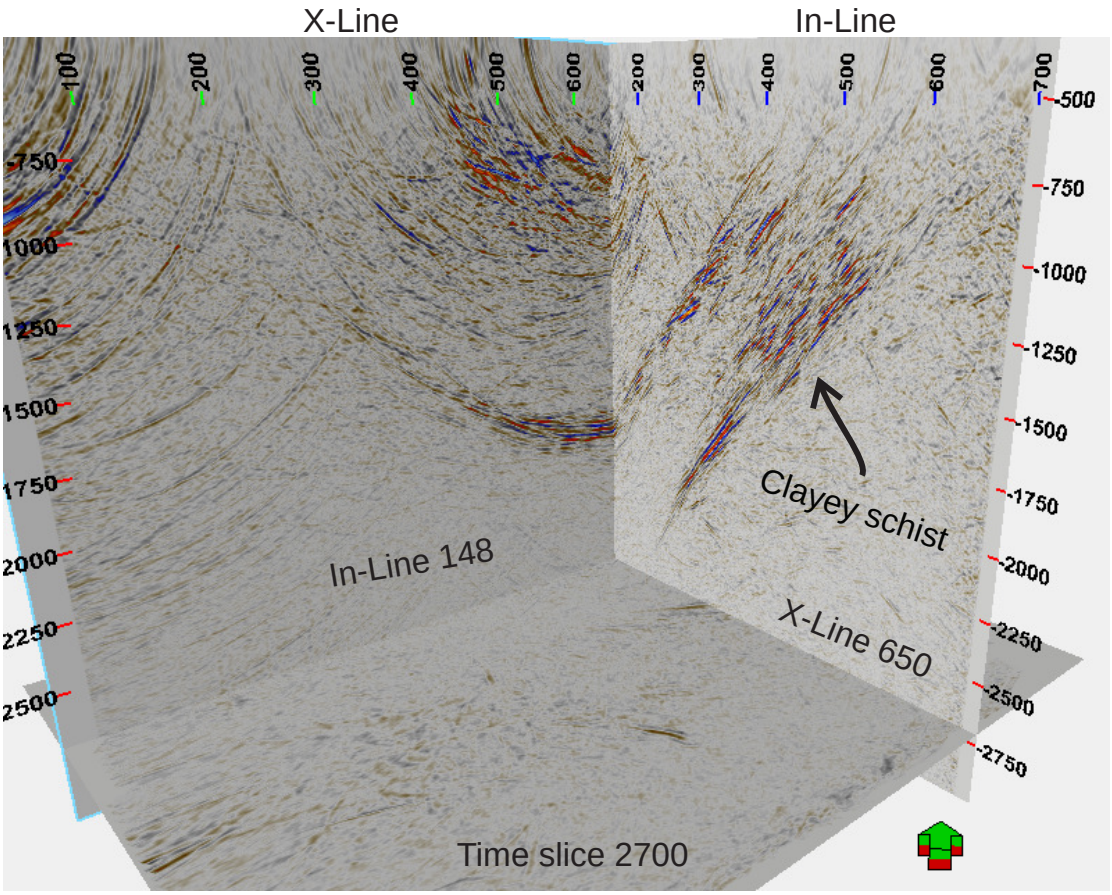

Figure 4.31.: Migrated coherence weighted stack view1.

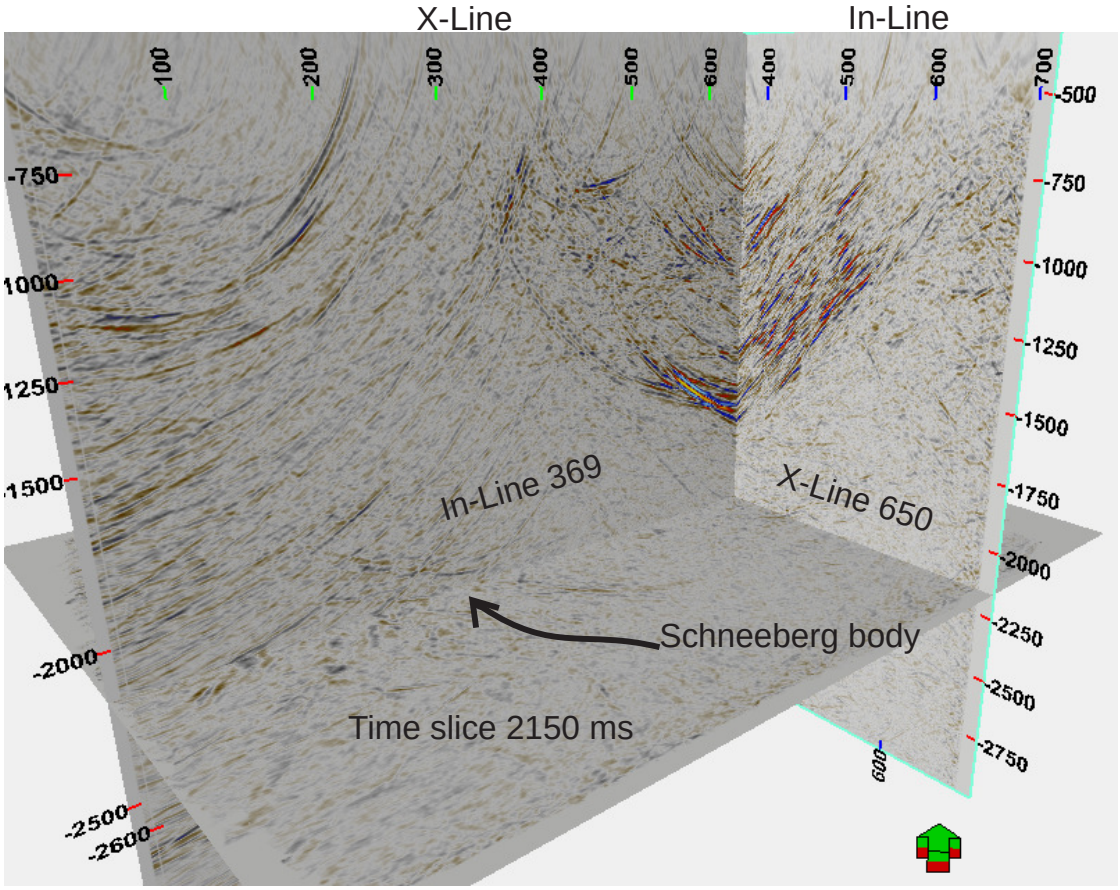

Figure 4.32.: Migrated coherence weighted stack view2.

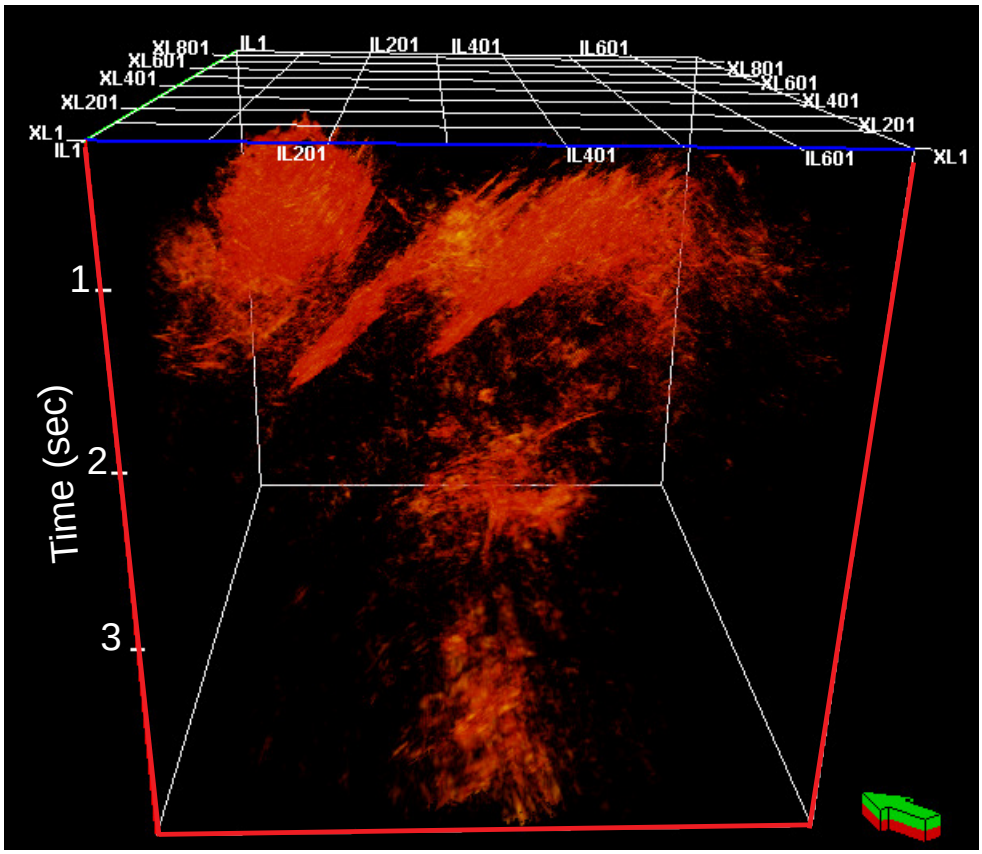

Figure 4.33.: Migrated coherence transparency.

5. Summary

Conclusions and discussion

In the present study, there were two important problems to be resolved. One is how to handle big 3D seismic dataset in feasible time frame. The other is that if the data comprising poor S/N ratio and low resolution, how to get a good seismic image out of it. To solve these problems, two steps were taken. First, to optimize the parallelization of the 3D CRS code. The original 3D CRS code had problems relating to the computation. These problems were relating to memory leaks and the search strategy. Also not all of the available resources were being utilized while computing the search steps.

In the 3D CRS workflow, almost 90-94% of the computational cost is utilized by coherence analysis. In modern machines, there are virtual cores and the threads available on CPUs. To improve the optimization (MPI based code), the code was optimized that the output is saving the time and cost both. In ideal conditions, the efficiency is up-to 10 times faster. Under special conditions, the efficiency is even more better than that. All effort to optimize (hybrid MPI with OpenMP) the code is to generate the threads that can be utilized in the processing if available on machines and cumulative performance gets better.

Upto now, the studies using the hybrid approach reveal that, the performance of this code is improved. Some tests on 2D, small 3D data proved that it is cost efficient and can save days, weeks, and even months when the data is huge. This code was tested on the Schneeberg 3D seismic dataset. The data was 500 GB in volume which is quite huge by academic standards. The hybrid code is able to handle it efficiently. The output of old code is similar to the new hybrid code. The code works more efficiently in the shared memory architecture than parallel memory because of the demand of the code. The data tunneling and communication is better in the new code. However, there are still some issues like memory leaks and some search strategies are not so well optimized. The code still needs to be written from scratch in a professional style in order to achieve better results in terms of

efficiency. For the Schneeberg 3D seismic dataset, the code worked fairly well. Thus the high performance computing (HPC) helped a lot in working with the huge datasets. Although the efficiency is not reached to the industrial level where specialized hardware for high performance computing like GPUs and FPGA is used. For the academic level, the performance of accelerated code is quite satisfactory. This is a leap in leading towards the improvement in the efficiency of code.

Application of a 3D CRS-based workflow to the Schneeberg 3D hardrock reflection seismic data is purely a data-driven approach. The S/N ratio of these data is very low and the initial automatic CMP stack indicated that multi-parameter processing methods, which use more traces in the stack might improve the image quality. Although the comparison of conventional CMP stacking with automatic CMP stacking is unfair, but the studies show that the conventional CMP stacking has not produced the reasonable results from these hardrock dataset (Lüschen et al. 2015. The data are dominated by diffractions generated at various steep dipping fracture zones. Steep structures and a huge number of diffraction tails interfere or lead to a complicated pattern of conflicting dips. The CRS stack showed a considerably improved S/N ratio and provided a reasonable basis for geological interpretation. However, plots of the coherence actually delivered good images for interpretation for this particular type of hardrock data. Despite the reduced resolution compared to the stack, the coherence is considered as a suitable imaging attribute, since it is an objective measure of the local similarity in the wavefield and directly reflects the physical relevance of the corresponding seismic event. For the considered data the coherence is a data-driven imaging attribute particularly helpful for the interpretation of hardrock data. Weighting, i. e., multiplying the stacks with the coherence further improved the S/N ratio of the resulting sections and supported the interpretation of the images. Similar conclusions apply to the display of the coherence-weighted time slices, which provided the best images.

The reflections from top and bottom of the clayey schists represent the most prominent features in the data. A sequence of conjugate faults is also nicely mapped. Their lateral extent at depth seems to be small which does not coincide with the surface expression of these faults. There are some surprised results revealed from the study of these hardrock dataset. Prior to this experiment the Roter Kamm was expected to be the most prominent structure in the data. However, it is noted that there are only faint hints of this fault in the data and the respective coherence is much smaller than the coherence of the sequence of conjugate faults. Another prominent feature of the data was detected in the SW of the survey area. This feature represents a region with a very high number of aligned events below 1.5 s TWT named as Schneeberg body. This area of high coherence is located in a region where several fracture systems intersect and may have a high fracture density. Whether these fractures are open or mineralized cannot be

decided from the current state of processing. Open fractures would make this area a favorable region for a geothermal heat exchanger. It is known, however, that many fracture systems in the North of the measurement surface are mineralized, which initiated the mining activities in this area. Different features are still un-interpreted specially in higher traveltime and several are still unexplored due to the data quality.

6. Outlook

Many options are open for optimizing the 3D CRS code, like sorting problem of the memory leaks and the data I/O etc. One way to get the high performance computing with 3D CRS code is to rewrite it for modern hardware. However analyzing the parts of the code (which needs to be optimized) also needs considerable time. The alternating approach is to convert the code into FPGA (field programmable gate array) based code which is also possible with either the hardware design language or using the Max-compiler on Maxeler machine.

Imaging Schneeberg data from crystalline environment opened new horizons to think about the problems which are faced during the seismic data processing from complex environment and it rails the research in different directions to improve the S/N ratio of seismic data. Pre-stack time and depth migration of hardrock data will rely on the respective velocity model input. Because of the poor data quality, the estimation of CRS attributes is not necessarily stable and all processes relying on these attributes may be compromised. This includes the computation of migration velocities. All options to improve the signal quality of the pre-stack seismic data will help to better image the subsurface of hardrock systems. Key element in the successful processing of hardrock data is the enhancement of the pre-stack data quality. Partial CRS stacks (e.g., Baykulov and Gajewski 2009) might be an option to improve the data quality in the pre-stack domain. Seismic data from a hardrock subsurface are largely dominated by diffractions, which are not optimally fitted by the CRS operator. Processing the data with the i-CRS operator (e.g., Schwarz et al. 2014) might improve the determination of wave field attributes, since it better fits diffractions. High quality attributes will result in more reliable time migration velocities, capable of improving NIP wave tomography and better pre-stack data enhancement opportunities. Another option of pre-stack data improvement is given by the partial time migration introduced by (Dell et al. 2012). This tool also has a pre-stack data enhancement facility and requires reasonable time migration velocities to be applied effectively. 3D NIP wave tomography (Klüver, 2007) can be used to estimate the velocity model using the attributes by picking reliable events. Anisotropy is one of the main targets which can help in better imaging such type of dataset. Conflicting dips are main issue in CRS processing and can lead to wrong estimation or lead to the loss of events in the stacked section.

Handling conflicting dips in 3D CRS processing can lead to improvement in the imaging of criss-cross patterns in the stacks. The method suggested by (Walda and Gajewski, 2015) can be implemented for 3D case to resolve this issue. As the data is dominated by diffractions, a specialized processing and tomography recently discussed by (Bauer, 2014) and (Schwarz, 2015) may lead to a new methodology for velocity model building entirely based on zero-offset data.

A. Electronic Supplements in DVD

* In the DVD, there are animated videos with slide shows of 3D volumes from different directions and different angles. These volumes are imaged with the transparency. This means that there is certain threshold for the signal to visualize. Most of the noise is attenuated which is below the threshold. Therefore most of the signal is visible and the unwanted noise disappears. Different colour scales are used to visualize the volumes. The videos are of migrated coherence weighted stack, migrated coherence (animated slides) and migrated stack.

* Electronic pdf version of thesis is also available.

* The DVD supplement is not available online and can be accessed on request from the department library or by writing an email khawar-ashfaq.ahmed@uni-hamburg.de.

Used softwares and hardwares

During the research work, differnet types of operating systems have been used, which are Linux (Debian and CentOS) free version licenses and (Windows XP/7/8.1).

The hybrid approach for High Performance computing (HPC) developed in this thesis is based on 3D ZO CRS stack code as implemented by Alex Müller (2007), concurrent programming using C++ and integrated approach to use (OpenMP with MPI) for using the threads. This has been successfully implemented and done with the help of DKRZ (Specially Dr. Hendryk Bockelman).

Migration of the 3D seismic volumes has been done by using the ProMAX & SeisSpace software from Hilliburton.

For visualization of the 3D cubes and inlines, crosslines, slices, Opendtect, Petrel (Seismic to simulation) from Schlumberger, Seismic Un*x (Colorado School of Mine) were used.

For some visualization, drawing, editing and generating images, Corel Draw (Graphic suit X6) and Inkscape has been used.

SeisSee (free) has been used for header investigation.

For animation and 3D visualization, Avizo Earth (in collaboration of DKRZ) has been used.

The Wave Inversion Technology (WIT) consortium provided further software for the CRS processing:

1. 3D ZO CRS stack (by Alex Müller)

2. Automatic picking of input data for tomographic inversion (by Tilman Klüver)

3. 3D NIP-wave tomography (by Tilman Klüver)

4. 3D Migration velocity analysis for diffractions (by Sergius Dell)

5. 3D Diffraction mapping
6. C/C++ for programming

Four types of hardware machines have been used:

1. Desktop machine core i7 based.
2. Tornado (little endian) 2000cores based.
3. Thunder (little endian) cluster 32cores (64 threads) based.
4. Blizzard (bigger endian) cluster 8000 cores based.
5. Laptop core i5 based.

The thesis is written on laptop and desktop based OS in LATEX.

Aknowledgements

- I have no words to express my humble thanks and love to Professor Dr. Dirk Gajewski for accepting me as PhD student, giving me chance to work under his supervision and gave me lot of freedom to express my skills. It is his highness that he trusted me while accepting even without knowing me. His door was always open for every problem and help either in research or moral support is needed. He gave me the opportunity to express my research across the globe in conferences and meetings.

- I am also grateful to Dr. Claudia Vanelle for the co-supervision of my thesis and also for allowing me to further develop my skills. Special thanks for the proof reading of this thesis.

- I would also like to say thank you to Dr. Hendryk Bockelman from DKRZ for sharing precious ideas and sparing time to resolve issues relating to software and coding.

- I am thankful to Benjamin Schwarz for sharing office, we did lot of benificial discussions and we shared every feeling and problem and resolved together. I always enjoyed his company.

- I would also like to say thank you to Dr. Sergius Dell from CGG, London, for sharing office, nice discussions, wonderful ideas of seismic imaging and always being helpful in every problem.

- I also like to say thank you to Dr. Ekkehart Tessmer for being with me in every time of difficulty relating to computer, cluster and coding and all other problems which I share to him.

- I am as well grateful to Dr. Mikhail Baykulov (Addax Petroleum) for sharing wonderful ideas relating to research.

- I am thankful to Dr. Christian Hübscher for giving nice advices and discussions relating to my work.

- I would like to say thanks to Dr. Ali Dehghani for always being helpful.

- Helping effort of Dela Spickermann and Michael Böttinger from DKRZ is also appreciated specially for visualization and animations.

- Thanks to Prof. Dr. Boris Kashtan from Russian Academy of Sciences, Saint Petersburg, Russia for nice helpful discussions.

- Discussions with project parteners from LIAG, Hannover and TU Freiberg is also appreciated.

- Thanks to Prof. Dr. Zulfiqar Ahmad and Prof. Dr. Shahid Nadeem Qureshi for always encouraging me for research work.

- My special thanks also goes to Christel Mynarik and specially Paola Dal Corso who always helped me with administration issues.

- I would like to thanks Hendrik Niehaus, Leonie Pick, Jan Walda, Malik Faisal Peracha, Ivan Abakumov, Phillip Witte, Martin Vögele, Muayyad Younis Mahmoud Al Hseinat, Mahmood Sultan, Syed Faraz Ahmed, Syed Awais Haider and Shehzada Yasir Ummar for always being with me for support and help during my PhD.

- I gratefully acknowledge the Wave Inversion Technology (WIT) consortium for funding of my position and the conference attends. The Code provided by the consortium represents the basis for the work presented in this thesis.

- I like to thank BMWi for data and financial support. Funding by the Federal Ministry for Economic Affairs and Energy of Germany (0325363A) is gratefully acknowledged

- Obviously, I like to say infinite thanks to my family starting from specially my parents, father Ashfaq Ahmed Qazi, mother Nighat Yasmin, wife Hira Khawar, brother Khurram Ashfaq Qazi for always being with me in any situation and always supporting me financially, physically, morally and spritually in my progress. They always standby on my decisions and never let me down in any difficult situation. Thanks to my beloved brother Manazar Ahsan Hashmi, sister Asma Manazar, and nephew Abdul Moiz Hashmi and Abdul Azeem Hashmi for giving me infinite love and moral support. Indeed, I am incomplete without any of them in my life.

- Always thanks to Almighty ALLAH for blessings on me.

Bibliography

M. Al-Chalabi. Series approximation in velocity and traveltime calculation. *Geophysical Prospecting*, 21(4):783–795, 1973.

A. Bauer. From zero-offset to common-offset with diffractions. Master's thesis, University of Hamburg, 2014.

M. Baykulov. *Seismic imaging in complex media with Common Reflection Surface Stack*. PhD thesis, University of Hamburg, 2009.

M. Baykulov and D. Gajewski. Prestack seismic data enhancement with partial common-reflection-surface (CRS) stack. *Geophysics*, 74(3):V49–V58, 2009.

M. Baykulov, S. Dümmong, and D. Gajewski. From time to depth with CRS attributes. *Geophysics*, 76(4):S151–S155, 2011.

H. J. Berger, M. Felix, S. Görne, E. Koch, O. Krentz, A. Förster, H. J. Förster, H. Konietzky, Ch. Lunow, K. Walter, H. Schütz, K. Stanek, and St. Wagner. *Tiefengeothermie Sachsen*. Number 9 in Schriftenreihe. Landesamt für Umwelt, Landwirtschaft und Geologie, 2011.

S. Bergler, P. Hubral, P. Marchetti, A. Cristini, and G. Cardone. 3D common-reflection-surface stack and kinematic wavefield attributes. *The Leading Edge*, 21 (10):1010–1015, 2002.

W. Bruce, N. Flesjå, O. E. Kristiansen, F. Vignati, A, and A. Aronsen, H. Shallow water 3D multiple attenuation:A case study in methods. WorldOil, 2009.

B. Chapman, G. Jost, and R. Van Der Pas. *Using OpenMP : portable shared memory parallel programming*. The MIT Press, Cambridge, Massachusetts, London, England, 2008.

J. F. Claerbout. *Imaging the Earth's Interior*. Blackwell, 1985.

J. F. Claerbout and S. M. Doherty. Downward Continuation of Moveout Corrected Seismograms. *Geophysics*, 37(5):741–768, 1972.

S. Dell and D. Gajewski. Common-reflection-surface-based workflow for diffraction imaging. *Geophysics*, 76(5):S187–S195, 2011.

S. Dell, D. Gajewski, and C. Vanelle. Prestack time migration by common-migrated-reflector-element stacking. *Geophysics*, 77(3):S73–S82, 2012.

S. Dümmong and D. Gajewski. A multiple suppression method via CRS attributes. *2008 SEG Expanded Abstracts*, pages 2531–2535, 2008.

E. Duveneck. Velocity model estimation with data-derived wavefront attributes. *Geophysics*, 69(1):265–274, 2004.

D. W. Eaton, B. Milkereit, and M. H. Salisbury. *Hardrock seismic exploration.* Number 10. SEG Books, 2003.

R. Emmermann and J. Wohlenberg. *German Continental Deep Drilling Program (KTB).* Springer, 1988.

S. Fomel. Velocity analysis using AB semblance. *Geophysical Prospecting*, 57:311–321, 2009.

J. Gazdag. Wave equation migration with phase-shift method. *Geophysics*, 43: 1342–1351, 1978.

B. Gelchinsky, E. Landa, and V. Shtivelman. Algotithm of phase and group correlation. *Geophysics*, 50:596–608, 1985.

N. A. Gnatus, M. D. Khutorskoy, and V. K. Khmelevskoi. *Petrothermal Energy and Geophysics.*, volume 66. Moscow University Geology Bulliten, Allerton Press, Inc.,ISSN 0145-8752, 2011.

H. P. Harjes, K. Barm, H. J. Dürbaum, H. Gebrande, G. Hirschmann, M. Janik, M. Klöckner, E. Lüschen, W. Rabbel, M. Simon, J. Thomas, J. Tormann, and F. Wenzel. Origin and nature of crustal reflections: Results from integrated seismic measurements at the KTB superdeep drilling site. *Journal of Geophysical Research*, 102(B8):18,256–18,288, 1997.

T. Hertweck, J. Schleicher, and J. Mann. Data stacking beyond CMP. *The Leading Edge*, 26:818–827, 2007.

P. Hubral. Computing true amplitude reflections in a laterally inhomogeneous earth. *Geophysics*, 48(8):1051–1062, 1983.

P. Hubral and T. Krey. Interval velocities from seismic reflection traveltime measurements. *Soc. Expl. Geophys.*, 1980.

R. Jäger, J. Mann, G. Höcht, and P Hubral. Common-reflection-surface stack: Image and attributes. *Geophysics*, 66:97–109, 2001.

T. Klüver. *Velocity model building using analytic and model-based diffraction traveltime functions.* PhD thesis, University of Karlsruhe, 2007.

U. Kroner, T. Hahn, R. L. Romer, and U. Linnemann. *The variscan orogeny in the Saxo-Thuringian zone - Hetrogeneous overprint of Cadomian/paleozoic Peri-Gondwana crust.*, volume 423. Geological Society of America, Spec. Pap.„ 2007.

S. A. Levin. Principle of reverse time migration. *Geophysics*, 49(5):581–583, 1984.

U. Linnemann and R. L. Romer. *Pre-Mesozoic Geology of Saxo-Thuringia (From the Cadomian Active Margin to the Variscan Orogen).* Schweizerbart Science Publishers., 2010.

S. Luo and D. Hale. Velocity analysis using weighted semblance. *Geophysics*, 77(2): U15, 2012.

E. Lüschen and R. Schulz. 3-D Seismic Surveys Explore German Petrothermal Reserves. *EOS Transactions, American Geophysical Union*, 95(26):237–244, July-2014.

E. Lüschen, S. Görne, H. von. Hartmann, R. Thomas, and R. Schulz. 3D seismic survey for geothermal exploration in crystalline rocks in saxony, germany. Geophysical Prospecting (Special Issue Hardrock), 2015.

A. Malehmir, R. Durrheim, G. Bellefleur, M. Urosevic, C. Juhlin, D. J. White, B. Milkereit, and G. Campbell. Seismic methods in mineral exploration and mine planning: A general overview of past and present case histories and a look into the future. *Geophysics*, 77(5):WC173–WC190, 2012.

J. Mann, R. Jäger, T. Müller, and P. Hubral. Common-reflection-surface-stack - a real data example. *J. Appl. Geoph*, 42(3,4):283–300, 1999.

W. H Mayne. Common reflection point horizontal data stacking techniques. *Geophysics*, 27:927–938, 1962.

B. Milkereit, E. K. Berrer, A. R. King, A. H. Watts, B. Roberts, E. Adam, D. W. Eaton, J. Wu, and M. H. Salisbury. Development of 3-D seismic exploration technology for deep nickel-copper deposits-A case history from the Sudbury basin, Canada. *Geophysics*, 65(6):1890–1899, 2000.

N-A. Müller. *Determination of interval velocities by inversion of kinematic 3D wavefield attributes.* PhD thesis, TH Karlsruhe, 2007.

Nils-Alexander Müller. The 3D Common-Reflection-Surface stack – Theory and application. Master's thesis, University of Karlsruhe, 2003.

N. S. Neidell and M. T. Taner. Semblence and other coherency measures for multichannel data. *Geophysics*, 36:482–497, 1971.

J. A. Nelder and R Mead. A simplex method for function minimization. *Computer Journal*, 7:308–313, 1965.

H. Paschen, D. Oertel, and R. Grünwald. Possibilities of geothermal electricity generation in Germany (in German with English abstract). *TAB Rep. 084, Off. of Technol. Assess, German Bundestag, Berlin*, 2003.

Schlumberger. Oilfield glossary, 2015.

W. A. Schneider. Integral formulation for the migration in two and three dimensions. *Geophysics*, 43:49–76, 1978.

B. Schwarz. *Moveout and Geometry*. PhD thesis, University of Hamburg, 2015.

B. Schwarz, C. Vanelle, D. Gajewski, and B. Kashtan. Curvatures and inhomogeneities: An improved common-reflection-surface approach. *Geophysics*, 79(5):S231–S240, 2014.

R. H. Stolt. Migration by fourier transform. *Geophysics*, 43:23–48, 1978.

R. H. Stolt. Seismic data mapping and reconstruction. *Geophysics*, 67:890–908, 2002.

R. H. Stolt and A. K. Benson. Seismic migration theory and practice. *Geophysical Press, London*, page 382pp, 1986.

M. T. Taner and F. Koehler. Velocity-spectra digital computer derivation and applications of velocity functions. *Geophysics*, 34:859–881, 1969.

J. Walda and D. Gajewski. Handling the Conflicting Dip Problem in the CRS/i-CRS Methods. In *77th Annual International Meeting, EAGE*, page WS06. Expanded Abstracts, 2015.

A. Williams. *C++ Concurrency in Action (PRACTICAL MULTITHREADING)*. Manning Publications Co. PO Box 261 Shelter Island, NY 11964, USA, 2012.

O. Yilmaz. *Seismic Data Processing, Vol. I and II*. SEG, Tulsa, 2001.